CLIMATE CHANGE IN LOS ANGELES COUNTY: GRID VULNERABILITY TO EXTREME HEAT

A Report for:

California's Fourth Climate Change Assessment

Prepared By:
Daniel Burillo[1], Mikhail Chester[1], Stephanie Pincetl[2], Eric Fournier[2], Daniel Walton, Fengpeng Sun, Marla Schwartz, Katharine Reich[2], Alex Hall[2]

[1] Arizona State University
[2] University of California Los Angeles

Edmund G. Brown, Jr., *Governor*

August 2018
CCCA4-CEC-2018-013

ACKNOWLEDGEMENTS

The Climate Change in Los Angeles County: Grid Vulnerability to Extreme Heat Report was prepared with contributions from the following:

California Energy Commission, with support through Agreement No. EPC-15-007
Southern California Edison
California Independent System Operator
California Center for Sustainable Communities
CLEAN Coalition
Janet Reyna, Ph.D., National Renewable Energy Laboratory
Alan H. Sanstad, Lawrence Berkeley National Laboratory
Alex Ricklefs, The Energy Coalition
David Stoms, California Energy Commission
Guido Franco, California Energy Commission
Sudath Edirisuriya, California Energy Commission
David Fink, Climate Change Policy Consultant
Bill Pennington, California Energy Commission
Susan Wilhelm, California Energy Commission
Al Alvarado, California Energy Commission
Shawn Pittard, California Energy Commission
Tom Flynn, California Public Utilities Commission
Pamela Doughman, California Energy Commission
Mark Wallenrod, Southern California Edison
Felicia Federico, University of California Los Angeles
Laurel Hunt, University of California Los Angeles
Nathan Johnson, Arizona State University
Benjamin Ruddell, Northern Arizona University
Andrew Fraser, Arizona State University
Sam Markolf, Arizona State University
Emily Bondank, Arizona State University

PREFACE

California's Climate Change Assessments provide a scientific foundation for understanding climate-related vulnerability at the local scale and informing resilience actions. These Assessments contribute to the advancement of science-based policies, plans, and programs to promote effective climate leadership in California. In 2006, California released its First Climate Change Assessment, which shed light on the impacts of climate change on specific sectors in California and was instrumental in supporting the passage of the landmark legislation Assembly Bill 32 (Núñez, Chapter 488, Statutes of 2006), California's Global Warming Solutions Act. The Second Assessment concluded that adaptation is a crucial complement to reducing greenhouse gas emissions (2009), given that some changes to the climate are ongoing and inevitable, motivating and informing California's first Climate Adaptation Strategy released the same year. In 2012, California's Third Climate Change Assessment made substantial progress in projecting local impacts of climate change, investigating consequences to human and natural systems, and exploring barriers to adaptation.

Under the leadership of Governor Edmund G. Brown, Jr., a trio of state agencies jointly managed and supported California's Fourth Climate Change Assessment: California's Natural Resources Agency (CNRA), the Governor's Office of Planning and Research (OPR), and the California Energy Commission (Energy Commission). The Climate Action Team Research Working Group, through which more than 20 state agencies coordinate climate-related research, served as the steering committee, providing input for a multisector call for proposals, participating in selection of research teams, and offering technical guidance throughout the process.

California's Fourth Climate Change Assessment (Fourth Assessment) advances actionable science that serves the growing needs of state and local-level decision-makers from a variety of sectors. It includes research to develop rigorous, comprehensive climate change scenarios at a scale suitable for illuminating regional vulnerabilities and localized adaptation strategies in California; datasets and tools that improve integration of observed and projected knowledge about climate change into decision-making; and recommendations and information to directly inform vulnerability assessments and adaptation strategies for California's energy sector, water resources and management, oceans and coasts, forests, wildfires, agriculture, biodiversity and habitat, and public health.

The Fourth Assessment includes 44 technical reports to advance the scientific foundation for understanding climate-related risks and resilience options, nine regional reports plus an oceans and coast report to outline climate risks and adaptation options, reports on tribal and indigenous issues as well as climate justice, and a comprehensive statewide summary report. All research contributing to the Fourth Assessment was peer-reviewed to ensure scientific rigor and relevance to practitioners and stakeholders.

For the full suite of Fourth Assessment research products, please visit www.climateassessment.ca.gov. This report contributes to energy sector resilience by investigating the vulnerability of Los Angeles County's electricity grid to projected heat waves as well as resilience options to safeguard reliability.

ABSTRACT

Grid vulnerabilities to potential future heat waves described by climate change projections were assessed throughout Los Angeles County (LAC). Heat waves have posed serious challenges to power infrastructure in Southern California, including a major blackout in 2011 and emergency curtailment in 2014, and understanding how future temperature change might impact the power system is critically important for its continued reliable operation. Potential increases in peak demand, resource adequacy requirements, and component over-loadings were forecast for ranges of scenarios from 2021-2060. The Intergovernmental Panel on Climate Change's (IPCC) Representative Concentration Pathway (RCP) 4.5 and RCP 8.5 scenarios were used to project daily maximum temperatures at 2 km^2 resolution throughout LAC. The range of average annual maximum temperatures across LAC in the historical period (1981-2000) was 35-43 °C (95-110 °F), and highest average future temperatures across scenarios and periods ranged from 44.6-45.5 °C (112-114 °F). Peak hour electricity demand was projected to increase in residential and commercial sectors by 2060 by 0.2-6.5 GWh (2-51%) depending upon population growth (California Department of Finance vs SCAG projections), building efficiency (single-family vs multi-family), air conditioning (AC) penetration, AC efficiency, and warming. All grid components, except those located near Santa Monica Beach, were projected to experience 2-20% capacity loss due to air temperatures exceeding 40 °C (104 °F). Under SCAG high population growth projections, it is expected that the higher peak demands could be satisfied in the in-basin area without infrastructure capacity expansion through the implementation of aggressive energy efficiency measures. However, the central LAC region, spanning from West Valley to Pomona, was projected to experience increases of approximately 1.5 GWh even with aggressive energy efficiency measures, and the northern regions of Lancaster, Palmdale, and Santa Clarita were projected to have 300-900 MWh increase in peak hour load. Based on current substation load factors, an additional 0.9-1.1 GW of delivery system capacity will be needed by 2060 to maintain reliable operations, some of which may be met more cost-effectively via distributed energy resources than via new substations and/or transmission lines.

Keywords: California, Los Angeles, climate change, extreme heat, peak demand, vulnerabilities

Please use the following citation for this paper:

Burillo, Daniel, Mikhail Chester, Stephanie Pincetl, Eric Fournier, Daniel Walton, Fengpeng Sun, Marla Schwartz, Katharine Reich, Alex Hall. (University of California Los Angeles). 2018. ***Climate Change in Los Angeles County: Grid Vulnerability to Extreme Heat.*** California's Fourth Climate Change Assessment, California Energy Commission. Publication number: CCCA4-CEC-2018-013.

HIGHLIGHTS

- The vulnerability of Los Angeles's electricity infrastructure to rising air temperatures was estimated as a 2-20% loss of rated component capacity by 2060 based on RCPs 4.5 and 8.5 with average temperature rises of 0.9 to 3.2 °C (1.6 to 5.8 °F), and worst-case maximum temperatures of 54.3 °C (129.7 °F).
- The effects of population growth, building densification, AC penetration, AC efficiency, and rising air temperatures were modeled, and peak hour electricity demand was projected to increase in residential and commercial sectors by 0.2-6.5 GWh (2-51%) by 2060.
- Air temperature was estimated to have a non-linear effect ranging 2-5% per 1°C, which could increase to 3-7% by 2060 depending upon change in the other factors modeled.
- By 2060 the western-facing coast of Santa Monica Bay is projected to be the least impacted region of LAC, with inland areas experiencing the greatest vulnerability.
- Inland regions, specifically the San Gabriel Valley and the Antelope Valley, were projected to experience the highest temperatures at up to 54 °C (129 °F).
- Santa Clarita is the community at the greatest risk of service interruptions due to substation overloading (load factor $\geqslant$2) by 2060.
- Depending upon the choice of population growth scenario, California Department of Finance or SCAG, an additional 0.9--1.1 GW (8-11% increase from today) of substation capacity, DER, or peak load shifting, will be needed throughout Los Angeles county to keep substation load factors at or below one during the worst-case heat waves by 2060.
- The SCAG population growth projections can be satisfied within the in-basin area of the county without significantly increasing peak demand by pursuing the development of high-efficiency, high density housing. However, the portion of SCE service territory in California Building Climate Zone 9, spanning from West Valley to Pomona, would require 700 MW additional capacity, DER, or load shifting to avoid overloading local substation capacities.
- Multi-family (shared wall) housing units were estimated to reduce peak demand by up to 50% per capita relative to single-family detached housing.
- While further improvements in air conditioner ratings beyond SEER 16 can be effective in reducing total energy consumption, a new "peak performance rating" at or above 45°C would be useful to adapt air conditioners' performance for extreme heat.
- Use of projected climate change impacts should continue to be used in the demand forecast and related analysis for California to ensure changing conditions are taken into account in energy planning.

TABLE OF CONTENTS

1: Introduction

This report quantifies potential increases in peak demand and risk of electric power outages in Los Angeles County to 2060 with consideration for future record-breaking heat waves. Additionally, several policy options to mitigate or adapt to those risks are discussed at the end of this report in terms of infrastructure planning and building and appliance standards. Climate change assessments have considered various emissions scenarios in the past, but were limited in their actionable effectiveness due to a lack of consensus on which future scenarios to plan for, uncertainty in the models, and a lack of transparency in the data as to what the scenarios meant in terms of stress on the infrastructure [1]. Prior studies have shown how rising temperatures in Los Angeles County, coupled with technological changes (e.g., building shell, appliance technologies, air conditioning use, etc.), can increase annual electricity demand, as well as the efficacy of energy saving strategies [2]. Most past studies considered climate change in terms of changes in mean temperatures, and subsequent effects on *T90* (a.k.a. 90th percentile, or 1-in-10 hottest day's historical summertime temperatures) [3], [4], [5], [6], [7]. While these metrics have been useful in planning and preparing for cooling degree days and total volumetric energy demand, they are insufficient in evaluating the vulnerabilities of the system that are a risk to public health, commerce, and security—namely service outages. In order to consider the potential for service outages, the most stressful operating conditions must be studied. In the context of extreme heat, those conditions are peak demand (evaluated in this study at an hourly timescale) and de-rated component capacities (i.e., heat-related reductions in Wattage of electricity generation, substations, or transmission). In short, electric power flow generates heat, and all of the system's components can only tolerate so much before protection gear trips or physically breaks [8]. Thus, as ambient air temperatures rise, components' ability to cool themselves can lower too, and their capacity to support power flow can decrease. Understanding the effects of high air temperatures in this context enables estimation of vulnerabilities to the County.

Electricity infrastructure vulnerabilities were evaluated in terms of absolute air temperatures, which were extracted from the multiple climate change scenarios projections used per the recommendations in the Little Hoover Commission report per [1]. In Chapter 2: Climate Modeling for Heat Events, specific 'extreme' temperatures were obtained from data developed for Los Angeles County, specifically at 2 km^2 resolution [9], [10]. These temperatures were projected using the low and high scenarios as standardized by the Intergovernmental Panel on Climate Change (IPCC). The most extreme projected air temperature was identified as 54 °C (129 °F) in certain desert locations. Because Los Angeles County is such a large and climatically diverse region, two temperature measures were developed and used for the vulnerability assessment. The first, 'composite' measures were calculated as the daily maximum air temperatures experienced in each grid cell for the entire scenario analysis period (historical 1981-2000, early-century 2021-2040, and mid-century 2041-2060). This metric captures the hottest temperatures for each gird cell at any time and was used to analyze all of the potential neighborhood-level infrastructure capacity issues. The second metric, the 'hottest day' temperatures, were calculated as the temperature at each cell on the projected day with the highest average temperature throughout the County. That metric represents the hottest conditions for the County at large and was used to consider total resource adequacy requirements. The range of uncertainty between climate change scenarios was found to be relatively small, 2°C (3.6°F) by 2060, when compared to the range of annual maximum

temperatures observed in historical conditions, 8°C (14.4°F) from 1981-2000. In accordance with ISO31000:2009 risk management principles [11], this study, and the concepts developed within, also serve as a draft to update long-term weather-adjustment planning processes. Instead of using coarse maps of 'slightly fuzzy' (i.e. ±1 °C) historical *T90* values for different cities, the forecasts developed in this study used high-resolution maps of 'slightly fuzzy' projected *maximum* air temperature values.

In addition to the stress of rising air temperatures, Los Angeles County has other forces driving increases in peak demand and stressing the electric infrastructure system. Approximately 41% of residential buildings in the County currently have air conditioning [2], [12], which results in increases in peak demand of roughly 300-400 MW or 2-5% per 1 °C (1.8°F) from 25-40 °C (77-104 °F), after which it gradually decreases at higher temperatures due to AC duty cycling saturation [13]. Because new development favors installation of central AC, those rates are expected to increase in the future, especially in neighborhoods that have very little AC installed [12], [14]. Moreover, the county is one of the largest and fastest growing metropolitan regions in the USA [15]; population is expected to increase by 1.2—3.2 million people (12—32%) by 2060 (Figure 1) with commensurate increases in residential and commercial buildings and energy use [16], [17], [18], and much of the infrastructure is already operating at or near capacity [13], [19]. The U.S. Geological Survey has projected growth primarily on the fringe and in the northern (and hotter) region of the County [16], whereas the Southern California Association of Governments (SCAG) has projected both growth in the northern region and growth via further densification of the already developed central basin area [17]. While new buildings will be constructed to meet Title 24 building energy standards—with significant improvements in building attics, walls, water heating, and lighting efficiency—percent reductions in peak demand from those standards are not nearly as significant as increased in annual energy consumption [20]. Moreover, while high-density multi-family housing is generally more efficient per capita, a net increase in population can still result in a net increase in annual energy consumption and peak demand. The projections developed in Chapter 3: Electricity Demand Forecast consider all of these factors at the Census Block Group (CBG) scale, enabling both a total resource adequacy assessment for the county and a neighborhood-level assessment of delivery system component vulnerability to overloading.

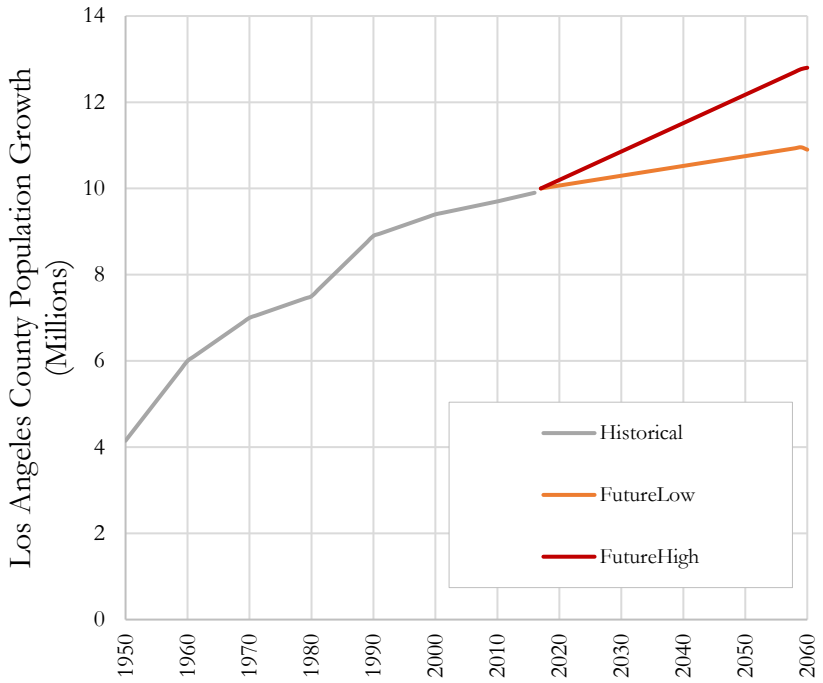

Figure 1. Historical and Estimated Future Los Angeles County Population Growth.

Los Angeles County's vulnerability to extreme heat, in the context of the electric power sector, is the potential for component outages and service interruptions. Reliable electricity ensures that energy will be available as needed for activities that allow for basic provisioning, protect people directly against environmental hazards such as extreme heat or cold weather, and drive economic activity (i.e., cooking, lighting, heating, ventilation, air conditioning, computing, entertainment, etc.). The combination of reliable electricity and affordable AC technologies has resulted in cities growing and expanding into regions with temperatures that are otherwise very uncomfortable and often pose public health risks, including the very hot northern San Fernando and Antelope Valley areas [21], [22], [23]. While this study does not focus on the climate change issues of sea-level rise, drought, and wildfire, it is important to note that electricity infrastructure in LAC is vulnerable to those climate change factors as well [24], [25], [26], [27], [28], [29]. Heat waves specifically can result in service interruptions via a combination of high demand, and (i) insufficient cumulative generation resources [24], [26], or (ii) insufficient capacity in delivery components (substations and lines) for electric power to flow from generators to loads [30], [31], [32], or (iii) widespread cascading failures due to a combination of multiple instances of either of the former two [25], [33], [34]. Therefore, Los Angeles County's generation and delivery capacities were assessed by type and location in Chapter 4: Infrastructure Vulnerability Analysis using the results from the climate modeling and peak demand forecasts, as well as generator, transmission line, and substation data published by the US Energy Information Agency, Department of Homeland Security, and the major investor owned utility, Southern California Edison.

Because electric power infrastructure is a critical system [35], long-term investments are in many ways a matter of public policy. Between the Zero Net Energy plan [36], building energy standards [20], renewable portfolio standards [37], climate action plans [38], and more as cited in [39] California, and Los Angeles specifically, have been leaders in developing policies that affect the electric power sector, reduce greenhouse gas emissions, and conserve limited natural resources. Moreover, according to Senate Bill X1-2 (Simitian, Chapter 1, Statutes of 2011), all retail sellers of electricity shall serve 33% of their load with renewable energy by 2020, and according to SB 350, 50% by 2030 [40]. California was at 30% renewable energy as of November 2017, with 57% originating from solar PV [41], and more is planned [42], [43]. Not all of that energy has the same value throughout the day however, as California now has so much Solar PV surplus during mid-day off-peak hours that it actually pays Arizona to take it [44], [45]. Because of these time-of-day usage and reliability issues, a mix of solar PV in conjunction with some form of fast-ramping storage, central generation (e.g., natural gas), and or power imports must be implemented to meet future California demand as regulated by California policies. Based on the analysis of different building types and appliance technologies' effects on peak demand, as well as potential size and location of component capacity overloading, various specific investment and policy options are discussed in Chapter 5: Conclusions – Mitigation and Adaptation as to how to maintain reliable electric power services in light of various trade-offs, competing priorities, and geographic constraints.

2: Climate Modeling for Heat Events

2.1 Summary

"Downscaled" global climate model data was used from previous work in [9],[10] to produce 2-km^2 resolution projections of historical and future daily maximum air temperature (T_{max}) in Los Angeles County from 1981 to 2060. This study did not consider changes in wind speed, air pressure, humidity, or solar radiation that may also change in the future. Two climate change scenarios were considered based on the Intergovernmental Panel on Climate Change (IPCC's) standardized Representative Concentration Pathway scenarios (RCPs) [46]. These scenarios describe potential time series of greenhouse gas emissions throughout the 21st century. As greenhouse gas concentrations in the atmosphere increase, more outgoing radiation is absorbed and re-emitted downwards towards the Earth. This increases the amount of radiation that is absorbed by the surface of the earth and has a total net average warming effect. The IPCC has defined four standardized RCPs for global climate change models: 2.6, 4.5, 6, and 8.5. California's Fourth Climate Change Assessment guidance for adaptation planning purposes was to use RCP 4.5 as the best-case "mitigation" scenario and RCP 8.5 as the "worst-case" scenario (often referred to as "business-as-usual") with increased emissions rate. Each scenario corresponds to an increase in the amount of radiative forcing in terms of Watts per square meter by the year 2100. By comparison, during high noon in summer, solar radiative energy reaching the surface of the earth in LAC is approximately 1,000 W/m^2. Simulation results showed average warming of 0.7 to 2.3 °C (1.3 to 4.1 °F), with less warming near the coast and more inland.

2.2 Approach

2.2.1 Global Climate Model Downscaling

Global climate models (GCMs) are powerful tools for simulating the global climate system and projecting future climate under various scenarios of atmospheric forcing due to anthropogenic greenhouse gas emissions. However, they are too low in spatial resolution to answer certain questions about climate change at the scales on which resource managers and other stakeholders make decisions. This is particularly true in topographically complex areas such as the LAC region, where coastlines and mountain ranges create microclimates. To perform calculations, climate models discretize geographic areas into a grid and output data for each grid cell. A typical GCM grid resolution is 100 km by 100 km, far too coarse to capture the variations in climate across LAC. To account for these variations, global climate model information was "downscaled" in [9] and [10] to a much higher spatial resolution over a domain covering LAC and other parts of the greater Los Angeles region as shown in Figure 2. The grid cells in these simulations are 2 km^2, a spatial scale that is sufficient to resolve important local topographical features governing climate in the region.

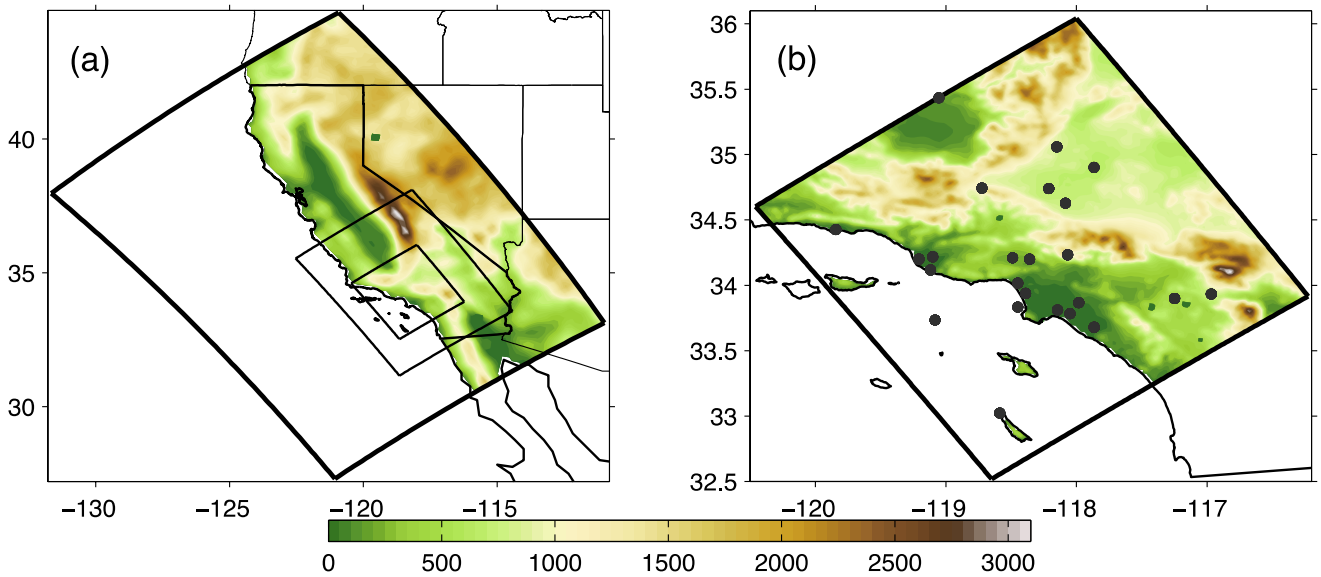

Figure 2. (a) Model setup with three nested Weather Research and Forecasting (WRF) domains (D1, D2, and D3) at resolutions of 18, 6, and 2 km (area sizes 1188 × 1566, 486 × 612, and 276 × 288 km2), respectively. Topography (m) is shown in color. (b) The innermost domain (D3) of the regional simulation, with 2-km resolution. Black dots indicate the locations of 24 stations used for surface air temperature validation.

This resolution was achieved with a novel methodology called "hybrid downscaling." There are two basic categories of downscaling techniques, each with strengths and limitations:

- *Dynamical* downscaling involves using a regional climate model, similar to a GCM but designed to be run over smaller domains at higher spatial resolution. A strength is physical realism, but a limitation is high computational cost.

- *Statistical* downscaling involves using empirical mathematical relationships to go from large-scale predictors to fine-scale predictands. A strength is that statistical downscaling is computationally cheap, but a significant limitation is that it is not inherently physically realistic.

About three dozen GCMs have been developed at modeling centers around the world, and differences in construction from model to model lead to differences in outcomes. When using GCMs to create high-resolution projections of regional climate change, it is desirable to downscale multiple GCMs in order to account for these differences. This task is not computationally tractable if one uses dynamical downscaling alone. On the other hand, if one uses existing statistical techniques alone, the projections produced may not be physically realistic.

The hybrid downscaling technique previously developed overcomes these issues by combining dynamical and statistical downscaling in a way that capitalizes on their strengths and minimizes their limitations. A complete technical description of the methodology is available in [9], and a summary is as follows:

1) The Weather Research and Forecasting [47] (WRF) regional climate model was forced with a high-resolution reanalysis data set [48] to create a 2-km simulation of a 1981–2000 historical period. This simulation provides a "baseline" against which to compare future climate.

2) The accuracy of the 1981–2000 simulation was assessed by comparing it with observed historical data.

    a. Detailed statistical analyses of the model are provided in Section 2 "Dynamical Downscaling" of Walton et. al. 2015 [9]. In short, the WRF model was most accurate, with $R^2 \geq 0.93$, during summer and winter months, wherein modeled values were on average 1°C cooler than observed values in the summer. Therefore, modeled summertime temperature values used in this report should be considered highly accurate, but probably slightly conservative.

3) A subset of five GCMs from the Coupled Model Intercomparison Project, Phase 5, [49] (CMIP5) archive was chosen that samples the archive members' range of warming outcomes. These GCMs are listed in Table 1 below.

4) Warming signals from these GCMs were used to produce five dynamically downscaled future climate projections under RCP 4.5 and RCP 8.5. The initial work included simulations for the 2041-2060 and 2081-2100 periods. Model results for the 2021-2040 period were added for this assessment report.

5) The dynamically downscaled projections were used to develop a statistical model that mimics the WRF model.

6) This statistical model was used to create future monthly-mean temperature projections for the GCMs that had already been dynamically downscaled, and the dynamical and statistical model results were compared to assess the physical accuracy of the statistical model. Monthly means are produced to maximize computational efficiency, and the research team determined that monthly means are adequate to project future changes in heat extremes, as explained in further detail in [10].

7) The statistical model was applied to an additional 27 GCMs in the CMIP5 archive to produce future climate projections under business-as-usual greenhouse gas concentrations.

Table 1. Global climate models (GCMs) chosen for dynamical downscaling.

Model	Country	Institute
CCSM4	United States	National Center for Atmospheric Research
CNRM-CM5	France	Centre National de Recherches Météorologiques
GFDL-CM3	United States	NOAA/Geophysical Fluid Dynamics Laboratory
MIROC-ESM-CHEM	Japan	Atmosphere and Ocean Research Institute (University of Tokyo), National Institute for Environmental Studies, and JAMESTEC
MPI-ESM-LR	Germany	Max Planck Institute for Meteorology

2.2.2 Creation of Maximum Temperature Projection Images

From the 2-km-resolution temperature data, two sets of maximum temperature projection images and peak demand forecasts were created to analyze two distinct grid vulnerability issues. First, ***composite*** images of the highest projected T_{max} in each grid cell for each time period and RCP were created. Second, ***hottest day*** images were created of the T_{max} in each grid cell on the day that the highest average T_{max} occurs across the county for each period and RCP. The two issues that these images inform respectively are the highest peak demand in each spatial unit, and therefore the capacity requirements for local delivery system components, as well as the total resource adequacy requirements for the region as a whole during a possible "realistic" record-breaking heat wave.

The definition of what exactly constitutes the single hottest day across a large and geographically diverse region is something that can be subject to debate. In deference to this fact, different definitions of the term were evaluated using the methods in Chapter 3: Electricity Demand Forecast: the day with the highest single-cell T_{max}, the day with highest average T_{max} across all grid cells, and the day with the most number of grid cells over 35°C (95°F).

2.3 Results

2.3.1 Temperature and Extreme Heat Findings

Increases in both average temperatures and the number of extreme heat days, defined as days on which temperatures exceed 35° C (95° F) were analyzed. This threshold is commonly used in climate change impact studies and was chosen in part for its relatability to the public and stakeholders. Results are summarized below, and more detail is available in [10]. Ensemble-mean warming, i.e., the average of all of the hybrid-downscaled GCM results, is shown in Figure 3 for the different time slices and greenhouse gas pathways. Spatial variations in warming are due to 1) generally lower warming over the ocean given its relatively larger effective heat capacity and more efficient energy transfer through latent heat fluxes, which allows enhanced downward infrared radiation in the warmer climate to be balanced with a

smaller surface temperature increase over the ocean compared to land; and 2) the land–sea breeze circulation, which introduces a marine influence in the coastal zone, in this case bringing the milder warming of the ocean to the coastal zone. The annual-mean warming is highest in mountain areas mainly because they experience significant snow albedo (reflectiveness) feedback[1], which is strongest in the spring months.

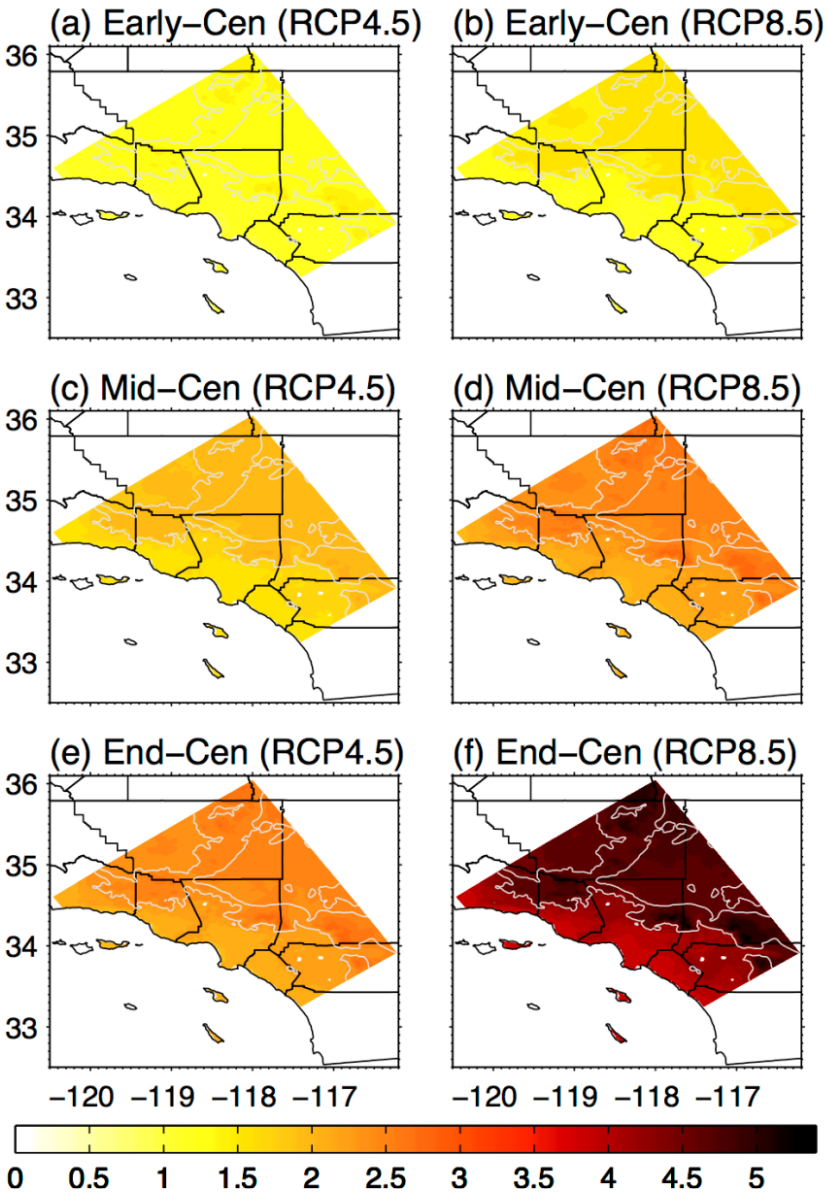

[1] Albedo is a measure of a surface's ability to reflect solar radiation. Snow is a high-albedo surface that is highly reflective of solar radiation. Snow albedo feedback is a phenomenon in which warming causes snow cover to retreat, exposing lower-albedo surfaces. These surfaces absorb more solar radiation than snow would have, causing greater local warming. This local warming exacerbates snow melt, which uncovers more radiation-absorbing surfaces, which causes more local warming, and so on.

Figure 3. Ensemble mean of downscaled annual-mean surface warming (°C) for early-, mid-, and end of century periods 2021–2040, 2041–2060, and 2081–2100.
White contours are plotted at 1000-m elevation and county lines are marked in black.

As shown in Figure 3c & 3d and Figure 4, the emissions scenario has only a relatively small influence on the warming at mid-century. The midcentury warming under RCP 4.5 is about 75% of the warming under RCP 8.5. By the end of century, however, the gap between the scenarios grows much larger. Under RCP 4.5, end-of-century warming increases modestly beyond mid-century warming, whereas under RCP 8.5, end-of-century warming approximately doubles compared with mid-century warming, shown in Figure 3e & 3f and Figure 4. This indicates that, although the impact of global measures to reduce greenhouse gas emissions would be modest in the near-term, the cumulative effect would be significant by the end of the century.

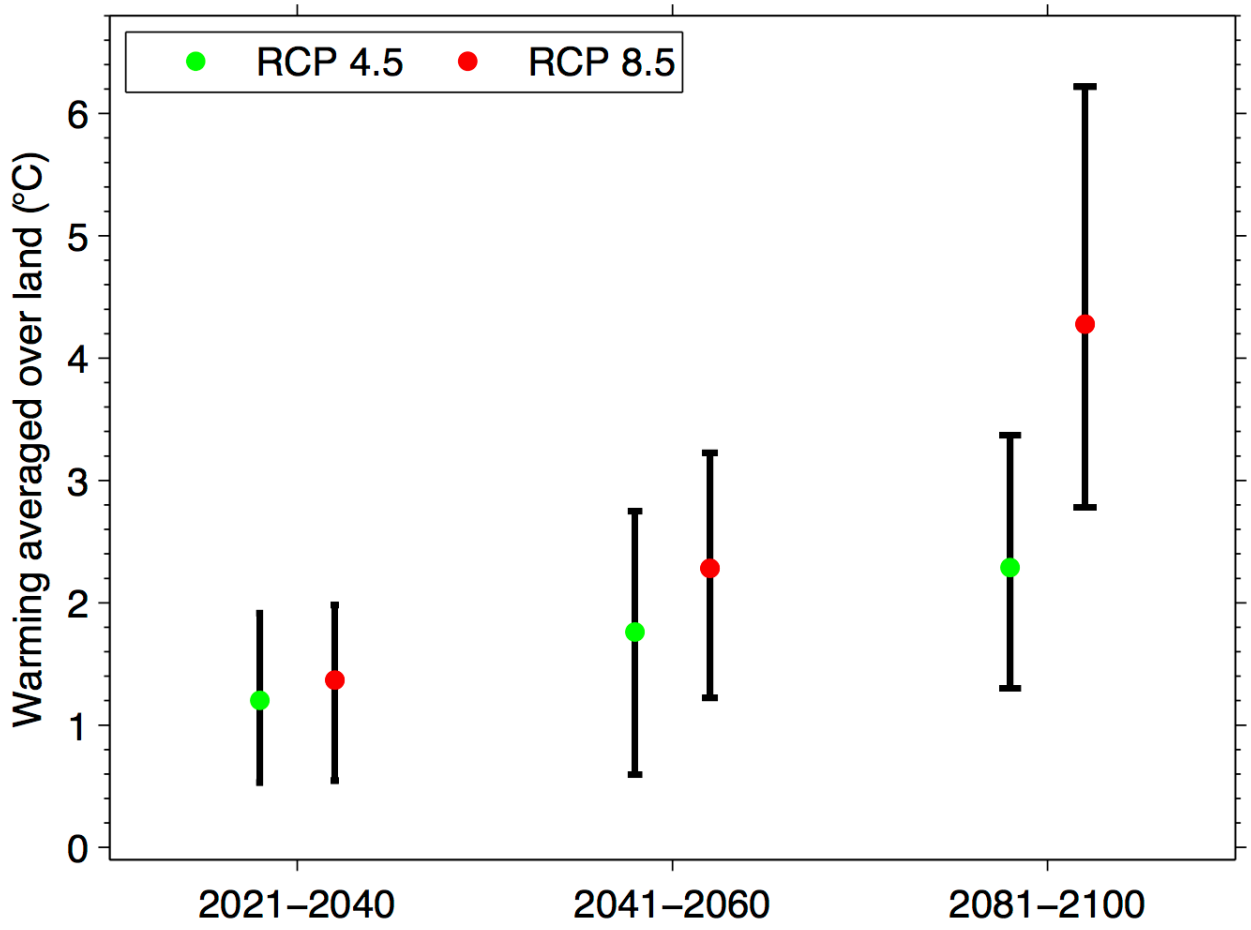

Figure 4. Land-averaged annual-mean surface warming (°C) downscaled from each GCM for early century (2021–2040), midcentury (2041–2060), and end-century (2081–2100) under "mitigation" (RCP4.5, green dots) and "worst-case" (RCP8.5, red dots) scenarios. Dots represent the ensemble mean across all GCMs for each scenario/time slice. The vertical bars represent the full range of GCM results.

In the baseline period, most of the coastal and mountain areas have fewer than 10 extremely hot days per year. As shown in Figure 5, in contrast, inland regions such as the Mojave Desert,

Coachella Valley, and Central Valley all contain areas exceeding 100 extremely hot days per year. While frequent extreme temperatures are mostly limited to inland regions, parts of the coastal zone have more than 60 extremely hot days per year. These regions are valleys that are somewhat removed from the moderating effects of the sea breeze, despite lying on the coastal side of the major mountain complexes. Strong gradients in the number of extremely hot days—such as those within the coastal zone—are an important reason to perform dynamical downscaling to such high resolution. With lower resolution, it could be difficult to distinguish important differences in extreme temperature changes between these locations.

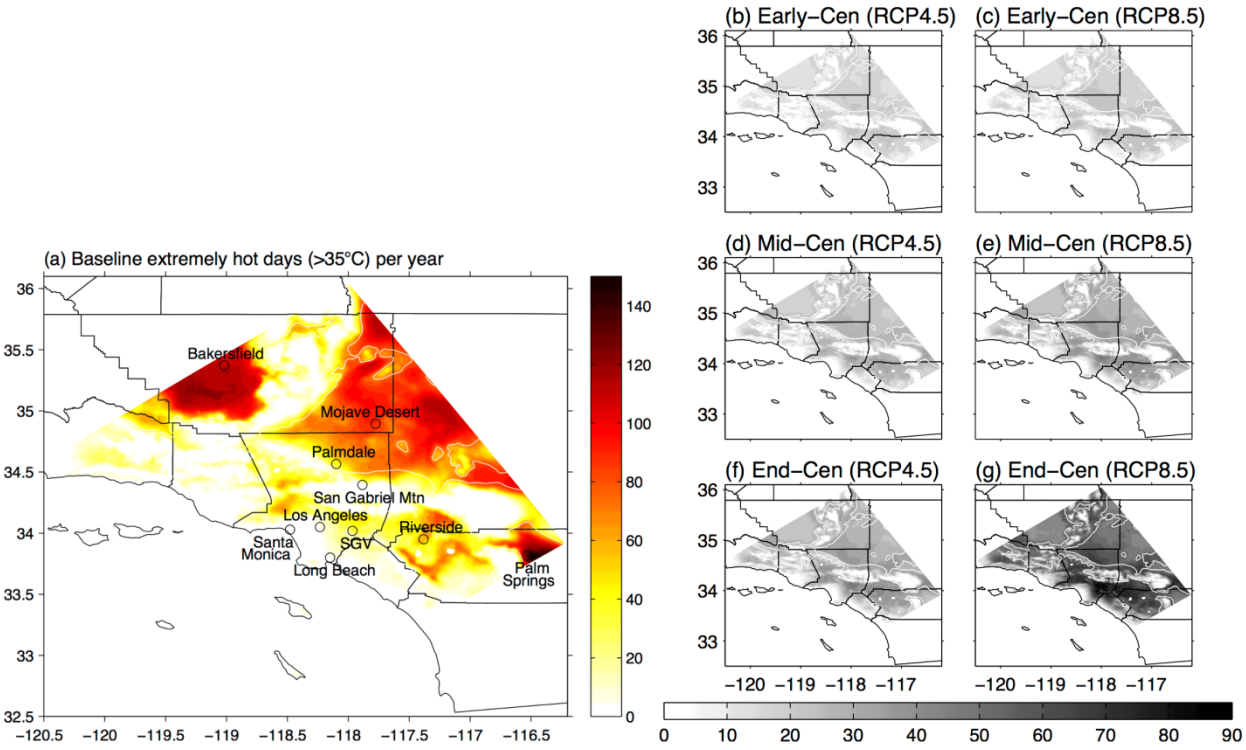

Figure 5. (a) The number of extremely hot days per year (Tmax > 35°C, or (95 °F) for the baseline; and the change in the number of extremely hot days per year for (b) the early century (2021–2040) RCP4.5, (c) early-century RCP8.5, (d) midcentury (2041–2060) RCP 4.5 (e) midcentury RCP 8.5, (f) end of century (2081-2100) RCP 4.5, and (g) end of century RCP 8.5. The 1000-m elevation contour is shown in white and county lines are shown in black. SGV denotes the San Gabriel Valley.

The distributions of future daily maximum temperatures were found to be approximately equal to the baseline distributions shifted by the change in average temperature. These results are not shown, but were applied to create future distributions of daily maximum temperatures by shifting the baseline distributions by the temperature changes provided by the statistical model.

For mid-century under both RCPs, the spatial pattern is similar to RCP8.5 at end-of-century, but the increases are smaller. Many land areas may experience increases of roughly 20–40 additional extremely hot days per year. Downtown Los Angeles is projected to experience a dozen or so more extremely hot days, roughly a tripling from baseline conditions, while Riverside may experience approximately a 50% increase. Little to no change in extremely hot days is projected in the region's highest elevations and near the coast.

By the end of the century, the number of extremely hot days increases most under RCP8.5. With the exception of the highest elevations and a narrow swath very near the coast, where the increases are confined to a few days, most land locations are projected to experience an additional 60–90 extremely hot days per year by the end of the century, as listed in Table 2. Thus, most land areas may effectively experience a new season of extreme heat. Downtown Los Angeles is projected to experience an increase from 6 to 54 extremely hot days, while at Riverside the number of days roughly doubles from 58 to 128.

Table 2. Average number of extremely hot days (daily Tmax > 35 °C, or 95 °F) per year for selected sites in the Los Angeles region.

Location	Baseline	2021-40 RCP4.5	2021-40 RCP8.5	2041-60 RCP4.5	2041-60 RCP8.5	2081-2100 RCP4.5	2081-2100 RCP8.5
Bakersfield	111	124	126	129	134	134	154
Long Beach	4	9	10	12	16	16	37
Los Angeles	6	13	14	17	22	22	54
Mojave Desert	90	106	108	113	119	119	141
Palm Springs	135	146	148	152	158	158	179
Palmdale	36	54	57	63	71	71	105
Riverside	58	79	82	89	98	99	128
San Gabriel Valley	32	53	57	64	74	76	117
San Gabriel Mountains	0	0	0	1	1	1	9
Santa Monica	0	1	1	1	1	1	3

Although areas with more extremely hot days during the baseline period generally also are projected to experience larger increases in temperatures, the largest increase actually occurs in the San Gabriel Valley, a part of the coastal zone. This phenomenon can be understood by examining the baseline and future temperature distributions shown in Figure 6. Within the San Gabriel Valley, where the largest increase in extremely hot days occurs, the peak in the baseline maximum temperature distribution occurs at about 32.5 °C (90.5 °F). Thus, a warming of 4°C (7.2 °F) pushes the peak of the distribution well past the 35 °C (95 °F) threshold, resulting in nearly a quadrupling of the number of extremely hot days per year, from 32 in the baseline to 117 at the end of the century. In contrast, in the Mojave Desert, which is located farther inland, the increase is smaller (from 90 to 141), even though the baseline number of extremely hot days is larger. Despite the fact that the warming is about 0.7°C (1.3 °F; 17%) larger here than in the coastal zone, the increase in extremely hot days is smaller because the baseline distribution is broader and its peak already lies above the 35°C (95 °F) threshold. In much cooler coastal locations, such as Santa Monica, few baseline days are close to the threshold; therefore, a warming of 4°C (7.2 °F) only results in an increase from 0 to 3 extremely hot days per year. Another way to conceptualize extreme heat changes is to compare a city's future extreme heat days to another city's baseline heat days. For example, under RCP 8.5, at the end of the century, cities in the San Gabriel Valley become analogous to present-day Bakersfield, and Long Beach becomes analogous to present-day Palmdale.

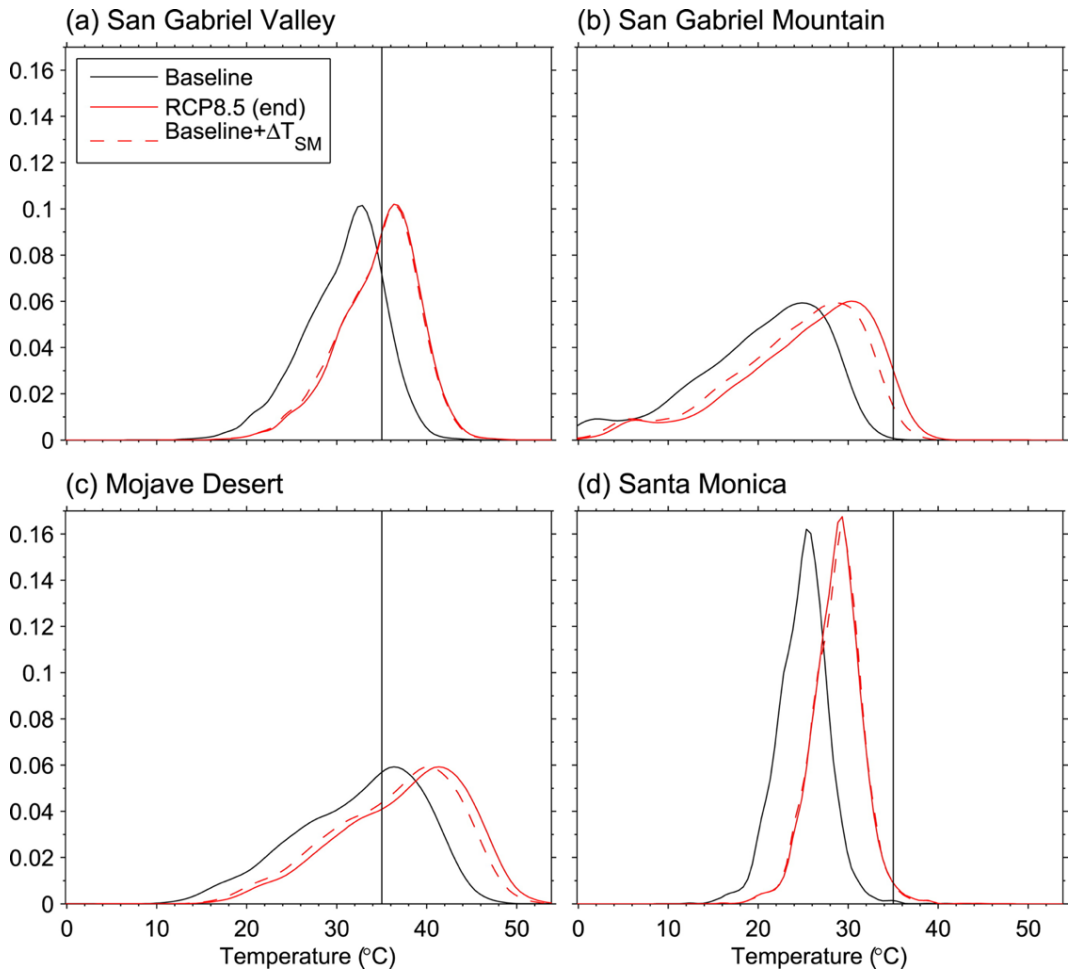

Figure 6. Probability Distribution Functions (PDFs) of daily maximum temperature at selected sites during warm months (June–October) for baseline period (solid black), end-of-century under RCP8.5 (solid red), and baseline shifted by warming (dashed red). Vertical line indicates the 35 °C (95 °F) threshold.

2.3.2 Maximum Temperature Projection Images

The results of the three hottest day definitions were compared, and the day with highest average T_{max} across all grid cells was decidedly the hottest. Foreshadowing the results in Chapter 3: Electricity Demand Forecast, the results for the residential and commercial sectors for the base period using the different definitions of hottest days were: 5.6 and 7.2 GWh for the day with highest average T_{max} across all grid cells, 4.09 and 6.23 GWh for the highest single-cell T_{max}, and 4.8 and 6.82 GWh for the day with the most number of grid cells over 35°C (95°F). Spatial comparison of the results for "hottest days" are shown in Figure 7, where it is noticeable that on the day with the highest average temperature, the region experienced multiple concurrent heat waves of lower magnitude, whereas in the days with alternate definitions, the northern region of the county experienced more severe heat waves. A summary of all of the climate scenario statistics are listed in Table 3. The range of hottest days for lowest, median, and highest years are shown in Figure 8, where the range of average T_{max} between the lowest and highest years' hottest days was 8°C (15°F).

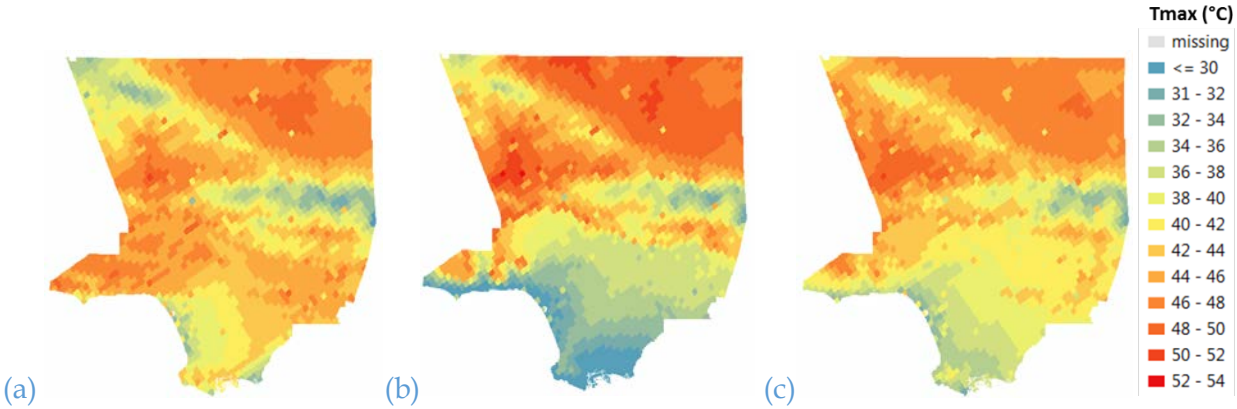

Figure 7. Baseline period hottest days comparison for (a) highest average T_{max} (b) highest grid cell T_{max} (c) most cells over 95 °F.

Table 3. Summary of climate scenario projection statistics.

Time period	RCP	Projection	Average grid cell Tmax °C (°F)	Max grid cell Tmax °C (°F)	Date (MM/DD/YYYY)
Historic (1981-2000)	n/a	Composite	45.9 (114.6)	52.2 (126.0)	n/a
		Hottest day (lowest year)	35.2 (95.4)	41.4 (106.5)	08/17/1981
		Hottest day (median year)	40.5 (104.9)	48.4 (119.1)	07/01/1997
		Hottest day (hottest year)	43.3 (109.9)	50.4 (122.7)	06/03/1985
		Alt. hottest day (max cell)	41.7 (107.1)	52.2 (126.0)	07/06/1989
		Alt. hottest day (>95°F)	42.7 (108.9)	50.7 (123.3)	08/05/1997
Early-century (2021-2040)	RCP 4.5	Composite	47.2 (117.0)	53.4 (128.1)	n/a
		Hottest day	44.6 (112.3)	51.6 (124.9)	-
	RCP 8.5	Composite	47.7 (117.9)	53.9 (129.0)	n/a
		Hottest day	44.7 (112.5)	51.7 (125.0)	-
Mid-century (2041-2060)	RCP 4.5	Composite	47.3 (117.1)	53.5 (128.3)	n/a
		Hottest day	45.1 (113.2)	52.1 (125.8)	-
	RCP 8.5	Composite	48.2 (118.8)	54.3 (129.7)	n/a
		Hottest day	45.5 (113.9)	52.5 (126.5)	-

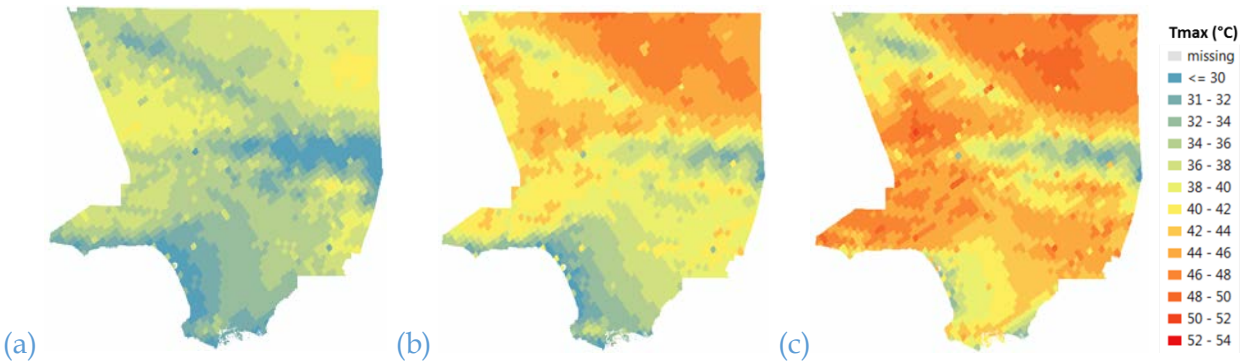

Figure 8. Baseline period hottest days for (a) lowest, (b) median, and (c) highest years.

The maximum temperature projection images are shown in Figure 9 for historical and future periods for composite and hottest days. Spatial patterns are similar to those in the projections of extremely hot days with cooler parts near the coast and mountains, and hotter parts in the valleys and deserts. T_{max} ranged in the historical period throughout the region from approximately 30-54 °C (86-129 °F) and was projected to increase up to 3.2 °C further by 2060 under RCP 8.5. In viewing the composite and hottest days images side by side, the reader can see how higher magnitude heat waves are capable of impacting different areas of the county, but not necessarily all simultaneously on the same day. Several grid cells in the Manhattan Beach coastal area had temperatures ~8°C higher than surrounding grid cells in the composite images. The anomaly was likely due to a pixilation issue with gradient classification between water and non-water land cover types at the shoreline in the underlying Weather Research and Forecasting (WRF) model used in [10]. Those few higher temperature value pixels were replaced with adjacent values based on [50].

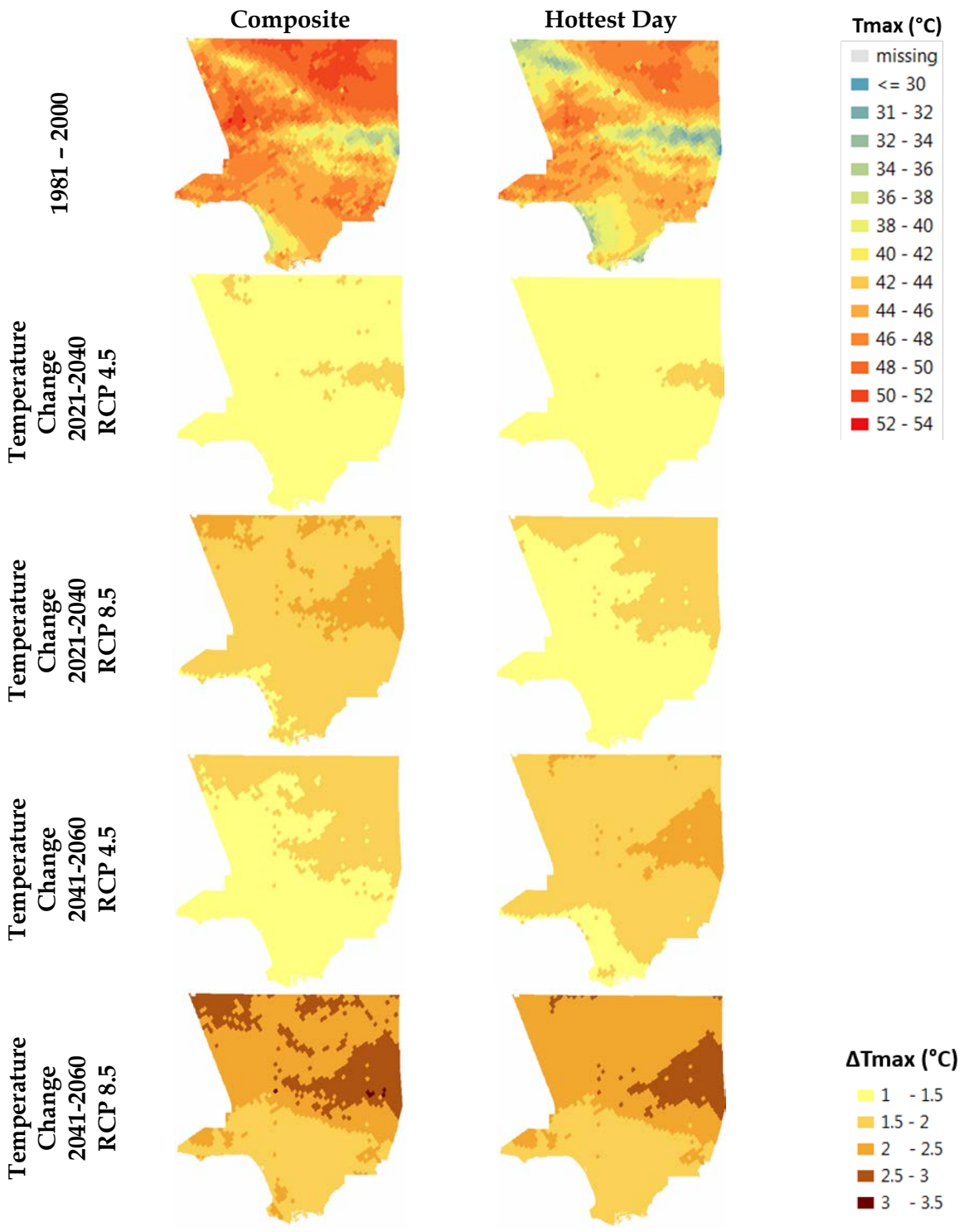

Figure 9. Historical and future maximum temperature projection images. Top images are the baseline period, the bottom images are future changes from the baseline period. The actual values of temperature increases range from 0.9 to 3.2 °C. Composite images are of the highest projected Tmax in each grid cell for each time period and RCP. Hottest day images are of the Tmax in each grid cell on the day that the highest average Tmax occurs across the county for each period and RCP.

3: Electricity Demand Forecast

3.1 Summary

Los Angeles County (LAC) is a large urbanized region which had about 9.7 million residents as of 2010[2], and will require new and retrofitted electricity infrastructure over the next several decades. Population forecasts predict LAC will become home to an additional 1.2 – 3.1 million residents by 2060, and climate projections predict air temperatures will increase by 1-4°C in the region between RCPs 4.5 and 8.5 (Chapter 2: Climate Modeling for Heat Events). Both of these factors are expected to result in higher summertime peak demand due to more buildings, with a higher percentage of installed air conditioners, and increased loading on those air conditioners. In order to understand potential electricity infrastructure reliability issues due to excessive peak demand, a long-term forecast was conducted at census block group resolution, taking into consideration those factors. Residential and commercial building energy models calibrated for LAC specifically were used to forecast how changes in population, building vintage, building density, AC efficiency, AC penetration, and daily high air temperatures are likely to affect peak demand by 2040 and 2060.

LAC's residential and commercial sectors were estimated to consume approximately 9.5-12.8 GWh of electricity during the base-period peak demand hour, and forecasted to increase to 12.3-16.7 GWh (~30%) by 2040 and 13.1-19.2 GWh (~45%) by 2060. While increases in ambient air temperature only accounted for 3.9-8.3% of future increases in peak demand for climate change scenarios RCP 4.5 and RCP 8.5, the range of hottest day temperatures over 20-year periods resulted in a difference of peak demand of 40% to 66% from year to year as temperatures fluctuated between 30-45°C. Population growth of at least 1 million persons is anticipated to occur mostly in the peripheral cities of Palmdale, Lancaster, and Santa Clarita, bringing an additional 0.4-1 GWh of peak demand in those areas. If building and AC efficiency standards continue to improve and replace older units, then peak demand will decrease in Climate Zone (CZ) 6 and 8 along the coast and in-basin areas. These measures should support the level of population increases predicted by SCAG's highest growth forecasts without corresponding increases in peak demand if they are able to be combined with the development of high-efficiency multi-family dwelling units within those areas.

3.2 Approach

In order to estimate potential increases in electricity demand, peak demand was modeled for recent historical climate and infrastructure conditions and then projected into the future for a number of different scenarios. Specifically, peak demand was modeled within LAC for residential dwelling units (DUs) and commercial buildings in terms of kWh for the peak hour at a spatial resolution of census block groups (CBGs). Residential sector buildings have relatively low electricity use variance in terms of building properties as opposed to commercial sector buildings, and lastly the industrial sector, which has higher variance. The industrial sector is inclusive of more than buildings, and includes factors such as streetlights and mass transit. The

[2] LAC had a population of 10.2 million as of 2017 [51], but 2010 population values were used for the base period throughout the as they were available spatially congruent with all of the calibrated infrastructure models and base-period building stock.

industrial sector was not modeled as the factors that influence that sector's demand do not scale directly with population and climate. A sample of the image transformation from grid cell to CBG resolution (for data processing purposes) is shown in APPENDIX A: Energy Simulation Weather Files, where minor differences were incurred with up to a 1°C (1.8°F) effect on summary statistics. Technically, the peak demand forecast was conducted in three phases: weather file creation (based on the climate modeling in the previous chapter), characterization of individual building energy model performance, and spatial allocation of those individual buildings' energy consumption throughout LAC.

Because building energy simulations were conducted using EIA's Energy Plus and BEOpt software, special "EPW" weather files had to be created to conduct the analysis, which adds an additional layer of uncertainty to the analysis. This was done, however, in order to complete the analysis in a practical amount of time with the computational power available to the research team. EPW files require 8,760 inputs, one set of 12 parameters for each hour of the year, including: time, dry bulb temperature, dew point temperature, relative humidity, atmospheric pressure, horizontal infrared radiation from sky, direct normal radiation, diffuse horizontal radiation, wind direction, wind speed, visibility, and a variable for present weather observation. EIA sample historical weather data from a hot day in Los Angeles was modified to simulate a range of hourly dry bulb temperatures such that daily T_{max} ranged from 20°C to 60°C in order to characterize building peak electricity consumption respectively. The complete list of EPW input variables and hourly parameter values used are listed in APPENDIX A: Energy Simulation Weather Files. The dry bulb temperature was increased by 1°C for each hour each day up to T_{max} = 60°C, then decreased back to T_{max} = 20°C, and so on as shown in the appendix. This artificial raising and lowering of the input weather data was repeated four times throughout the 8,760 EPW file such that multiple simulations output data were created for each T_{max}, and error due to day of week or holiday usage patterns coded into the building models would be minimized.

Peak demand values were estimated based on model simulation runs in the software as the average of the hourly consumption from noon-6pm per residential peak pricing times in the area [52], [53]. Base period results were verified as within a reasonable range as described within the Uncertainty and Validation section. The core building models consisted of 15 commercial buildings types from [54] and 4 residential building types from [2]: single family detached (SFD), single family attached (SFA), multifamily small (MFS), and multifamily large (MFL), calibrated for Los Angeles County specifically, with several variations for different vintages, climate zones, and AC efficiencies. Individual buildings' peak demands were characterized as a function of T_{max} and then allocated by respective building counts to each CBG based on the scenario factors. The analysis is significantly more detailed for residential buildings than commercial buildings as existing residential building models were much better calibrated for electricity consumption in LAC than commercial building models. Further explanation and detailed performance characterization for residential and commercial buildings are included in Appendix B. The climate and urban infrastructure scenarios are summarized in

Table 4 and Table 5, and described in detail in the following sub-sections. A sensitivity analysis was conducted to understand how significantly each factor contributed to peak demand, and what opportunities exist for developments in residential buildings or improved AC efficiencies to mitigate potential hazards due to excessively high peak demand during potential future record-breaking heat waves.

Table 4. Summary of climate scenarios.

Time period	RCP
Historic (1981-2000)	n/a
Early-century (2021-2040)	RCP 4.5
	RCP 8.5
Mid-century (2041-2060)	RCP 4.5
	RCP 8.5

Time period	RCP
Historic (1981-2000)	n/a
Early-century (2021-2040)	RCP 4.5
	RCP 8.5
Mid-century (2041-2060)	RCP 4.5
	RCP 8.5

Table 5. Summary of urban infrastructure scenarios.

Case	Model parameter(s) affected	Low	Medium	High
Growth	Population growth* • # of new dwelling units per period (3 people per DU) • # of additional commercial buildings	1.2 million CA Department of Finance / USGS projections	Average	3.1 million SCAG projection
	Building turnover rate [18] (replacement with new buildings)	0.03% per year	0.3% per year	3% per year
	AC penetration	Central AC in all new buildings from turnover and population growth		
Energy Efficiency	Housing Density** Percent allocation of new dwelling units by residential building type. Total ratio of (MF/SF) for new DUs	SFD - 47 SFA - 08 MFS - 24 MFL - 21 (45/55)	SFD - 28 SFA - 05 MFS - 36 MFL - 31 (67/33)	SFD - 09 SFA - 01 MFS - 45 MFL - 45 (90/10)
	Residential ACs (all DUs, new and pre-existing)	SEER 16	SEER 19	SEER 21

*Acronyms: United States Geological Survey (USGS), Southern California Association of Governments (SCAG). single-family detached (SFD), single-family attached (SFA), multi-family small (MFS), multi-family large (MFL).
**Low housing density values are current distribution [2], medium values use SCAG projected 67% MF and 33% SF [55] with current ratio within sub-categories, high density assumes 90% multifamily & 10% single family.

3.2.1 Urban Infrastructure Scenarios

The key urban infrastructure characteristics that change over time and affect peak demand are the numbers of buildings and their operative energy consumption efficiencies. Changes for energy efficiency factors included residential building types (density) and AC efficiency, which were forecasted for residential and commercial sectors for 2040 and 2060 with low, medium, and high ranges. Other changes, including growth factors for population, residential building stock turnover, and AC penetration, were also estimated. These factors were chosen because they are known to significantly affect peak demand and can be influenced by policy. Factors that may affect industrial loads as well as potential new demand-side technologies, such as solar photovoltaics, micro-grids, energy storage, and electric vehicles, were not considered.

Such factors may significantly affect future electricity demand and loads and are the subject of other complementary research efforts. Demand and load should be kept distinct in energy modeling and forecasting, as demand is what is actually consumed, whereas load is what is visible to the grid from the perspective of the meter. Some distributed energy resources may have no effect on demand, but may significantly affect loads in the future, and could pose unforeseen problems for service reliability if demand and load were not accounted for explicitly.

Urban infrastructure scenarios were defined relative to base-case models for residential and commercial building stock in each CBG. The base residential building stock included 2.3 million buildings or 3.2 DUs classified by the 51 archetypes in [2], indexed by 2010 CBGs and California's previous Climate Zones, and based on the 2014 LAC assessor database. The base commercial building stock included 55,865 buildings classified by the 45 NREL codes from the UCLA Energy Atlas [56] indexed by 2014 CBGs. All new buildings were modeled as having the highest efficiency performance levels associated with their corresponding building types in compliance with California's state mandated Title 24 building standards.

3.2.2 Population Growth

Population growth can be influenced by land use zoning [57], and two forecasts from two different government agencies were found to exist. The low-growth case used the California Department of Finance's county-level population projections (and spatially allocated by the USGS) from [16] as described in [58] with total population values for LAC of 9.7 million in 2010, 10.3 million in 2040, and 10.9 million in 2060. The Department of Finance made three population projections (low, central, and high), but they were all the same through 2060 and did not diverge until 2061. The high-growth case used the Southern California Association of Governments (SCAG) population projections from [17] as described in [55] and [59], with total projected population values of 11.4 million in 2040 and 12.8 million in 2060. The medium case used the average of the two projections in each CBG. The major differences between the low and high cases are that the high case has 10% and 17% more total population in 2040 and 2060, and much more growth in already developed urban areas than new areas. The projected population increases are shown in Figure 10. In all cases, new residential buildings were added in each CBG proportional to population increases from the historic building stock in [2] at a rate of 3 persons per DU per current rates from SCAG [55] and the US Census [60]. Commercial buildings were assumed to increase proportionally by count in each CBG in the same proportion as they exist currently. While SCAG projected slight decreases in population per dwelling unit with aging population (2.9 persons per DU), that factor was not considered. The technical details of data processing of these forecasts from the sources are in Appendix C.

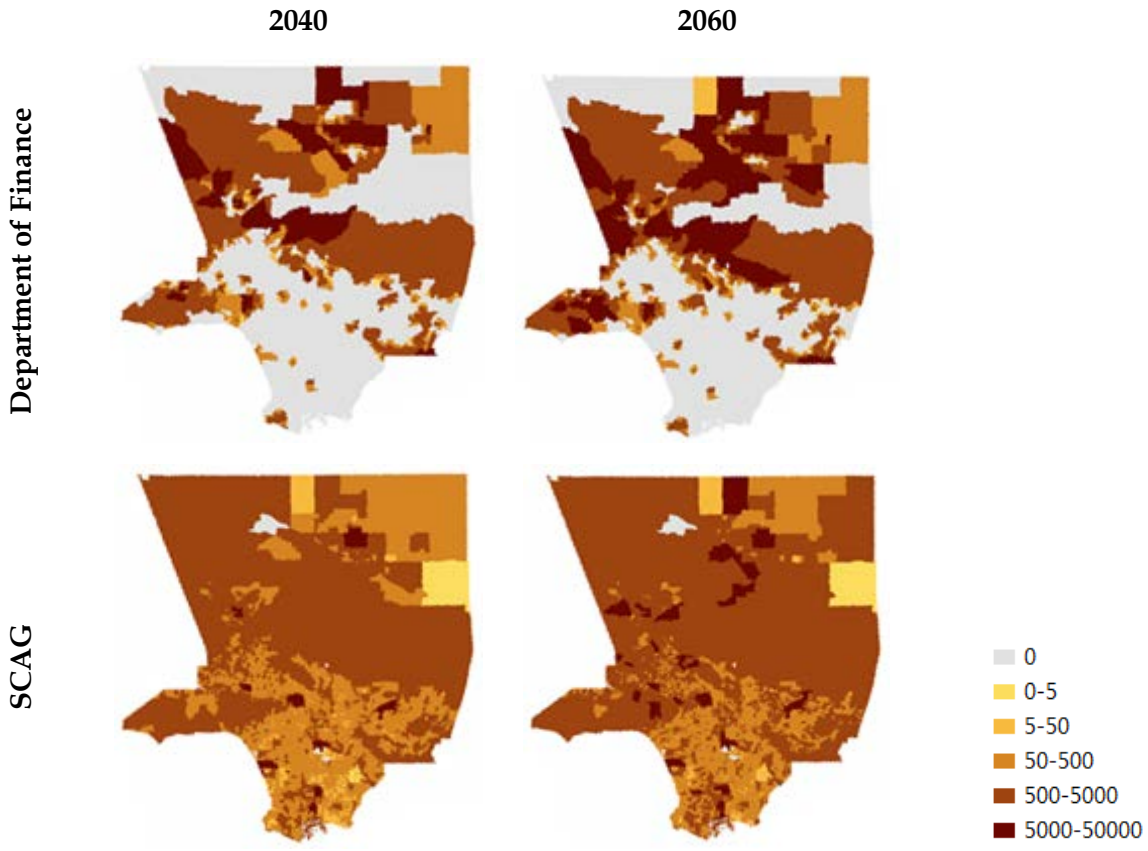

Figure 10. Population projections from 2010 to 2040 and 2060 from CA Department of Finance/USGS and SCAG by census block group.

3.2.3 Residential Building Stock Turnover

Replacement of older vintage buildings with new buildings is important to consider as new buildings must be constructed according to the most recent iteration of Title 24 building standards, as were coded in the models developed in [2] based on the 2008 Residential Appliance Saturation Survey (RASS). Distribution level solar PV energy production may reduce apparent load as viewed from the grid-side of the meter; it would not affect demand, as is the focus of this study. Technically, solar panels on building rooftops would reduce incoming solar radiation and therefore some demand for AC, but the significance would be proportional to the coverage, and modeling this variable is beyond the scope of this study. Turnover was considered for residential buildings only. The commercial building models available were not sufficient to consider building turnover in that sector due to a lack of calibration for electricity consumption by vintage as explained in Appendix B. Previous work classified the current residential building stock in LAC (2.3 million buildings, and 3.8 million DUs) by CBG in terms of the 51 building archetypes as listed in Table 6. Older buildings were replaced by newer construction of the same type unless otherwise specified per the housing density scenario. Low, medium, and high turnover rates of 0.03%, 0.3%, and 3% DUs per year per CBG were used based on the range identified for LAC in [18]. It was assumed that all older vintage buildings without central AC would be replaced by newer construction possessing central AC. Thus, a higher turnover rate will result in a larger peak demand, as AC accounts for 60-70% of electricity consumption while in use [61]. While newer buildings are generally more energy

efficient per square foot, newer buildings also tend to be constructed with larger footprints, so the net correlation between building vintage alone and energy consumption is not consistent in the models [2].

Table 6. Residential building archetype divisions and names. Note: CZ = climate zone.

Multifamily Small (MFS), apartment or condo (2-4 units)						Multifamily Large (MFL), apartment or condo (5+units)				
	CZ 6	CZ 8	CZ 9	CZ 14	CZ 16	CZ 6	CZ 8	CZ 9	CZ 14	CZ 16
<1940	6MFSD-5	8MFSD-4	9MFSD-5	14MFSD-5	16MFSD-4	6MFLD-5	8MFLD-5	9MFLD-5	14MFLD-5	16MFLD-4
1940-1949	6MFSD-5	8MFSD-5	9MFSD-5	14MFSD-5	16MFSD-4	6MFLD-5	8MFLD-5	9MFLD-5	14MFLD-5	16MFLD-4
1950-1959	6MFSD-5	8MFSD-5	9MFSD-5	14MFSD-5	16MFSD-4	6MFLD-5	8MFLD-5	9MFLD-6	14MFLD-5	16MFLD-4
1960-1969	6MFSD-5	8MFSD-5	9MFSD-6	14MFSD-5	16MFSD-4	6MFLD-6	8MFLD-6	9MFLD-6	14MFLD-5	16MFLD-4
1970-1982	6MFSD-6	8MFSD-6	9MFSD-6	14MFSD-5	16MFSD-6	6MFLD-6	8MFLD-6	9MFLD-6	14MFLD-5	16MFLD-4
1983-1997	6MFSD-6	8MFSD-6	9MFSD-6	14MFSD-5	16MFSD-6	6MFLD-6	8MFLD-6	9MFLD-6	14MFLD-6	16MFLD-4
1998-2008	6MFSD-6	8MFSD-6	9MFSD-6	14MFSD-5	16MFSD-6	6MFLD-7	8MFLD-6	9MFLD-7	14MFLD-6	16MFLD-4
Single family detached (SFD)						**Single family attached (SFA), townhouse, duplex, etc.**				
	CZ 6	CZ 8	CZ 9	CZ 14	CZ 16	CZ 6	CZ 8	CZ 9	CZ 14	CZ 16
<1940	6SFDD-5C	8SFDD-5C	9SFDD-5C	14SFDD-5C	16SFDD-7	6SFAD-6C	8SFAD-6C	9SFAD-6C	14SFAD-6M	16SFAD-7
1940-1949	6SFDD-5C	8SFDD-6C	9SFDD-6C	14SFDD-5C	16SFDD-7	6SFAD-6C	8SFAD-6C	9SFAD-6C	14SFAD-6M	16SFAD-7
1950-1959	6SFDD-5M	8SFDD-6M	9SFDD-6M	14SFDD-5C	16SFDD-7	6SFAD-6C	8SFAD-8M	9SFAD-7M	14SFAD-6M	16SFAD-7
1960-1969	6SFDD-7M	8SFDD-7M	9SFDD-7M	14SFDD-7M	16SFDD-7	6SFAD-6C	8SFAD-8M	9SFAD-7M	14SFAD-6M	16SFAD-7
1970-1982	6SFDD-7M	8SFDD-7M	9SFDD-7M	14SFDD-7M	16SFDD-7	6SFAD-7M	8SFAD-7M+	9SFAD-7M	14SFAD-6M	16SFAD-7
1983-1997	6SFDD-8M+	8SFDD-7M+	9SFDD-7M	14SFDD-7M	16SFDD-7	6SFAD-6M+	8SFAD-7M+	9SFAD-7M	14SFAD-6M	16SFAD-7
1998-2008	6SFDD-8M+	8SFDD-7M+	9SFDD-8M+	14SFDD-8M+	16SFDD-8	6SFAD-6M+	8SFAD-7M+	9SFAD-8M+	14SFAD-6M	16SFAD-7

3.2.4 AC Penetration

AC penetration was considered explicitly because, as previously mentioned, AC operation accounts for 60-70% of electricity consumption while in use, and a significant portion of homes in LAC do not currently have central AC. The base-case AC penetration estimate was obtained from [2] at 41% for LAC with allocations in each climate zone as listed in Table 7 as shown in Figure 11 [62]. AC penetration was modeled to increase with the addition of new buildings either due to population growth or building turnover. Details of AC energy efficiency are provided with the following subsection.

Table 7. Base-case AC penetration.

CZ	AC Penetration
6	0.393
8	0.418
9	0.39
14	0.777
16	0.605
Total	0.414

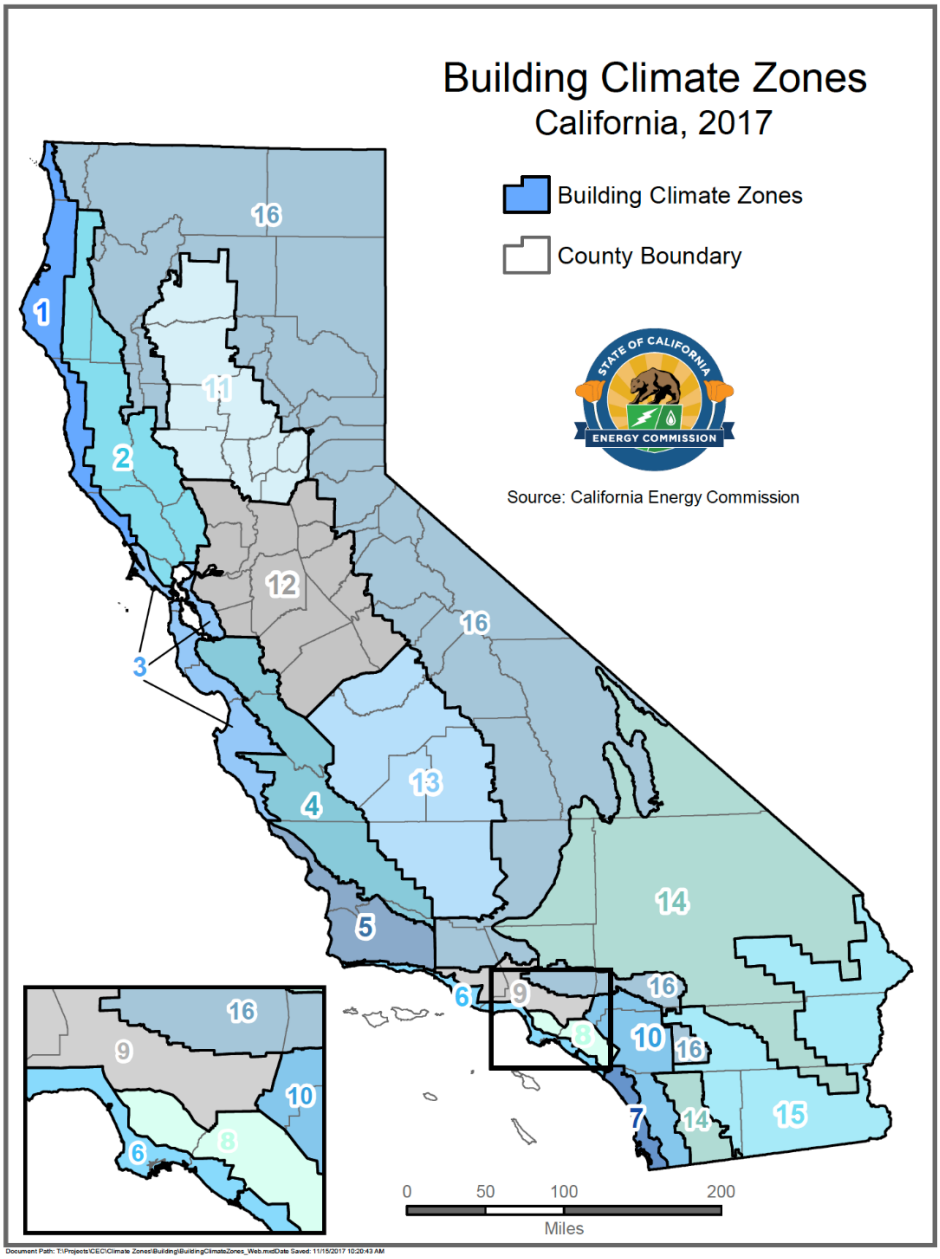

Figure 11. Los Angeles Building Climate Zone Areas.

3.2.5 Energy Efficiency – Housing Density

Housing density was considered because single family detached buildings are generally less energy efficient per square foot than multifamily attached buildings [18], and zoning policy can affect building types in the stock of particular locations [57]. Therefore, housing density was forecast in terms of the percent allocation of new dwelling units to the four types of residential buildings captured within the models: single family detached (SFD), single family attached (SFA), multifamily small (MFS), and multifamily large (MFL). The allocation values used for the base case were 47%, 8%, 24%, and 21%, respectively, as are current values per [2], and consistent with [55]. According to the Southern California Association of Governments 2016-2040 Regional Transportation Plan/Sustainable Communities Strategy, "66 percent of the 1.5 million new homes expected to be built in the SCAG region will be multifamily units, reflecting demographic shifts and anticipated market demand." [55]. Accordingly, the mid-case future scenario used this allocation of single family to multifamily units. The high case assumed 90% MF and 10% SF as an estimation of a potentially more aggressive scenario. For characterization of different building types' peak demands, see Appendix B.

3.2.6 Energy Efficiency – AC

Higher efficiency AC units use less electricity to cool the same volume of air to the same temperature. As AC energy efficiency standards have risen over time, further increases in AC efficiency were modeled in the building stock to consider potential effects of that continued trend on peak electricity demand. Seasonal Energy Efficiency Rating (SEER) was used in this study as an AC efficiency metric as it is the most common rating and was best available within BEOpt software. Note SEER ratings are based on performance over a weighted range of outdoor temperatures from 18-40°C (65-104°F) [63], whereas the range of outdoor temperatures in this study are up to 54.3°C (130°F). Previous building energy models developed in [2] clustered 20 different types of ACs; however, for a combination of practical and technical reasons, we further clustered residential AC in to three categories as listed in Table 8 based on SEER rating. Room air conditioners (RACs) were allocated to half SEER 8 and half SEER 16 per the model results and explanation in Appendix B. The low, medium, and high future scenarios used all SEER 16, 19, and 21 ACs as current standards require at least SEER 13 or EER 11.2 for residential sized ACs in California [20], and it is the Energy Commission staff's projection that these standards will rise to at least SEER 16 by 2040.

Table 8. AC technology categorization.

AC type	Definition	Clustering of (Reyna & Chester)	Base allocation
No AC	No AC	No AC	44%
Low efficiency	SEER 8	All SEER 10 or less + ½ of all RACs	26%
Medium efficiency	SEER 16	All SEER >10 + ½ of all RACs	30%
High efficiency	SEER 21	n/a	0%

3.3 Results

3.3.1 Countywide

Total Peak Demand. Peak demand was projected to increase for residential and commercial sectors from a base range of 9.5-12.8 GWh in the historical period to 12.3-16.7 GWh (~30%) in 2040 and 13.1-19.2 GWh (~45%) in 2060 for the scenarios listed in Table 9. Differences between

average T_{max} in the two RCPs was less than 1°C, and the effect of air temperatures on building peak demand ranged between 2% and 5% per 1°C as explained in the following subsection, and in Appendix B on an individual building basis. The other hottest day definitions tested included most grid cells over 35°C (95°F), and highest single cell T_{max}, which resulted in peak demand estimates of 4.09, 6.23, 10.32, and 4.8, 6.82, and 11.62 GWh for R, C, R&C sectors respectively in the base period.

Table 9. R&C sectors peak demand projections for hottest day scenarios.

Scenario	Ave. T_{max} °C (°F)*	Low (GWh)			Mid (GWh)			High (GWh)		
Sector		R	C	R&C	R	C	R&C	R	C	R&C
Base period	34-43 (93-110)	3.5	6.0	9.5	4.2	6.5	10.7	5.6	7.2	12.8
2040, RCP 4.5	43.7 (110.7)	4.5	7.8	12.3	5.4	7.8	13.1	8.8	7.8	16.6
2040, RCP 8.5	43.9 (111.0)	4.6	7.8	12.3	5.4	7.8	13.2	8.9	7.8	16.7
2060, RCP 4.5	44.2 (111.6)	5.1	8.0	13.0	6.6	8.1	14.7	10.7	8.2	18.9
2060, RCP 8.5	44.6 (112.3)	5.1	8.0	13.1	6.7	8.1	14.9	10.9	8.3	19.2

*Differences in T_{max} from values in Chapter 2 are due to allocation from grid cells to CBGs.
**Some values may appear the same between RCPs due to rounding

Spatial differences. Some CBGs must necessarily have significant increases in peak demand due to outward expansion of the urban landscape per the population projections in Appendix C. However, in most already developed areas, changes in peak demand ranged ±50% dependent upon the extent of efficiency improvements. Projections for combined R&C sectors are shown in Figure 12 for the composite heat images, which show the maximum potential peak demand in any CBG and relative percent change for any coincident heat waves in the scenario periods. Climate change was found to be responsible for 2% to 5% increases in peak demand. As shown in Figure 9, the areas closer to the ocean, located in climate zones 6 and 8, were projected to have fewer temperature increases over time (1-2°C), and climate zones 9, 14, 16, located further from the coast, were expected to experience more pronounced temperature increases (2-3°C).

The most electricity demand intensive areas in the base period in the model were in the Wilshire corridor, central downtown, east LA, West Glendale, and the Manhattan Beach areas due to high concentration of DUs and commercial buildings. Both SCAG and the CA Department of Finance projected approximately 1 million (~10%) population growth in the less developed and naturally hotter regions of Palmdale, Lancaster, and Santa Clarita; however, SCAG projections predict an additional 2 million in population across the western San Fernando Valley and LA Basin areas. The results in the high efficiency scenario were that peak demand decreased in the developed basin area in the low growth scenario by 2060 by about 20% overall on average, and as much as 50% in some CBGs, as AC efficiency standards forced replacement of older AC models with newer more efficient units in the model.

The highest increase scenario (19.2 GWh) considered approximately 700,000 new SFDs in the LA basin area. Figure 12 shows the lowest peak demand composite image for SCAG's high population growth scenario, which is 15.4 GWh total (hottest day is 14.7 GWh total) and arguably more feasible from a land use perspective as 90% of growth in that case is met with multifamily DUs that would require significantly less land area. In that case, peak demand

remains net constant in the in-basin area, at approximately 4 GWh, although there are certain pockets of increased demand in the Torrance and Long Beach areas, as well as by the coast. The central CZ 9 region's (from West Valley to Pomona) peak demand was projected to increase from 7.5 GWh in the base period to 9 GWh. The Santa Clarita and San Fernando Valley areas were projected to increase in the high efficiency cases from 320 MWh to 900 MWh for Department of Finance population growth or 590 MWh for SCAG population growth. Palmdale and Lancaster were likewise projected to increase from 560 MWh to 840 MWh and 570 MWh. Several CBGs appear green in the northern region in all cases due to little or no population growth, per the allocation procedures in Appendix C, and sufficient building turnover and or replacement of older ACs with newer ACs to result in a lower peak demand in the model. In all figures, CBGs with >50% area classified as protected lands are masked per the 2017 California Protected Areas Database [64].

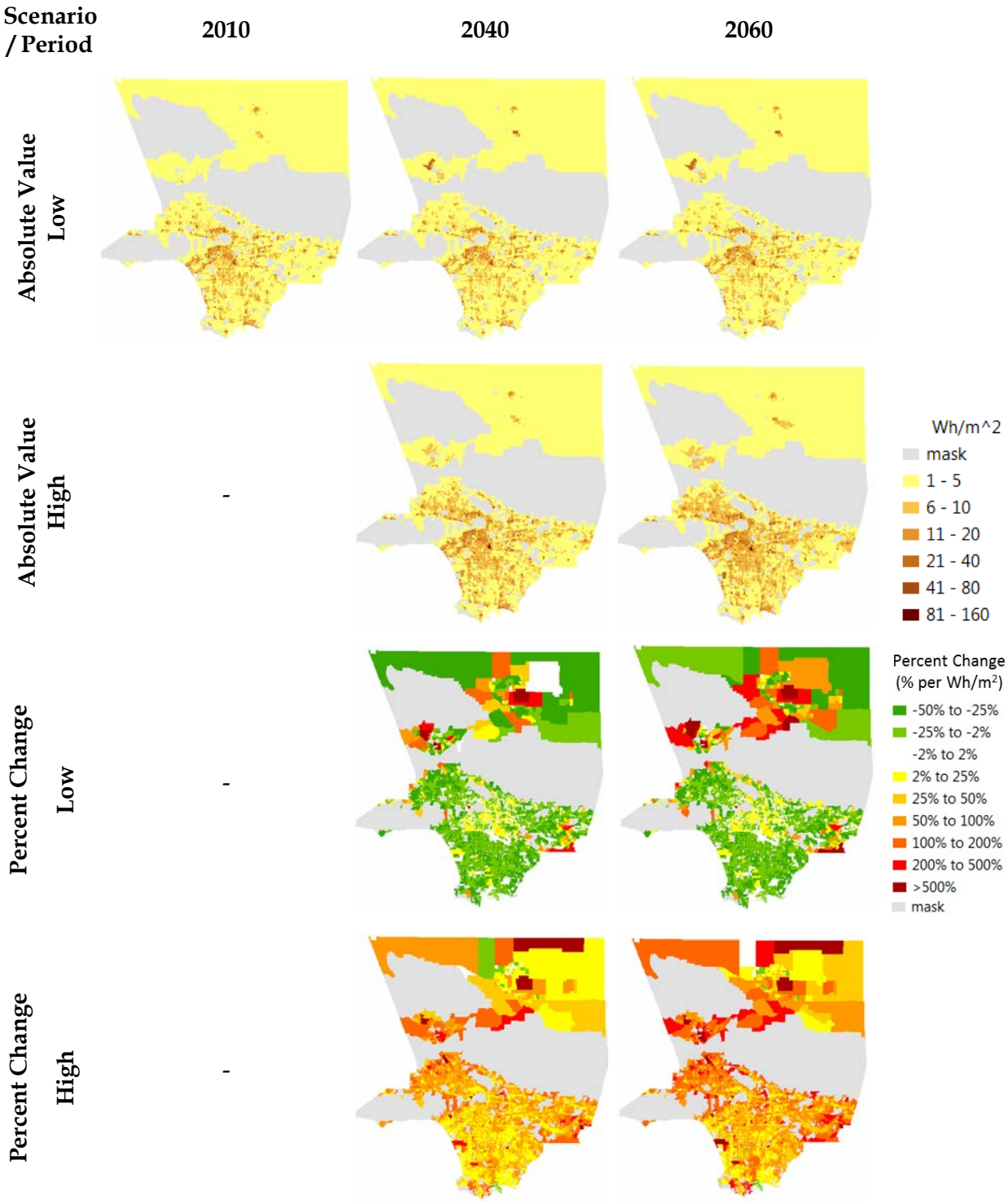

Figure 12. Composite peak demand projections and percent change for base and future period low and high scenarios.

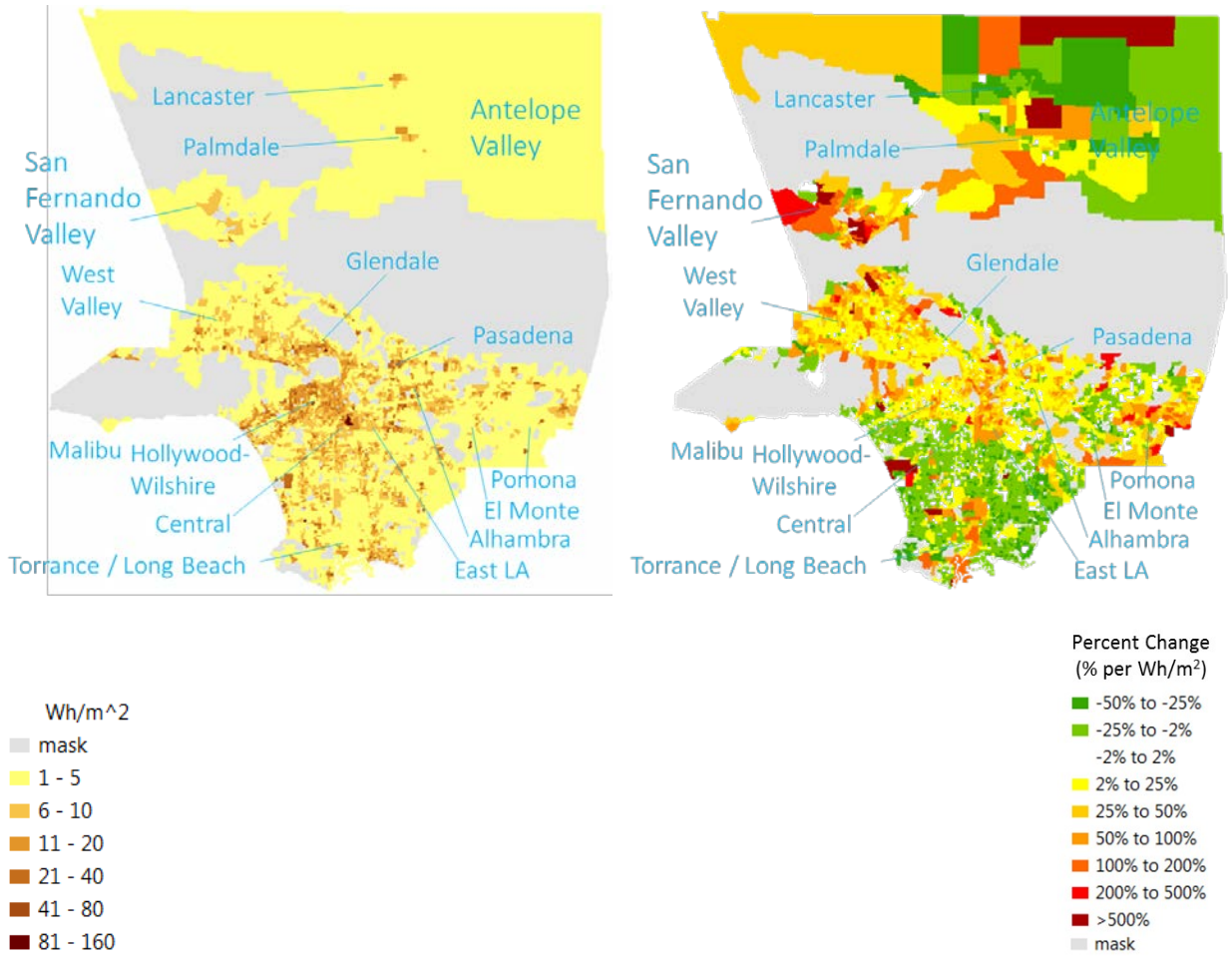

Figure 13. Composite high growth (SCAG) highest efficiency scenario for 2060. Left – absolute value. Right – percent change from 2010.

3.3.2 Factor Contributions

Air temperature. Effects of simulated heat waves resulted in increases in peak demand of 3-4% per 1°C in the base period, and 3-7% per 1°C in future periods relative to the peak at 30°C. As previously listed in Table 9, future hottest day average T_{max} were projected to increase from 42.7 °C (108.9 °F) to 44.6 °C (112.3 °C) in RCP 8.5 in 2060, a difference up to 1.9 °C (3.4 °F) from the base period when allocated by CBG. The total effect on peak demand, when compared to the base period hottest day, was an increase from 12.54 to 13.03 GWh in the 2060 low case, and 17.71 to 19.18 GWh in the 2060 high case (from 3.9% to 8.3%). Hottest day temperatures affected peak demand at higher rates in both low- and high- future cases as shown in Figure 14, due to higher AC penetration—65% and 100% respectively compared to the base case with only 45% AC penetration. To produce that figure, T_{max} was controlled in the model across LAC from 30 to 60°C for the scenarios as listed. Minor bumps in the graphs are artifacts of technical issues in building energy simulation modeling related to allocation of temperatures by day in BEOpt, which includes differences in behavioral usage patterns between weekdays, weekends and holidays as explained in Appendix B. The general trend was mostly linear however, with minor differences depending upon where slope measurements are taken. The slight s-curve pattern at

the temperature ends is due to AC duty cycling nearing 0% and 100% as was also predicted in [61]. Note: controlling every CBG's T_{max} to be equal to the scenario's average T_{max} produced total LAC peak demand results within 3% of using spatially differentiated temperatures for the hottest days.

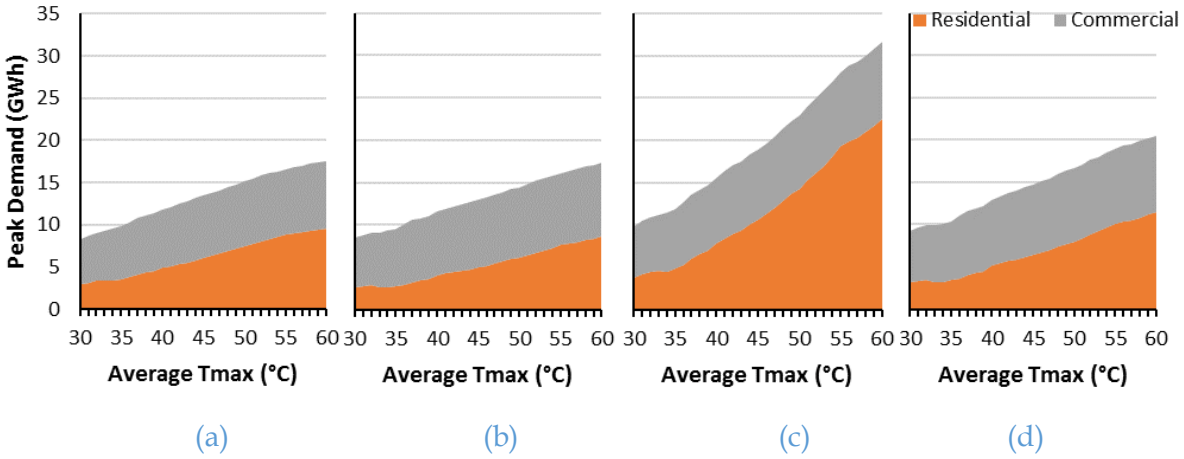

Figure 14. Peak demand sensitivity to T_{max}, in scenarios: (a) base-case, (b) 2060 low, (c) 2060 high, (d) 2060 SGAG low.
Per Table 9, the historical county wide average T_{max} range is 34-43°C (93-110 °F), and the future scenarios' 43.9-44.6 °C (110.7-112.3 °F).

Population growth. Without any efficiency improvements or increases in air temperature, peak demand increased 25—42% due to the addition of new buildings from population growth. Population growth affected peak demand forecast results by 6 -13% within each scenario. Figure 15 shows the effects of controlling for population within the low-case and high-case scenarios for each period. The effects on peak demand are directly proportional to the higher quantities of new buildings including AC penetration.

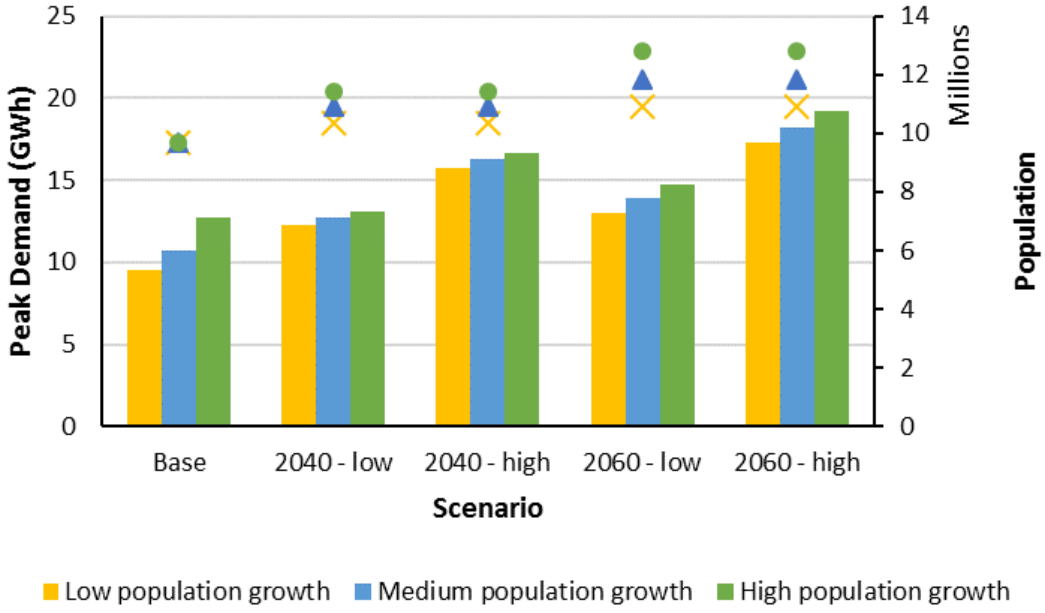

Figure 15. Scenario sensitivity to population growth factor.
Bars correspond to left axis, points correspond to right axis. Ranges in base period are for low, medium, and high historical hottest day images.

Building stock turnover and AC penetration. The effect of building turnover rate was 27 -30% in the model on forecasts of peak demand due primarily to increased AC installations at a rate of 0.5—0.6% increase in peak GWh per 1% increase in AC penetration. Differences in building efficiencies were inconsistent between newer and older vintage buildings, and improvements in building efficiency per square foot were generally negated in the models by larger total floor space per DU. As shown in Figure 16, if residential building turnover occurs at the highest modeled rate of 3%, then AC penetration would saturate at nearly 100% by 2040, and peak demand would be significantly higher than at low and medium turnover rates. Changes in AC penetration by climate zone are listed in Table 10 for each scenario.

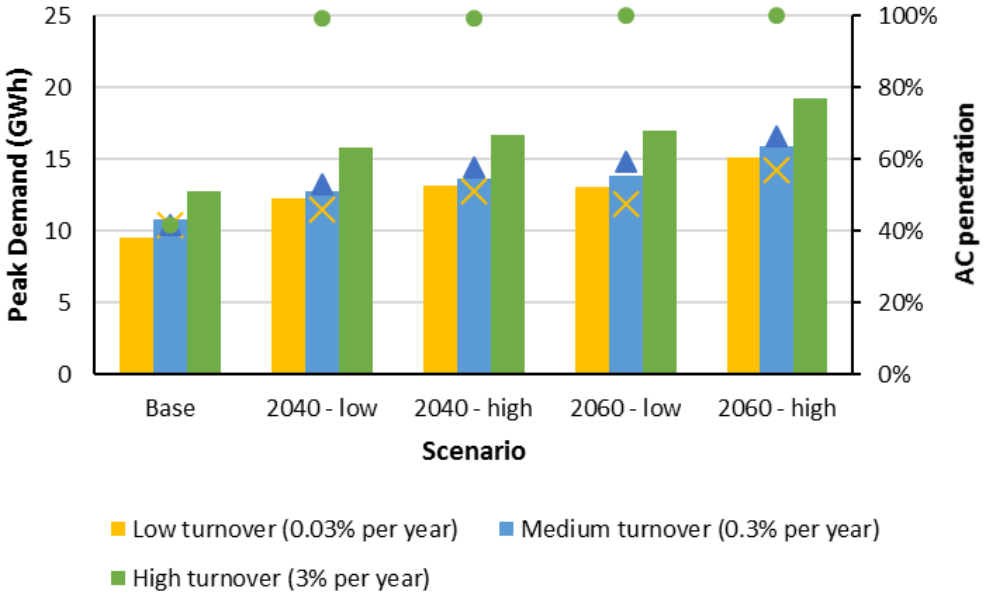

Figure 16. Scenario sensitivity to building turnover factor and AC penetration.
Bars correspond to left axis, points correspond to right axis. Ranges in base period are for low, medium, and high historical hottest day images.

Table 10. AC penetration by Climate Zone (CZ) for low and high population growth and turnover rates.

CZ	2010	2040 low	2040 high	2060 low	2060 high
6	0.393	0.413	0.993	0.419	1
8	0.418	0.429	1	0.435	1
9	0.390	0.433	0.991	0.45	1
14	0.777	0.86	1	0.888	1
16	0.605	0.764	1	0.828	1
Total	0.414	0.459	0.994	0.476	1

Housing density. New residential unit density affected total peak demand for LAC, and peak demand per capita, by 1-4% across the scenarios modeled. Figure 17 shows the effects of the low, medium, and high housing density factor (55%, 66%, and 90% MF for new building allocations) on the low and high future scenarios. The differences in peak demand are primarily due to the allocation of single-family detached units. Residential DUs that are attached via shared wall space can have up to 50% lower peak demand peak than single family detached DUs. For example, at SEER 16 AC units and T_{max} = 44°C, peak demand is 3.11, 2.36, 1.52, 1.54 kWh per DU in SFD, SFA, MFS, and MFL respectively when averaged across the five climate zones. The 2040 and 2060 high scenarios have higher peak per capita and greater variation therein. This is because the additional population growth and building turnover results in higher AC penetration for a larger quantity of buildings in the county.

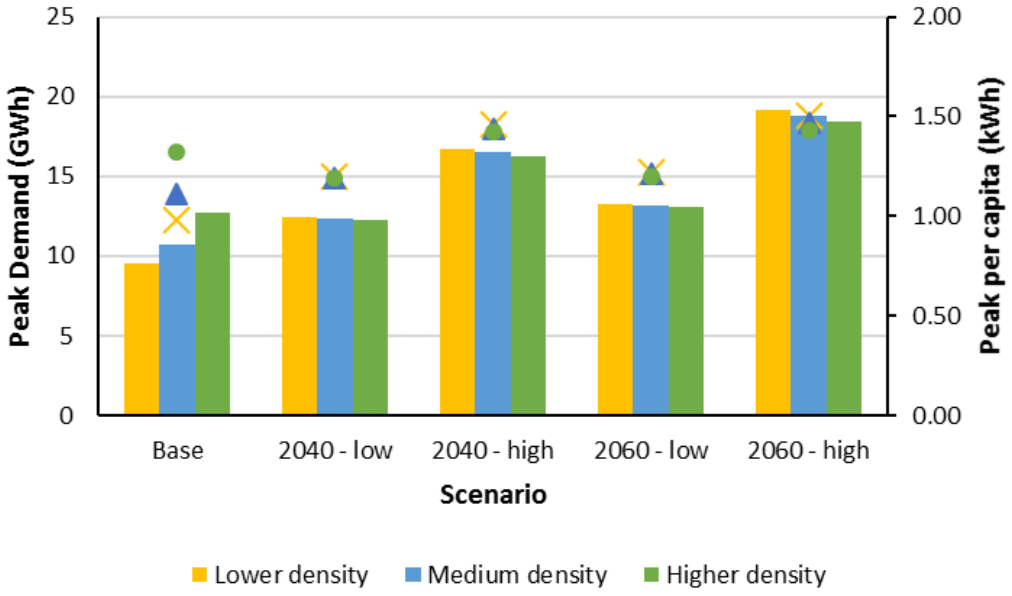

Figure 17. Scenario sensitivity to new housing density.
Bars correspond to left axis, points correspond to right axis.
Ranges in base period are for low, medium, and high historical hottest day images.

AC energy efficiency. Increases in AC SEER ratings from 16 to 21 increased peak demand by up to 2%. Future scenarios were modeled with all residential buildings as having either SEER 16, 19, or 21 central air conditioners. The range of effects on future peak demand is shown in Figure 18, where the highest case future scenario with the most SFDs had a 2% difference between a SEER 16 and SEER 21 standard. As shown in Appendix B, higher SEER rated AC units generally had lower electricity consumption at higher temperatures in the model. However, the performance differences saturated at higher SEER ratings, and in some cases reversed at very high temperatures. For example, in the highly populated CAZ 9, the newest model of SFD units had peak demands for SEER 16 and SEER 21 at T_{max}= 30, 38, and 44°C (86, 100, 111°F) of 1.17 & 1.15, 2.25 & 2.24, and 3.40 & 3.49 kWh respectively in the BE Opt simulations. In that specific model archetype, the unit with the SEER 21 AC unit could have lower annual energy consumption over course of an entire year, but during a heatwave with

temperatures in excess of 38°C (100°F) it would have a higher peak demand. SEER ratings are based on a weighted average of cooling energy efficiency for outdoor temperature ranges from 65-104°F (18-40°C), where it is assumed that 94% of operations occur at temperatures below 35°C or 95°F. Therefore, higher SEER rated AC units must be optimized for efficient performance during environmental conditions that are different from the hottest conditions when grid reliability is at risk. Future work should consider tradeoffs between annual energy consumption and peak load of AC units in engineering designs, as well as potentially different performance ratings other than SEER or EER, and their effects on peak demand—such as a peak performance rating.

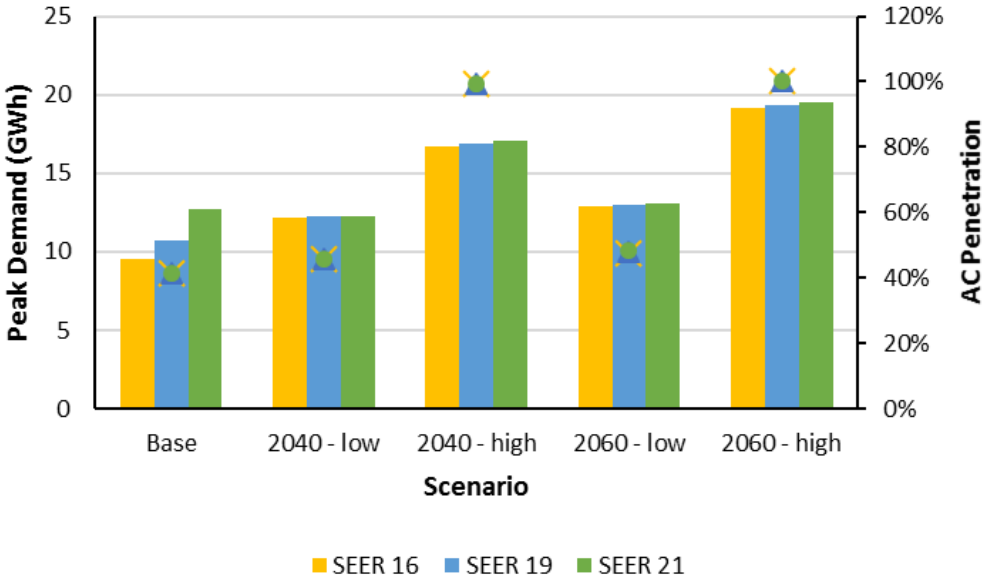

Figure 18. Scenario sensitivity to AC energy efficiency.
Bars correspond to left axis, points correspond to right axis.
Ranges in base period are for low, medium, and high historical hottest day images.

3.4 Uncertainty & Validation

In order to validate the feasibility of our conclusions, the results of the individual building models and total projections were compared to prior studies for the base period. Regarding future scenarios, a straight-line increase in peak demand with population growth would be 12% or 32% by 2060 for the Department of Finance and SCAG projections respectively. Therefore, given the range of building efficiency scenarios considered, and allocation of population to mostly warmer climate regions which already have higher AC penetration and demand, we do not consider the projected increases of 2-36% in the Department of Finance case, or of 16-51% in the SCAG case, to be unreasonable.

Countywide peak demand. The current base-period peak demand was modeled as 9.5 – 12.8 GWh for R&C sectors only, and is considered reasonable as the total peak demand for all sectors was estimated using the following three different approaches as being between 12.8–17.3 GWh. R&C sectors account for 64-68% of total electricity consumption per EIA records and

UCLA's Energy Atlas. If the same proportion were true for peak demand, then total peak demand would be 15-20 GWh, which significantly overlaps with the range of base period estimates, up to 20% higher in the high-cases. These estimates are necessary because sectoral data are either unavailable—in that residential, commercial, industrial, and other sector's consumption are not clearly disaggregated—or not reported with sufficient temporal resolution (hourly) to obtain a clear understanding of current peak demand. Therefore, as the ability to verify base-case model accuracy is limited, several ranges of historical temperature data were used to create a range base-case peak demand with which to compare future electricity demand forecast scenarios. The current peak demand estimations are as follows.

First, according to US EIA hourly balancing authority demand data, which are available for LADWP, which services almost half of LAC by geography and customer count, peak hourly demand for LADWP was 6,870 MWh in 2016 [65]. The peak demand was 2.0 times the average demand in that year. LADWP services 1.3 million residential, 89 thousand commercial, and 9.4 thousand industrial customers. This building stock is occupied by a population of approximately Rx3=3.9 million persons [66]. Scaling LADWP's historical peak demand per capita by the current population of LAC (9.8 million) yields a peak demand of 17.3 GWh.

Second, according the UCLA Energy Atlas, LAC's annual electricity consumption was approximately 20 billion kWh for residential and 16 billion kWh for commercial buildings, and 20 billion kWh for industrial and other in 2010, or 56 TWh total [56]. The average of the annual median electricity consumption for LAC in 2010 over a one year hourly period was 2.3, 1.8, and 2.3 GWh, or 6.4 GWh total [56]. If peak demand is 2 times the annual average measure, then it would be 12.8 GWh.

Third, peak demand for the entire state of California was 57-64 GW each year from 2005 to 2016 [67]. The population of LAC is approximately ¼ the state's population (37.3 million in 2010) [60], so a straight population allocation results in a peak demand estimate of 14-17 GW, applicable to a wider range of geography and an 11-year range of infrastructure and climate conditions.

CBG specific results. Uncertainty in input parameters and model procedures limit the accuracy of the CBG resolution results. For instance, population growth projections were allocated to CBGs as described in Appendix C for the three scenarios based on the percentage of spatial overlap and building density distribution factors were applied evenly across all CBGs. Realistically, this approach does not account for factors such as land areas that may be uninhabitable due to zoning regulations or other constraints. Moreover, population growth and residential building density are interdependent factors. In other words, some CBG values in the high-case may not feasible because higher density SFA, MFS, and MFL buildings *must* replace SFD buildings in some dense urban areas in order for the population to significantly increase within those geographies. These details do not affect the overall results or insights of this study, but are noteworthy in that they should be further examined by neighborhood specific land use studies before specific urban development plans are implemented.

Individual building electricity demand. While simulations of individual residential buildings resulted in average peak demands at 7pm that were approximately 50% larger than peak demand at 4pm, the overall model results based on the average of simulated electricity consumption from noon-6pm were within a reasonable historical range for total peak demand. Total peak demand historically occurs during the noon-6pm period as the additional coincident

demand from commercial and industrial sectors has been greater than the additional demand in the residential sector that occurs later in the day. While high penetrations of distributed solar PV are shifting the load on the grid to relatively lower levels during the daylight hours, that does not affect demand for actual electricity consumption, and forecasts in those changes in apparent load are beyond the scope of this report. The maximum hourly energy consumption values were tested in the model as well, which occurred at 7pm in the building energy simulations. Using the highest daily maximum values produced total peak demand results for LAC R+C sectors in the base period approximately equal to 60 GW. The task of further calibrating building models to hourly load profiles was beyond the scope of this work, but should be considered important future work as developing that sector-level hourly understanding is critical to addressing distribution-level grid modernization challenges associated with large scale solar PV integration, as well as increased energy storage systems and electric vehicles deployment.

The 2010 median annual electricity consumption for individual single family, multi-family, and commercial buildings were 6,726 kWh (0.5 Wh/ft^2), 9,612 kWh (0.43 Wh/ft^2), and 38,599 kWh (0.96 Wh/ft^2) respectively [56]. The low-end peak demand per DU across LAC in the base period was modeled at 1.5, 1.0, 0.7, and 0.7 kWh for the SFD, SFA, MFS, and MFL types, which were approximately twice the median values.

Commercial buildings were modeled as 108 kWh per building using the lowest value from the three vintages published. Those values overlapped the range of median values when considered over the range of building floor spaces listed in Appendix B. As previously stated, the use of the commercial building models exceeded their intended use in this report as they were not specifically calibrated for electricity consumption. The high temperature commercial peak demand values are likely an underestimation, where as shown in Figure 14 they did not significantly increase with air temperature in the model.

Temperature effects on peak demand. T_{max} affected peak demand at a rate of 3-4% per 1°C for the current infrastructure, which is consistent with historical observations found in [61] and [14]. The net increase in peak demand attributable to air temperature, for current infrastructure conditions, was approximately 300 MWh per 1°C, which was consistent with multiple previous regression analysis studies of California and LAC specifically in [61] and [3]. Increases in peak demand did not appear to decline until T_{max} = 53°C, approximately 10°C higher than estimated in [61], due to the method of averaging noon-6pm building consumption as opposed to the buildings' maximum consumption, which occurs later in the day. Again, future building energy modeling research should emphasize calibration for peak demand, and disaggregation of different customer sector hourly load profiles.

AC efficiency and power performance. Residential AC technologies were originally clustered into 20 types in previous work in developing the building energy models as were available for selection in the BEOpt and Energy Plus software. In this study, we further clustered AC technologies into three categories based on SEER ratings as were best available. The method of allocating room air conditioners into half SEER 8 and half SEER 16 may have resulted in high estimates of peak demand at maximum temperatures. Consequently, the percent demand reductions from upgrading ACs in high efficiency scenarios should be considered an upper estimate. Using only SEER ratings does not account for additional AC specifications that are known to affect performance, including compressor motor type [68]. Moreover, SEER ratings are based on performance over a weighted range of outdoor temperatures from 18-40°C (65-

104°F) [63], whereas the range of outdoor temperatures in this study are up to 54°C (129°F). Thus, the model results that some SEER 21 rated ACs performed less efficiently than SEER 16 at temperatures above 40°C is not implausible. Future work should consider tradeoffs between annual energy consumption and peak load of AC units if engineering designs were optimized for peak performance at very high outdoor temperatures instead of for current SEER and EER metrics. For example, AC units could have a peak performance rating analogous to EER, which is for outdoor temperatures of 35°C (95°F), but instead a PPR could be for 50°C (122°F).

AC penetration. This study used the AC penetration values from [2] for the base case by climate zone, which were different than the values as estimated in the Energy Commission's Residential Energy Demand Model, based on data from the Energy Commission Residential Appliance Saturation Surveys of 0.908, 0.514, 0.595, 0.730, and 0.742 for CZ 6, 8, 9, 14, and 16 respectively.

Persons per household. This study used a value of 3 persons per household for all scenarios. If that value were ranged from 2.7 to 3.3 (±10%) evenly across the county, then it would affect results likewise by ±10% as peak demand is directly proportional to building counts in the model.

Other factors. We did not consider peak demand from industrial sectors in this study, nor electrification of other technologies such as natural gas ovens, stoves, water heaters, nor petroleum-based vehicles. Electrification of household appliances could increase peak demand during the peak period. Assessing the impacts of electric vehicle deployment, including the possibility of EV batteries being used as a form of energy storage that can provide dispatchable local regulation services, should be the focus of its own dedicated study on the topic. Such a study should also consider time of use based prices and economic incentives for ratepayers.

3.5 Conclusions

Peak demand was projected to increase in LAC by at least 200 MWh by 2060. Peak demand was modeled and ranged from 9.5-12.8 GWh in the recent historical period for residential and commercial sectors. Increases by 2040 ranged from -0.5 GWh to 3.9 GWh, or a reduction of 4% to an increase in 30%, as conservatively estimated from the high range of the base period. By 2060, the range of increase in peak demand spanned from 0.2-6.5 GWh (+2-51%). The significant width of this forecasted range is due to the ways in which changes in climate, population, and urban infrastructure could potentially interact to influence demand.

Peak electricity demand increases significantly with increased air temperatures, and may or may not increase more in the future depending upon increases in AC penetration levels. Peak demand increases in LAC were found to occur during the base period at a rate of about 300 MWh or 2-4% per 1°C at 45% AC penetration. The range of the hottest day (average T_{max} across the county) of the year in the base period was 34-43 °C (93-110 °F) for the 20-year period. The modeled differences in peak demand across this 9 °C (17 °F) range was 3.3 GWh or 35% for the R+C sectors. By 2060, AC penetration was projected to be between 65%-100%, and the average T_{max} up to 2.3°C higher in RCP 8.5. The combined difference in peak demand over the range of hottest day temperatures in 2060 was 9.3 GWh to 13.0 GWh in the low case, and 11.4 GWh to 18.9 GWh in the high case, or 40% to 66% for R+C sectors. These results indicate that peak demand will probably be more sensitive to variations air temperature from heat waves in the future, and therefore the margin of error for underestimation of heat wave severity more critical for resource adequacy and delivery system capacity planning as well.

In addition to air temperature increases, population growth was found to be the other most significant factor driving peak demand within the model. The population forecasts used indicated an increase from 9.7 million people in the base period to 10.9-12.2 million by 2060, and resulted in a 25—42% increase in modeled peak demand without any efficiency improvements or increases in air temperature. Population growth in Palmdale, Lancaster, and Santa Clarita, which are less developed and naturally hotter regions, have building peak demands that are higher per capita than in the cooler basin areas. Approximately 2 million in population growth was projected in the SCAG scenario for estimates for the western San Fernando Valley and greater basin areas where current central AC penetration is ~40%. If all new buildings have central AC, then population growth could occur at a rate that raises peak demand almost 2x higher per capita than current conditions as AC use accounts for 60-70% of peak demand in residential buildings.

The benefits of switching from single family to multi-family housing are reductions of 25-50% in peak demand per capita. Therefore, if the current power delivery infrastructure in the LA Basin area is operating near its capacity limits, then the area can generally support population growth with the most energy efficient buildings, as they are able to outpace increases in AC penetration. For the SCAG projected growth of an additional 2 million people in the basin by 2060, at 90% multifamily dwelling units, the average CBG in the basin area from Central LA and south was forecasted to have an average decrease in peak demand of 7%. Torrance, Long Beach, and west Inglewood had increases in peak demand, indicating that new population growth may not be feasible to occur evenly across CBGs. The area from Pomona to West Valley, approximately climate zone 8, had an average increase in peak demand of 25%.

Implementing higher density residential building types can curb the growth of peak demand. Dwelling units with shared wall space, such as apartments, had as much as 50% less peak demand per capita in the models. While replacing older buildings with newer buildings generally improves thermal efficiency, and therefore energy efficiency as well, anticipated increases in building size and AC penetration rates mean that the net effect of building turnover will result in an increase in peak demand. Moreover, while significant improvements have been made over the last several decades in various building and appliance efficiencies, air conditioning is overwhelmingly the most significant factor in determining peak demand. Differences in lighting and other appliance efficiencies, while significant for total annual energy consumption, accounted for less than a 2% difference in peak demand. In our models, 60-70% of peak demand within residential buildings was attributable to AC use, where higher air temperature resulted in 3-7% increase in electricity demand per 1°C. If peak demand is going to be reduced within the residential sector in the future, then different, or differently optimized, AC technologies are necessary.

While improvements in AC SEER rating are significant for total annual electricity consumption, their effects on peak demand saturate, and different metrics are needed to optimize for peak performance. Higher AC SEER ratings negatively affected peak demand by up to 2% in the models above SEER 16 and high temperatures above 35°C or 95°F. SEER ratings are defined for a range of outdoor temperatures from 18-40°C (65-104°F), with the assumption that 94% of operations will occur while outdoor temperatures are less than or equal to 35°C [63]. Thus, higher SEER rated ACs are optimized to perform below outdoor temperatures of 35°C. Higher SEER rated AC units can actually be counter-effective to reduce peak demand during severe heat wave conditions (>45°C or 113°F). The other common AC rating, EER, is specifically for

35°C or 95°F and is problematic for the same reason. A different energy rating metric and optimized AC engineering design(s), is necessary to shave peak demand due to building cooling from ACs. A new "peak performance rating" for ACs could be useful to mitigate peak load during extreme heat conditions as there would be incentive for ACs to be engineered for more efficient performance at 50°C (122°F), for example.

Other important considerations for managing future grid reliability revolve around the fact that new technology implementations are both triggering shifts in demand profiles and creating differences between demand and load profiles [69]. Demand is the amount of power or energy that is being used behind the meter, whereas load is the amount of power or energy being consumed from the perspective of the grid connection. The shift from fossil fuel sources to distributed and intermittent renewable power sources has created a phenomenon known as the duck curve. The duck curve corresponds to conditions where total peak loads, which have historically occurred from noon-6pm, are shifting to slightly lower levels and occurring later in the day. This slight reduction in peak load, which occurs because of overlap between residential, commercial, and industrial sector demand profiles, is also associated with a very steep ramping rate as the output of solar generators decline rapidly in the early evening.

As a final consideration, electric vehicles are being deployed at an increasing rate. These vehicles will require grid charging and could potentially provide load shifting and regulation services if they are designed to support the two-way flow of power. In such a case, electric vehicles could potentially charge on solar during the day, supplement power to homes in the early evening to both reduce the ramp rate as the sun sets and reduce the later peak load, recharge in the middle of the night using cheap base-load power, and be fully charged again in the mornings. Such activity would decrease net load variance. Developing better understanding of the residential sector demand profile is critical to managing the duck curve at both a neighborhood circuit-level scale and a balancing authority scale. With a clear understanding of daily residential and commercial demand profiles, solar PV and battery storage systems can be located and sized in a way that reduces load variance and creates a smoother load profile to manage.

4: Infrastructure Vulnerability Analysis

4.1 Summary

Infrastructure vulnerabilities were analyzed throughout Los Angeles County for power generation plants, transmission lines, and substations for both the direct effects of higher ambient air temperatures, as well as the combined effects of increased air temperatures and increased future demand. Infrastructure components are vulnerable to rising air temperatures because heat generated from electric power flow is inherently dissipated into the ambient air. Higher ambient air temperatures mean that components' safe operating loads must be reduced. Vulnerabilities were analyzed to estimate maximum allowable loads on components to prevent physical hardware damage under climate change scenarios RCP 4.5 and RCP 8.5 to 2060.

Power plant derating factors were used based on findings from previous empirical studies of sensitivities to air temperature. Natural gas plant and solar PV generation capacities were vulnerable up to 6% each, or approximately 2% of total local generation capacity. Therefore, the

net heat wave risk is a minimum of 2% and maximum of 20% of delivery capacity depending upon location and neighborhood infrastructure constraints within Los Angeles County.

IEEE standards were used to calculate the steady state thermal ratings of substations and transmission lines throughout the systems. Distribution level substations are expected to generally be more vulnerable than transmission level substations due to lack of forced air or water cooling systems – i.e., lower voltage substations are more likely to rely on convective air cooling processes only. Substations in the Santa Clarita and West Valley areas were estimated to have the highest risk of failure due to heat waves in the future in the absence of system upgrades. About 20% of SCE's substations are already operating with load factors over 100%, and temperatures were projected to reach as high as 53.4 °C (128.1 °F) resulting in up to 20% reductions in loadability. Lower voltage transmission lines are generally expected to be more vulnerable than higher voltage lines due to higher resistance in conductor strands. The lower voltage lines in the basin area were estimated to be vulnerable at up to 20% reduced loadability, and while distribution-level lines were not specifically analyzed, their sensitivity to air temperature is likely on the high-end of that range.

The most significant short-term risk from heat waves is overload of distribution-level components in already congested areas from Alhambra to Pomona, and in San Fernando and Antelope Valleys. Infrastructure in the Santa Monica Bay area, along the western-facing coast up to 6 km (3 miles) inland, is not expected to experience air temperatures significantly above 40 °C (104 °F) at any time in the projected period. Long-term power service reliability is more susceptible to population growth and changes in technology that affect peak demands such as building and AC efficiency. Additional local generation and/or imported power, plus new delivery infrastructure, will be necessary to meet the demand needs of population growth in at least the northern half of the county and western valley areas. Under the highest efficiency scenario with the California Department of Finance population projections, the infrastructure in the in-basin area would realize reduction in peak hour load from 4 to 3.3 GWh (-17%). Under the highest efficiency scenario with SCAG's population forecast, then peak demand will remain approximately the same in the in-basin area.

4.2 Approach

The vulnerability of electricity infrastructure to rising air temperatures was considered relative to three categories of components: generation assets, substations, and transmission lines. Within each of these categories vulnerabilities were assessed in two parts. First, was the consideration of potential derating—i.e., decreases in percent loadability (MW capacity at generators, kVA capacity at substations, and ampacity in transmission lines) due to rising air temperatures only. Rising air temperatures were considered in terms of average temperature rise, and absolute degrees above 40 °C (104 °F). That temperature value was used based on ANSI/IEEE standards, which are also referenced several times as guidelines in LAC's major service provider's, Southern California Edison's (SCE), Interconnection Handbook [70]. Second, vulnerabilities were assessed for components in terms of total relative future capacity need considering both decrease in loadability and increase in future demand. Two sets of peak demand forecasts were used; one was based on the CA Department of Finance's projected population growth and the other based on SCAG's, each with low and high ranges for building types, energy efficiencies, and ambient air temperatures for 2040 and 2060 RCPs 4.5 and 8.5 (Table 11). It is important to

note that the demand forecasts were for residential and commercial buildings only (Chapter 3: Electricity Demand Forecast) and did not consider industrial or other sectors.

Therefore, the estimates developed should be considered low by 5 GWh, or 50% of listed values – depending upon whether the industrial building uncertainty would propagate additively or linearly – per Section 3.4 Uncertainty & Validation, especially in areas where significant industrial loads may exist now or in the future. Moreover, because demand was allocated to components spatially and did not consider specific power flow network topology or the ability of grid operators to make power routing decisions, results should be interpreted as more regionally insightful than prescriptive for any particular component. Vulnerabilities were estimated quantitatively as changes in absolute capacity (MW) of generation capacity, and as relative percent changes for substations and transmission lines as was most appropriate with the available data.

Table 11. Range of Peak Demand Projections for LAC for Residential and Commercial sectors only.

	LAC Total Peak Demand (GWh)			
Time Period	**Finance - Low**	**Finance - High**	**SCAG - Low**	**SCAG - High**
Hottest Day				
2010	9.5	12.7	-	-
2040	12.3	15.8	13.1	16.7
2060	13.0	17.3	14.7	19.2
Composite				
2010	-	13.5	-	-
2040	12.9	17.3	13.8	18.4
2060	13.6	18.8	15.4	20.9

4.2.1 Generation

Supply vulnerabilities were first assessed as potential derating values for generation capacity (MW) due to rising air temperatures in sensitive generation plants. Other factors that may affect availability of generation capacity, including availability of cooling water, cooling water temperature, and mechanical failures, were not considered. Moreover, LAC relies on energy that is imported from generators located in other neighboring regions, whose vulnerabilities were not identified in this study but could be significant factors in meeting future peak demand. LAC power plant data were obtained from the US EIA online at [71], including plant type, capacity, and geospatial location, as shown in Figure 19. In order to locate potential hazards, vulnerabilities were mapped for individual generators for worst case scenario temperatures in excess of 40°C (104°F) using the composite temperature projection images for 2060 RCP 8.5 (Chapter2: Climate Modeling for Heat Events). In order to consider potential effects on local resource adequacy of the entire County, vulnerabilities were tabulated for the total LAC generation fleet for both average temperature rises (up to 3°C or 5°F), and for the temperatures in excess of 40°C (104°F) for 2040 and 2060 future projected hottest days under RCPs 4.5 and 8.5.

Generation plants sensitive to high ambient air temperatures include dry-cooled natural gas plants, the dry-cooled portion of combined cycle natural gas plants, and solar PV plants with quantities and derating factors as listed in Table 12 [61]. Wet-cooled plants were not modeled to have any capacity losses with rising air temperatures per [72]. Total plant capacity values listed were assumed to be for ambient air temperatures of 40°C (104°F). The range of derating factors for natural gas generation plants was attributable to chiller performance at the air intake of dry combustion engines [26], [73], [74], [72]. The range of derating factors for solar PV was attributable to internal carrier recombination rates from thermal excitation [75]. While hydropower plants are known to be vulnerable to climate change, and the vulnerabilities were estimated as 0.4-14% to 2060 in the USA, those estimates were attributable primarily to reduced water availability from drought, as opposed to higher air temperatures directly [72], [24], [28]. Therefore, because hydropower accounts for only 2% of the generation in LAC, changes in those generation capacities due to ambient air temperatures were considered negligible in this study.

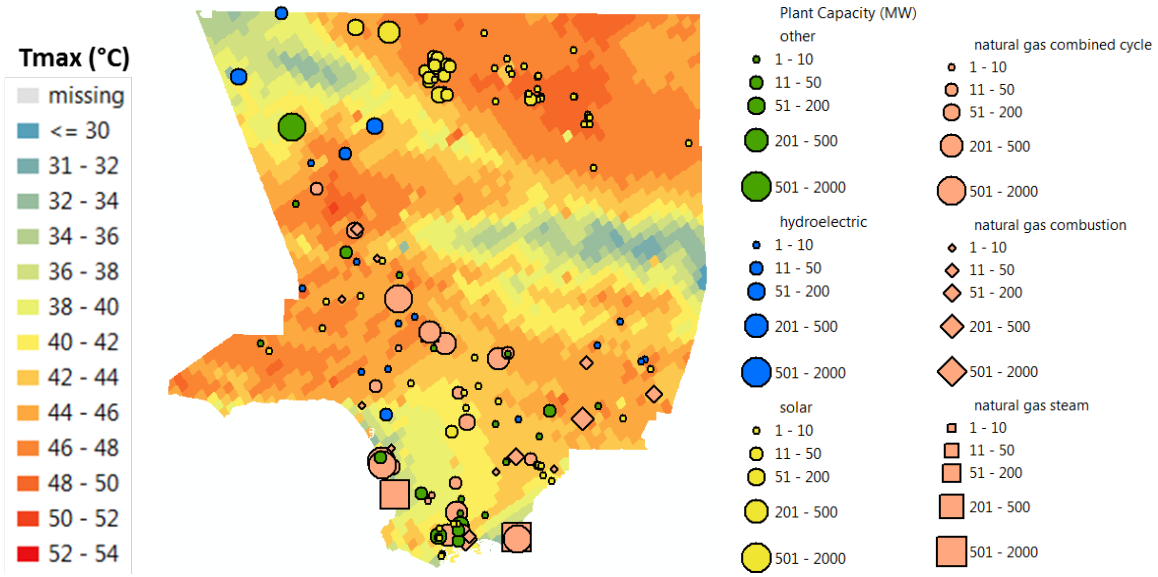

Figure 19. Map of power plants by type and capacity overlaid to historical hottest day.

Table 12. Power Plant Capacities by Type and High Air Temperature Derating Factors.

Generation type	Power Plants Count	Power Plants Capacity (MW)	Derating factor (%/1°C-T_{max})
Hydropower	18	284	-
Natural Gas (steam)	3	3,406	-
Natural Gas (combustion)	15	1,044	0.6% ± 0.1%
Natural Gas (combined cycle)*	23	5,742	0.3% ± 0.1%
Solar PV**	91	890	0.35% ± 0.25%
Other***	24	2,137	-
Total	174	13,503	0.20% ± 0.06%

*Includes three "natural gas other" plants with total capacity of 4.4 MW.
**Includes one 3.2 MW solar thermal plant without storage.
***Includes by size: pumped storage, biomass, other, and petroleum.

Vulnerabilities in generation were also quantified in terms of local reserve margin (LRM), which is the amount of total generation capacity in excess of total demand for the various forecasts in the region. The hottest day climate change scenarios were used for derated generation capacity and increased demand. LRM was projected to decrease for two separate and distinct reasons. First, plants will have reduced generation capacity under the stress of higher ambient air temperatures. Second, there will be higher demand for electric power with higher ambient air temperatures—which were evaluated for the range of population growth and technology change factors projected in Section 3: Electricity Demand Forecast. Future power plant generation capacity was explicitly not forecast and is instead discussed as an adaptation option in the concluding section of the report because significant interdependencies exist between generation and delivery capacity. For example, LAC is a net importer of electric power with 13.5 GW of generation capacity, and hottest day peak demand estimated at 15-20 GW. This means that transmission line imports are critical to meet demand on the hottest days, as depending upon the ambient air temperature (i.e., 1-in-2, 1-in-10, or highest summertime temperature), LAC presently operates with a small positive, neutral, or negative local reserve margin (LRM) [61]. Moreover, present peak demand was estimated for residential and commercial sectors only as between 9.5 and 12.7 GWh. In terms of total peak demand in LAC, the values in Table 11 should be considered low by 5 GWh or 50% as industrial and other sector processes are included. Considerations for future power generation are discussed in the adaptation section of this report including the context of vulnerabilities and risks in substations and transmission lines as well.

4.2.2 Substations

Substation vulnerabilities were first assessed in terms of derated capacity (kVA) of transformers due to rising air temperatures. Substation data were obtained from the US Department of Homeland Security (DHS) in [76], and included 410 geolocated substations total in LAC: 102 were labeled as having maximum voltage ratings, as shown in Figure 20, 43 were labeled 66KV to 138kV, 59 labeled 230 & 500 kV, and 308 were labeled unknown and assumed to be ≤69 kV. Air temperatures were spatially assigned to substations as they intersected temperatures from the 2 km² projections. As stated in IEEE Std C57.91™-2011 (Revision of IEEE Std C57.91-1995) Guide for Loading Mineral- Oil-Immersed Transformers and Step-Voltage Regulators [30], multiple types and ratings of transformers exist; however, the 65°C top oil temperature rise over 40°C ambient design has been industry standard since 1977. A short table of conservative

capacity derating factors for self-cooled, water-cooled, and forced-air cooled transformers are provided and specifically recommended for quick approximations. Those factors were considered reasonable to use in this study, as this is a broad spatial assessment of hundreds of substations with unknown physical attributes. The derating factors were listed as 1.5% kVA for each 1°C of daily 24 hour average temperatures above 30°C for air temperature for self-cooled transformers and 25°C for water temperature, and 1% kVA per 1°C for forced-air, oil-, and water-cooled transformers. The standard states that the associated maximum temperatures should not be more than 10 °C above the average temperatures. Therefore, the derating factors were applied to daily maximum temperatures from the climate projections relative to 40°C as an approximation consistent with the approach used throughout this report. High voltage substations (≥230 kV) were assumed to have some form of forced cooling, therefore rates of 1% kVA per 1°C were applied. Lower voltage substations were assumed to be sensitive to air temperature at a rate of 1.5% kVA per 1°C.

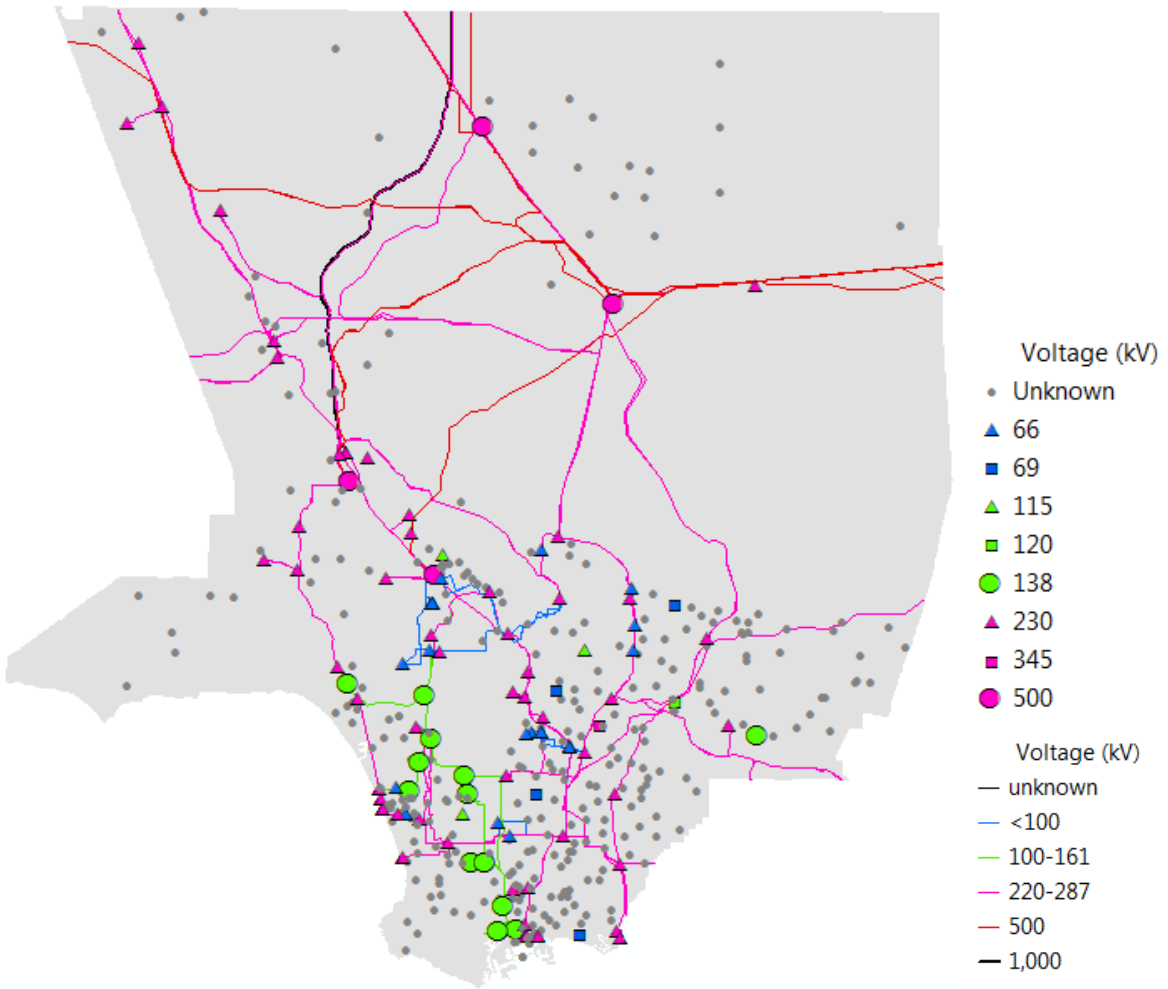

Figure 20. Substations and transmission lines.
Note: not all components are visibly distinguishable due to close proximity.

Vulnerabilities were also assessed by estimating percentage increases in temperature-adjusted load at substations. New substation construction was not forecast, but rather considered in mitigation and adaptation options. Temperature-adjusted load was defined as the base or forecasted load, plus 1-1.5% per 1°C above 40°C per the derating factors previously stated. Composite images were used for future demand forecasts to estimate the highest stress at any substation. Maps relating demand in CBGs directly to substation service areas were not available for the project. Therefore, peak demand, estimated at CBG resolution, was allocated to substations using a multi-layered Voronoi Tessellation clustering approach. Two substation layers were created to approximate for series and parallel operations of the substations. High voltage, >=230kV, and low voltage, <230kV, substations were clustered with like types within 2 km and 1 km respectively. Substation clusters were assigned to geographic areas such that boundaries were equidistant in between the center of the clusters. Details of how these procedures were performed are included in Appendix D. This estimation approach was considered a reasonable approximation for the purposes of this report as base period projections were validated within 15% of a sample of peak demand in SCE's substations in [77], which were representative of 50-70% of LAC's substations.

Lastly, risk of component overloading was estimated at SCE's substations for current and future conditions. Only SCE substation overloading was estimated, as those were the only substations where both load and capacity data were available to estimate load factor or utilization. As explained in further detail in Appendix D, the base peak load factors on SCE substations were estimated using the SCE Distributed Energy Resource Interconnection Map (DERiM) data [77], assuming those values corresponded to 40 °C (104 °F). Derated load factors were then estimated for present day circumstances using the composite maximum temperature projection images for the recent historical period and derating substations by any amount above 40°C as previously described. Future scenario derated load factors were estimated by scaling the load at the substations by the corresponding amount relative to the base period in the Voronoi polygons. Weather-adjusted load factor ratings were classified as described in Table 13 for the reasons as listed.

Automatic outages occur because the temperature of the oil or air pressure increases within the transformer, causing the relay mechanism to trip the transformer from the overloaded circuits. The standard calibration specifies that automatic outages occur at a load factor of two. Because load factors were estimated for the peak hour only, we were unable to conclude whether any conditions with load factors less than 2 would result in automatic outages, but the probability will certainly be higher that sub-hourly variability will result in automatic outages on substations with higher load factors than not. In the event that an automatic outage occurs, power flow is instantaneously redistributed to lines and substations operating in parallel, which could cause those components to trip resulting in cascading failures.

Table 13. Substation Derated Load Factor Risk Metrics.

Load Factor	Risk Level	Reference	Description
n/a	Unknown	n/a	Substation(s) exists in this space according to DHS database [76], but not SCE DERiM [77], so loading data were unavailable.
0.01-0.5	Very Safe	Assumption	Negligible thermal wear, probably n-2 reliable if in parallel/redundant configuration.
0.51-0.85	Safe	15% rule	Very low thermal wear, probably only n-1 reliable if in parallel/redundant configuration.
0.86-1.00	Caution	15% rule	Non-negligible thermal wear, probably not n-1 reliable.
1.01-1.20	Warning	[70], [8]	Thermal wear, component overloaded, automatic switching may occur in 24 hours to 30 days if loading continues at this level, or sooner with sub-hourly spike, depending upon switch gear settings.
1.21-2.00	Emergency	[70], [8]	Significant thermal wear, component very overloaded, automatic switching will occur in 30 min, or sooner with sub-hourly spike, depending upon switch gear settings.
> 2	Outage	[8]	Extreme thermal wear, switchgear will automatically trip to prevent hardware damage and failure.

4.2.3 Transmission Lines

Transmission line vulnerabilities were assessed as potential decreases in loadability factor due to rising air temperatures in terms of percentage of ampacity. Geospatial line data were obtained from the US Department of Homeland Security [78], and included 192 line segments for LAC, with one rated 1,000 kV, 12 rated 500 kV, 119 rated 220-287 kV, 31 rated 100-161 kV, 22 <100 kV, and 7 unknown. The 7 unknown line segments were removed from the data set; they were so short that they were not visible in the images produced in the results. Air temperatures were spatially assigned to lines by assigning the highest value of the intersecting temperatures from the 2 km^2 projections. The steady state balance equations in the IEEE Standard for Calculating the Current-Temperature Relationship of Bare Overhead Conductors [32] were used to estimate changes in loadability factor. The effects of higher ambient air temperatures on underground systems were not considered specifically, but conductive heat transfer in common duct banks could result in line sag, instrumentation errors, harmonic distortions, other quality issues, and/or shock hazards to field workers. These effects should be further investigated.

The IEEE standard provides generally accepted approaches for determining maximum allowable current on lines to prevent excessive sag or annealing that would occur if the lines were too hot. A line's temperature is a function of its physical attributes, the weather conditions, and its electrical load. Per basic physics, the heat gain from electricity conductance and solar radiation must equal the heat loss due to convection and radiation. Thus, if the ambient air temperature rises, then less energy is dissipated via convective cooling (if all else is held constant), the line temperature increases, and therefore the maximum current that a line can

carry without exceeding its safe operating temperature decreases. All input and calculated parameters used are listed in Table 14, with values and units for the base case. The only modification from the approach in the standard was the addition of a conductor electrical resistance increase factor, R(%), as an intermediary step for the conductor electrical resistance at 75°C, R(75°C), which was used for sensitivity analysis to create upper and lower ranges. The base case input values and ranges for conductor and weather parameters are summarized with explanations in Table 15.

Table 14. Transmission Line Ampacity Estimation Values.

Description	Parameter	Value	Units
Input parameters			
Climate			
Ambient Temp	T_a	40	C
Wind Speed	V_w	0.301	m/s
Angle between wind		1.571	radian
CDR elevation above sea level	H_e	300	m
CDR latitude in degrees	Lat	34	degrees
Solar hour	s_hr	16	#
Day of year	N	172	#
Conductor			
Conductor surface temperature, maximum allowable	T_s	100	C
conductor diameter	D_o	0.03	m
Coefficient of emissivity	ε	0.8	#
Coefficient of solar absorptivity	α	0.8	#
Conductor electrical resistance at 25°C	R(25°C)	0.00007	Ω/m
Conductor electrical resistance increase factor	R(%)	16	%
Conductor electrical resistance at 75°C	R(75°C)	0.0000812	Ω/m
Calculated Parameters			
Air Properties			
Wind direction factor	K_angle	1	#
film air temperature	T_film	70	°C
Air Density	p_f	0.993	kg/m^3
Dynamic viscosity of air	u_f	0.000020	kg/m-s
Thermal conductivity of air at temperature T_film	k_f	0.029	W/m-°C
Reynolds number	N_re	439	#
Solar Properties			
Solar hour angle	ω	60	degrees
Solar declination	δ	23.46	degrees
Solar altitude	H_c	37.08	degrees
Solar heat flux	Q_s	893	w/m^2
Solar azimuth variable	χ	-10.800	#
Solar azimuth constant	C	360	degrees
Solar azimuth angle	Z_c	275	degrees

Effective angle of incidence	θ	143	degrees
Conductor Properties			
Conductor electrical resistance at T_s	R(T_s)	0.000087	Ω/m
Heat loss rate due to forced convection	q_c1	58.10	W/m
Heat loss rate due to natural convection	q_cn	43.72	W/m
Output Parameters			
Heat gain rate from sun	q_s	13.01	W/m
Heat loss rate due to convection	q_c	58.10	W/m
Heat loss rate due to radiation	q_r	41.69	W/m
Thermal Ampacity Rating	I	1,000	A

Table 15. Transmission Line Ampacity Parameter Ranges and Explanations.

Parameter	Low	Base	High	Explanation
T_a	20	40	60	Same base and range values used throughout this study, with base attributable to SCE in [70].
V_w	0	0.301	0.4	Per [32] section G.3 Ambient-adjusted ratings, the wind speed should be no more than 0.4 m/s for temperatures above 43°C. The base value was set such that the base line rating would equal 1,000 A given the other parameters (0.301 m/s). Note: the typical design parameter is also listed as 0.6 m/s.
V_a	1.57	1.57	1.57	Constant.
H_e	0	300	3,000	Range of habitable altitude in LAC, 300 is base assumption.
Lat	33.6	34	34.8	Range of Latitude for LAC
s_hr	12	16	19	Noon to 7pm. 4pm is assumed current base-case peak demand period. 7pm is considered as potential future peak demand period.
N	172	172	273	Day 172 = June 21, was solved as the day with the highest solar radiative force in the model. Day 272 represents the furthest day from that within the summer period of June, July, August, and September.
T_s	85	100	200	Represents range of standard to emergency conditions. Per SCE in [70], standard ratings for aluminum and copper conductors are 85 °C and emergency ratings of 130 °C. ACSR are 90 °C and 130 °C. ACSS are 120°C and 200°C. Per IEEE [32], the highest value to be used in this approach is 200°C.
D_o	0.01	0.03	0.045	Range of values listed in [79] Appendix B Conductor Tables. Larger diameters include more conductor strands and are for higher kVA ratings. More conductor strands would have lower resistance in practice, although those parameters are independent

				in this model. Base value assumed at approximately top quartile of strand count classes consistent with R(25°C) range: Mallard, Cardinal, Rail, and Condor.
ε	0.2	0.8	0.9	Range provided in IEEE [32] Sec 5.4 Conductor emissivity and absorptivity, where 0.8 is used by convention in the absence of field measurement. Value increases with age and pollution.
α	0.2	0.8	0.9	Range provided in IEEE [32] Sec 5.4 Conductor emissivity and absorptivity, where 0.8 is used by convention in the absence of field measurement. Value increases with age and pollution.
R(25°C)	3E-05	7E-05	2E-03	Range as listed in [80] Table "Electrical Data for ACSR Conductors", Turkey to Bluebird. Base value assumed at approximately top quartile of strand count classes: Drake, Mallard, Tern, Condor, and Rail.
R(%)	10	16	25	Estimated to be consistent with listed R(25°C) and R(75°C) values as listed in [80].

Changes in ampacities were estimated as a linear percent decrease per 1°C increase in ambient air temperature based on sensitivity analysis of the IEEE thermal balance model. Model sensitivity to the input parameters is shown in Figure 22, where the most significant factors were the conductor resistance at 25°C, maximum allowable temperature, and diameter, all of which are associated with higher kVA rated lines. Ambient air temperature was the fourth most significant factor, followed by emissivity, solar hour, wind speed, change in resistivity, absorptivity, and elevation above sea level with ~5% effect. Latitude was not significant. The sensitivity of conductor ampacity to air temperature is shown in Figure 22, where all parameters were simultaneously set to the lowest, base, and highest conditions resulting in ampacity ratings of 71, 1,000, and 2,757 Amps respectively. Linear approximations of the three lines yields slopes of -0.27%, -0.87%, and -2.1% Amps per 1°C respectively with R^2>0.98. Therefore, all transmission lines above 200 kV were classified to decrease in ampacity at a rate of 0.6±0.3% per 1°C, and all transmission lines below 200 kV were classified to decrease in ampacity at a rate of 1.5±0.6% per 1°C.

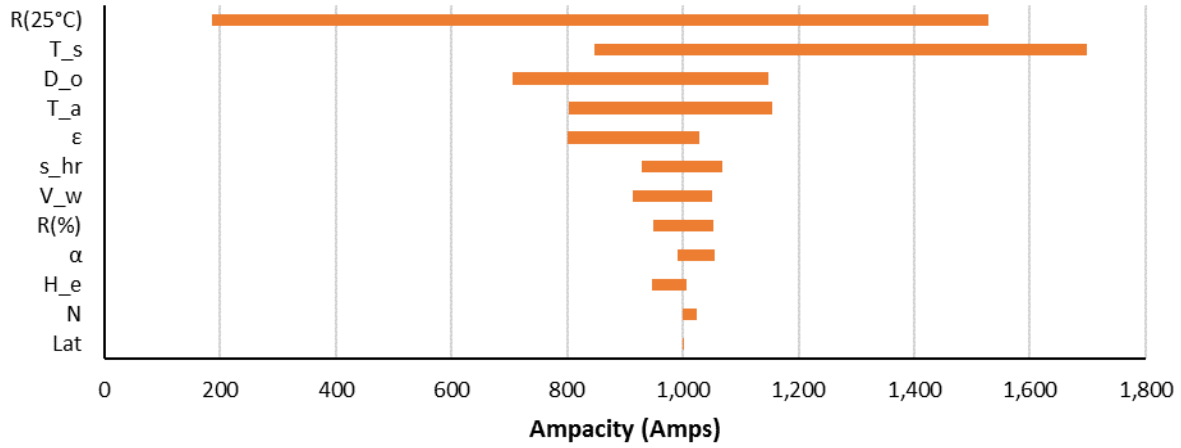

Figure 21. Sensitivity of Transmission Line Ampacity Input Parameters.

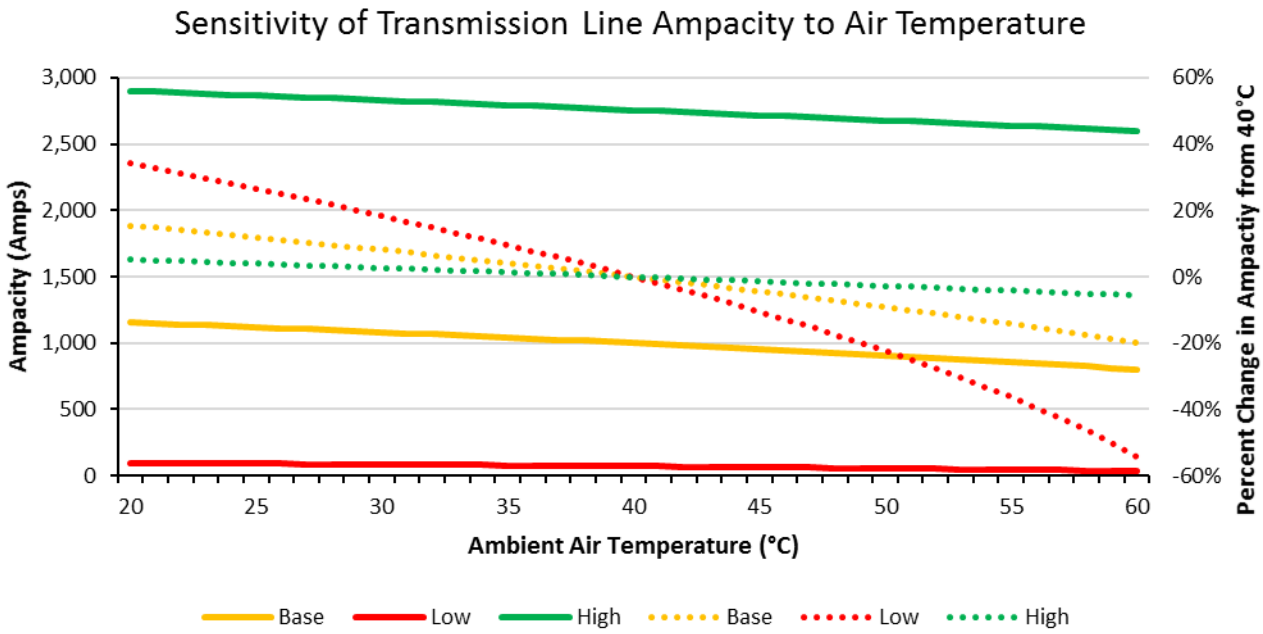

Figure 22. Sensitivity of Transmission Line Ampacity to Air Temperature.

Transmission line vulnerabilities were also assessed, similar to substations, by estimating percentage increases in temperature-adjusted load on the individual lines. Temperature-adjusted load was defined as the base or forecasted load, plus the derating factors previously stated for higher and lower voltage lines. Initial loadings on transmission lines were estimated based on the estimated values at high voltage substations. Load was allocated to lines under the assumption that the load on all of the lines was equal to the sum of the values at all of the high voltage substations. In other words, the assumption is that all of the load flow was collectively in one direction from the transmission lines, through the high voltage substations, and further into lower voltage delivery infrastructure. Specifically, load was allocated to lines from substations by dividing the MWh values in each substation cluster evenly amongst the

endpoints of the 185 lines as defined in the NHS database file. The endpoints at the border of the county were excluded such that those lines had only one allocation. All other lines had two endpoints. Factors such as differences in line impedance, or operator controls for routing, were not considered. Because absolute transmission line capacity (MVA) data were unavailable, the results of this analysis were only produced in terms of relative percentage changes in loading and did not estimate whether any lines would actually be loaded beyond their capacity. New line construction was not forecast, but rather considered in mitigation and adaptation options.

4.3 Results

4.3.1 Generation

Of LAC's 13.5 GW of local power generation, up to 240 MW (1.8%) is vulnerable to rises in air temperature. As shown in Figure 23, for worst-case 2060 temperature projections under RCP 8.5, the majority of the vulnerable generation capacity is the 23 combined cycle and 15 combustion natural gas plants located in the San Fernando Valley and on the outer basin areas away from the ocean. Please note that the figure is shown in units of MW, not percentages, so derating values are a function of both temperature change and size of the plant. Heat wave temperatures affecting natural gas plants ranged from 40-53 °C (104-127 °F) in that scenario, indicating that individual stations could experience 3-9% less capacity than their summertime ratings for 40°C (104 °F). Total combined weighted capacity of natural gas plants would be 69-104 MW less than present ratings. The 90 solar PV generation plants are also vulnerable, most significantly in Antelope Valley. Maximum temperatures at solar PV plants ranged from 44-54 °C (111-129 °F) in the model, and if such extreme temperatures were realized, individual solar PV output could be 1-8% lower than rated. The total spatially weighted capacity of solar PV on the realistically hottest day would be 8-45 MW less than present ratings.

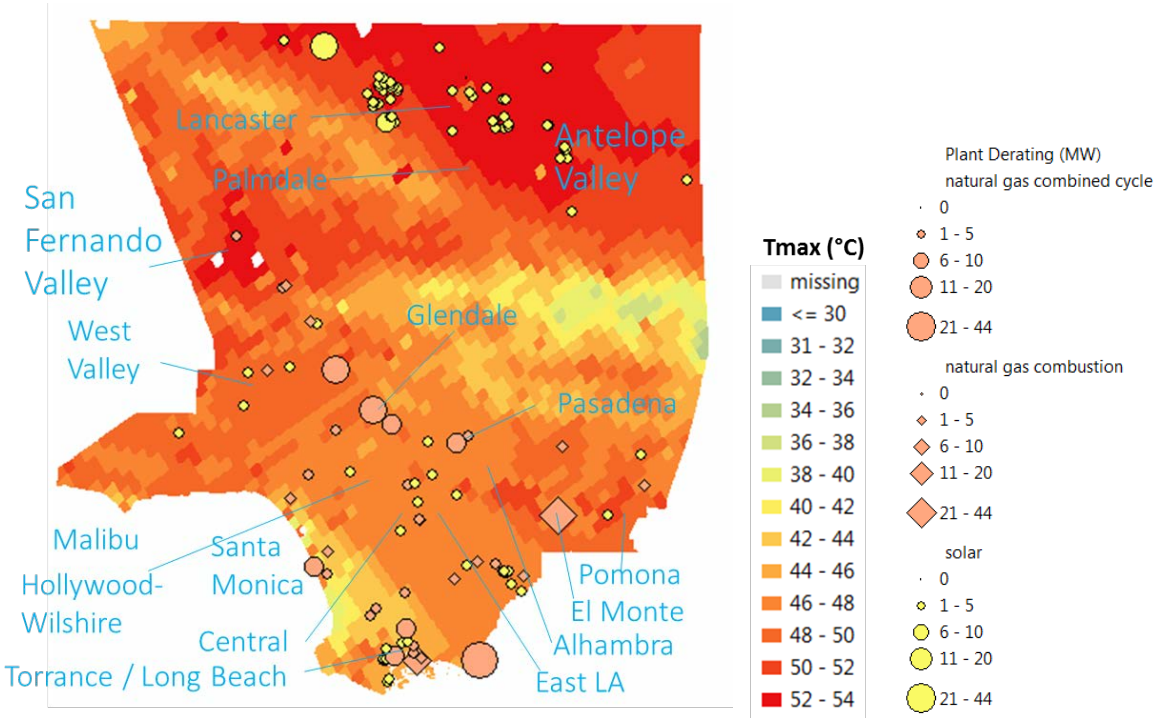

Figure 23. Map of worst-case losses in plant capacity for composite temperatures in 2060 RCP 8.5.

The expected capacity loss on a realistically hot day in the model for 2060 RCP 8.5 was 110 MW, or approximately half of the total vulnerable capacity when analyzed in terms of the composite thermal image. Total system capacity projections are listed in Table 16 for all generation in LAC for average temperature rise and hottest days temperatures in each time period and RCP. According to the range of temperatures already observed in the historical period, 75 MW of capacity is already vulnerable to temperatures in excess of 40°C given current heat waves. Average plant capacity losses are shown in Figure 24, overlaid to the average warming projection by 2060 under RCP 8.5, indicating total capacity would be 35 MW lower on average. Spatial differences for time periods and RCPs with less severe warming are fairly uniform and can be inferred specifically by considering temperature differences shown in Figure 9.

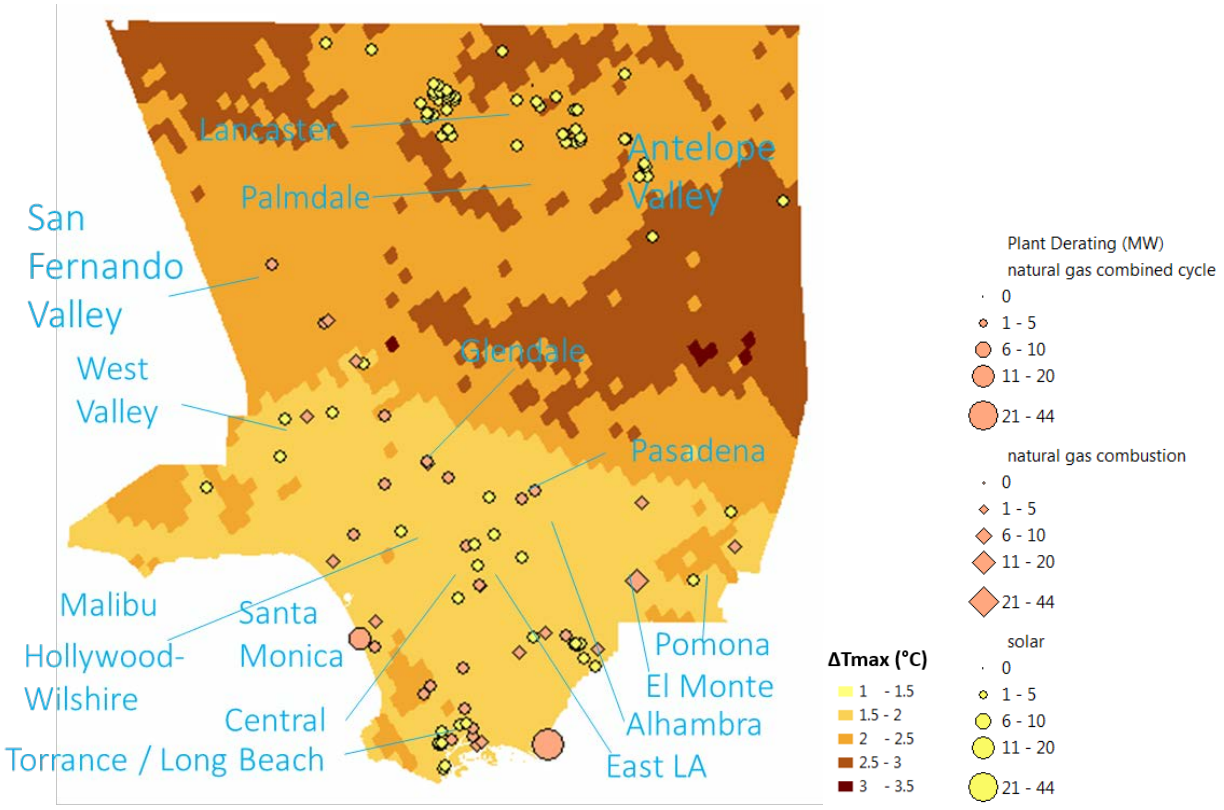

Figure 24. Map of average loss of plant capacity for average warming by 2060 in RCP 8.5.

Table 16. Total Generation Vulnerabilities by time period and RCP for hottest day projections.

Time Period	RCP	Average T_{max} at all plants °C (°F)	Average T_{max} increase at all plants °C (°F)	Total capacity (MW)	Loss from >40°C (MW)
1981-2000	-	44.3 (111.8)	0 (0)	13,428	75
2021-2040	4.5	45.5 (113.9)	1.2 (2.1)	13,409	94
2021-2040	8.5	45.6 (114.1)	1.3 (2.3)	13,407	96
2041-2060	4.5	46.0 (114.8)	1.7 (3.0)	13,400	103
2041-2060	8.5	46.4 (115.5)	2.1 (3.8)	13,393	110

Los Angeles County's current local reserve margin was estimated to be negative by 0.8-5.7 GW in the base period, inclusive of other sector peak demand as the lesser of 5 GW or 1/2 (R&C), and that shortage could increase up to 15 GW by 2060 without investments in local power resources. As listed in Table 17, the minimum increase in peak hour generation capacity needed to meet future demand is 3.9 GW by 2040 and 4.6 GWh by 2060 for the low growth, high efficiency scenarios under RCP 4.5. The details of the factor contributions are explained in the prior sections. While it is possible to invest in generation capacity outside of LAC and long-distance transmission imports to meet future peak demand, doing so exclusively would result in substantially negative LRMs, such that less than half of the county's power demands would be met locally if imports were unavailable for some reason.

Table 17. Estimated Local Reserve Margins for time period, population, and demand scenarios.

Time Period	Local Reserve Margin GWh (%)			
	Department of Finance - Low	Department of Finance - High	SCAG - Low	SCAG - High
Base	-0.8 (-6%)	-5.7 (-42%)	-	-
2021-2040	-3.9 (-29%)	-10 (-77%)	-4.7 (-35%)	-12 (-87%)
2041-2060	-4.6 (-35%)	-12 (-93%)	-6.3 (-47%)	-15 (-115%)

*Includes other sector peak demand as the lesser of 5 GW or 1/2 (R&C)

4.3.2 Substations

Of LAC's 410 substations, 99% are vulnerable to air temperatures over 40 °C (104 °F), including reductions in loadability of up to 20% of their kVA ratings. As shown in Figure 25, for worst-case temperature projections, 2060 RCP 8.5, 24 unknown substations (presumably low voltage convective air cooled) and one 138 kV substation, across Antelope Valley, San Fernando Valley, El Monte, and Pomona could experience temperatures up to 51-53 °C (123-127 °F) and be safely loadable at 16-20% less than their summertime 40°C kVA ratings. Substations within 5 km of the Santa Monica beach were projected to have capacity losses no more than 5% as temperatures were not projected to rise above 42 °C (108 °F). As shown in Figure 26, results at different time periods and RCPs were fairly uniform with a range of loadability reductions of up to 2% kVA. The majority of substations, 70%, were projected to experience average capacity losses of 1.5-3% kVA due to average warming, and 60% of substations, were projected to

experience capacity losses of 6-12% during heat waves due to temperatures in excess of 40°C (104 °F).

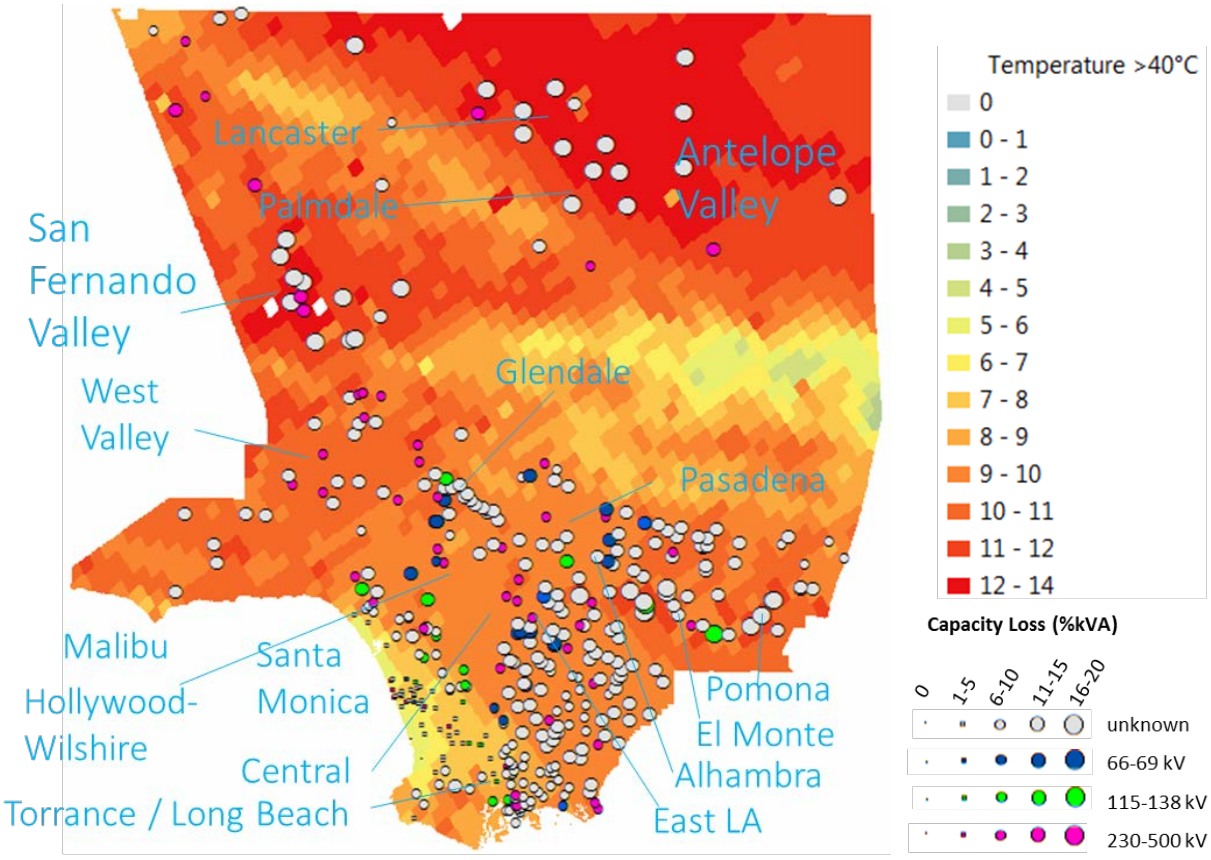

Figure 25. Map of worst-case losses of substation capacity for composite temperatures in 2060 RCP 8.5.

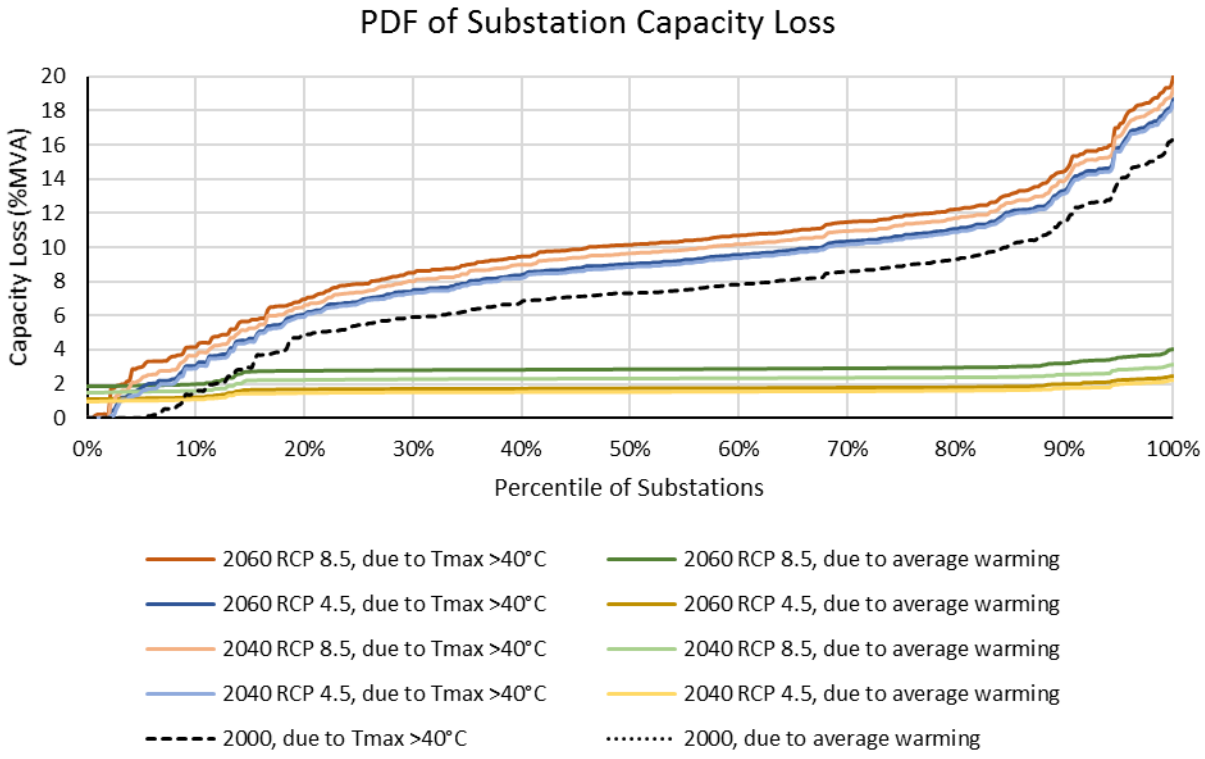

Figure 26. Empirical Probability Distribution Function of substation vulnerabilities by time period and RCP.

Year 2000 average warming values are all equal to zero and may not be visible.

Despite population growth, climate change, and warming, results indicate that substations in developed areas can still experience lower loads by 2060 if the high energy efficiency scenario is realized. As shown in Figure 27, the Voronoi Tessellation process resulted in 36 and 173 cluster areas for high- and low-voltage substations respectively, with base-period peak demand allocations as shown. The percent change differences in loading on substations are shown in Figure 28 and Figure 29. The low demand scenarios resulted in up to 21% reductions on substations in the in-basin region, with most increases occurring in the northern Palmdale, Lancaster, and San Fernando Valley Areas. The major difference between the Department of Finance and SCAG projections was all increases in loadings on substation clusters throughout CZ 9 from West Valley to Pomona, which are very clear visually in the low-demand scenarios. There were also a few clusters in the southern Torrance and Long Beach areas that had projected increases in the SCAG projections as well. Of course, without improvements in building and appliance energy efficiency, both population growth scenarios resulted in significant increases in loading on substations as shown in the high demand cases.

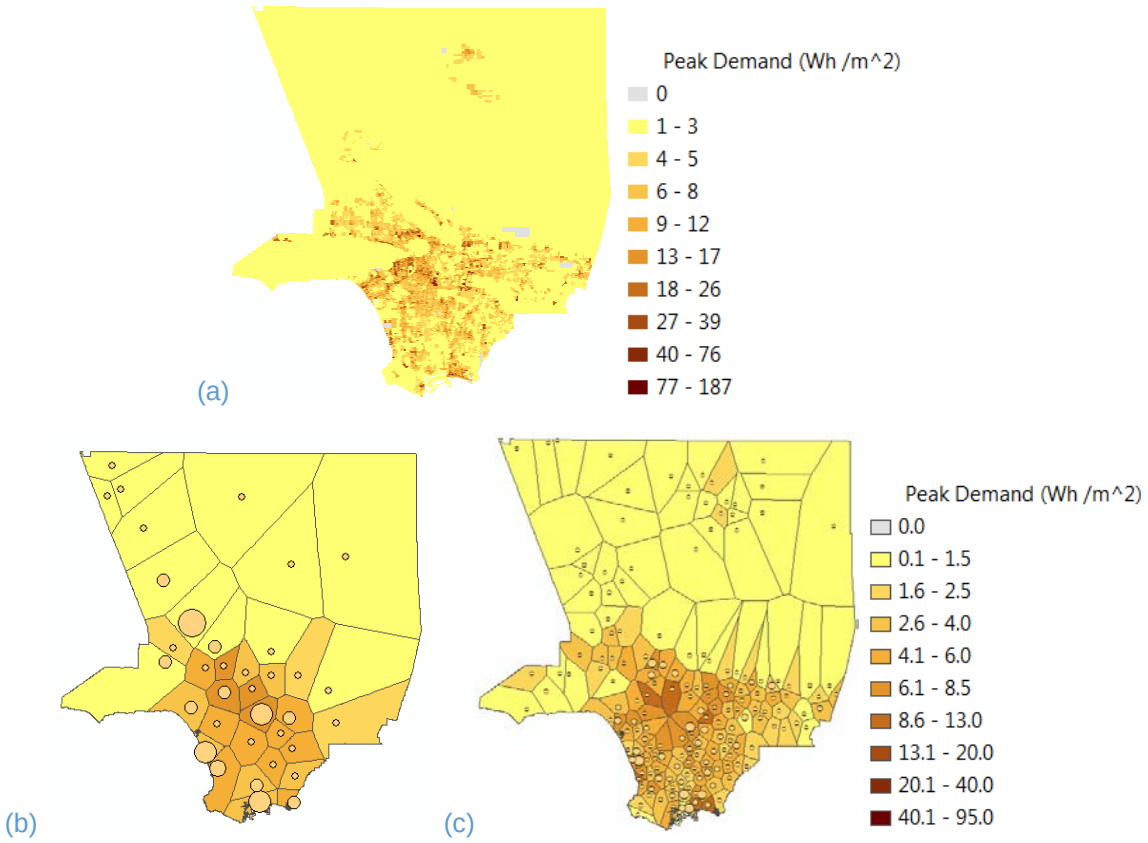

Figure 27. Base period model peak demand for composite heat image in (a) CBGs, (b) high-voltage substation Voronoi areas, and (c) low-voltage substation Voronoi areas.
Larger circles indicate higher quantity substations in the cluster.

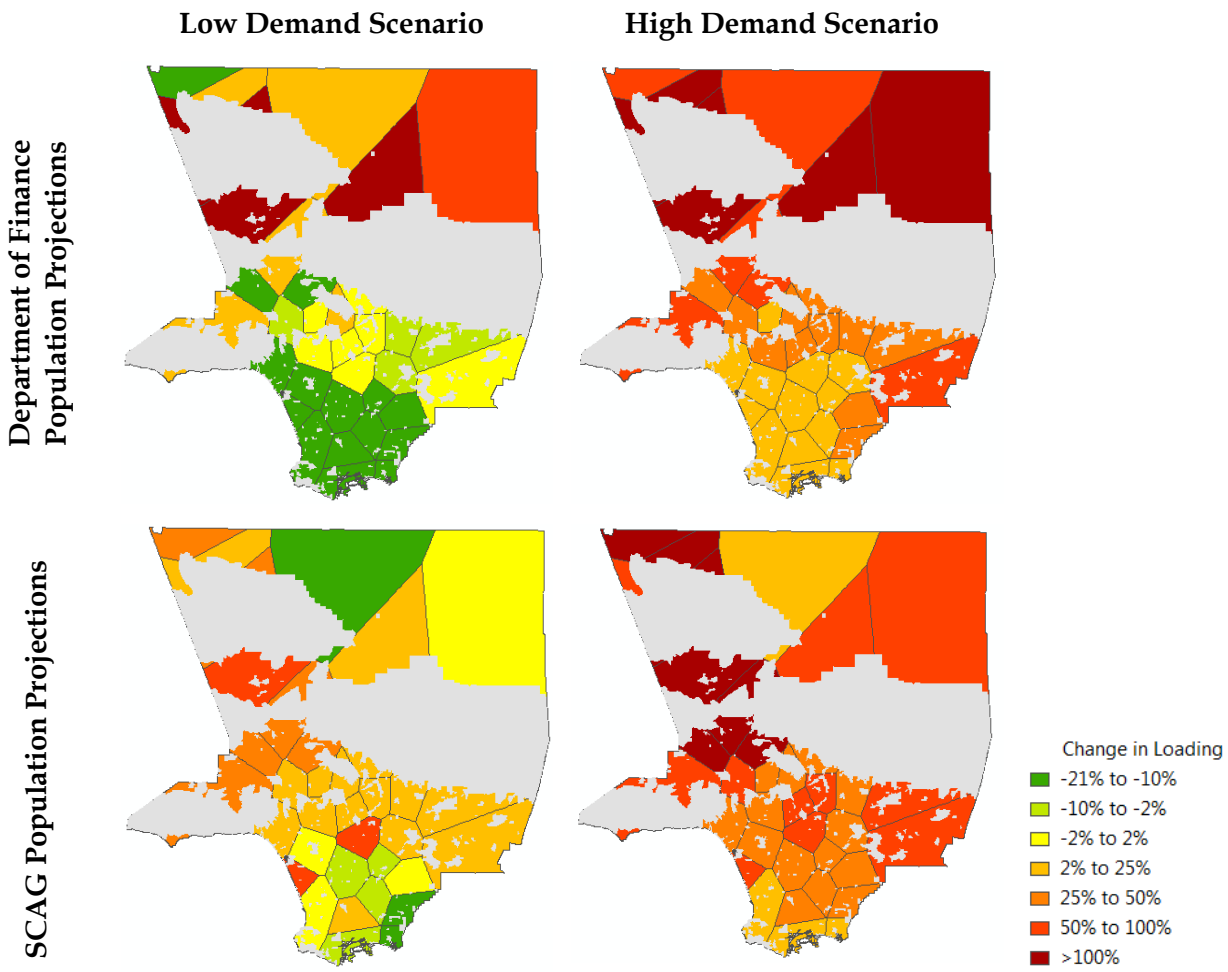

Figure 28. Percent change in high voltage substation loading for 2060 scenarios.

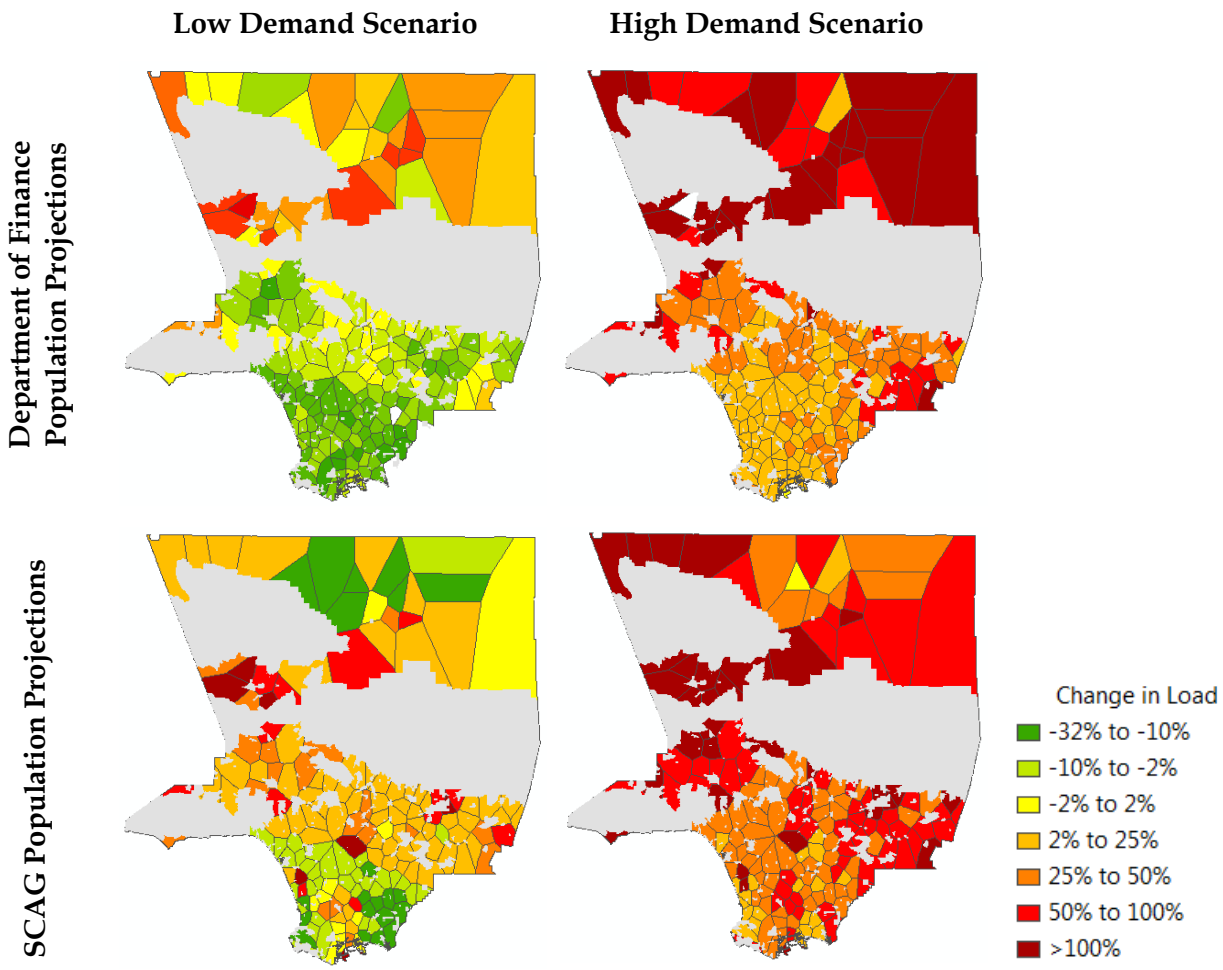

Figure 29. Percent change in low voltage substation loading for 2060 scenarios.

Over half of SCE's substations were identified as being at risk of overloading during the peak hour of the summer under current conditions, i.e., this summer 2018. As shown in Figure 30, the majority of substation areas throughout LAC, where data were available, were projected to have substations operating at a weather-derated load factor of 1 to 1.2 for the hottest historical heat wave temperatures. Components are technically overloaded at this point and automatic outage switching may occur within 24 hours to 30 days if loading continues at this level, depending upon switchgear settings. Due to high operating temperatures, substation mineral oil may experience accelerated thermal wear [81], and depending upon system redundancies, neighborhoods may not be n-1 reliable in this condition.

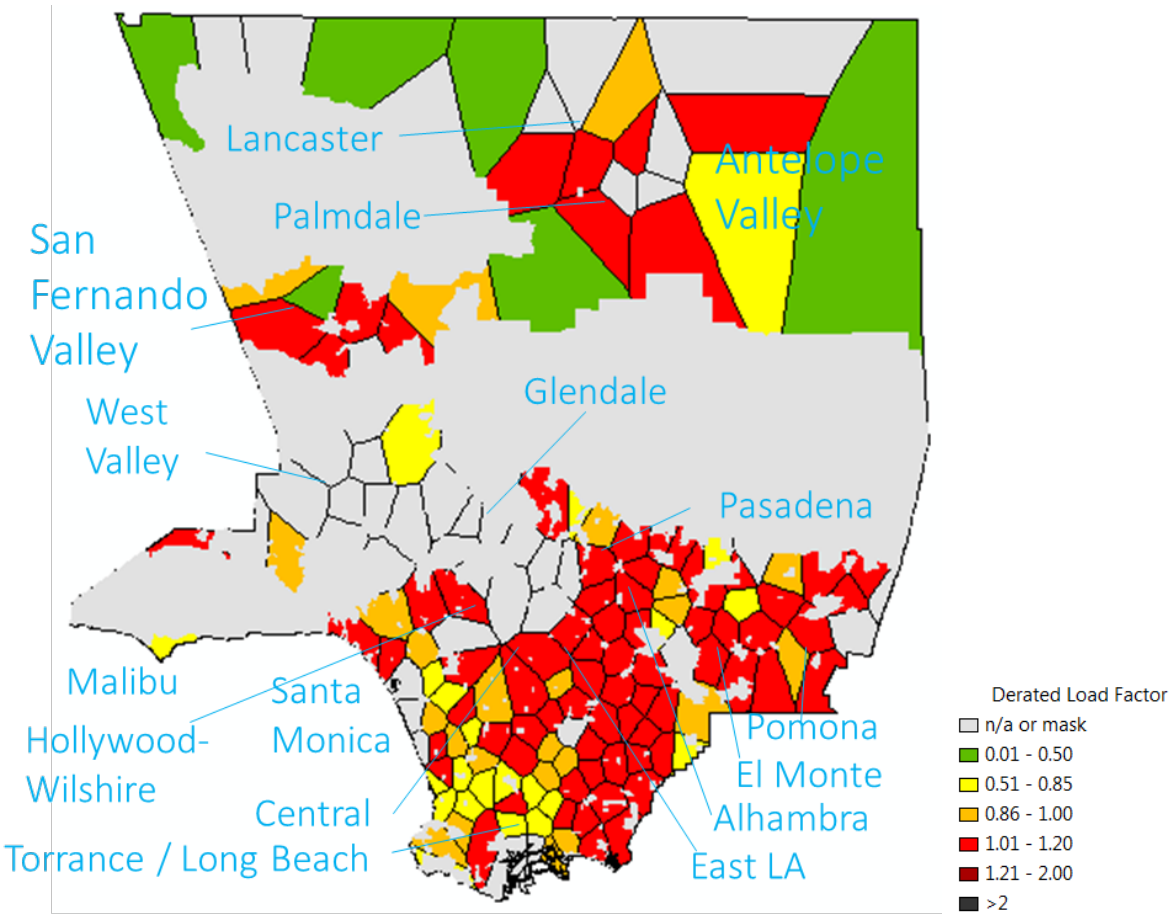

Figure 30. Map of today's substation risks. Current substation load factors derated for composite historical heat waves. I.e., this is what the peak hour could look like this summer in any spot on the map.

In all future scenarios, by 2040 and 2060, at least a few substations were projected to exceed tolerance for automatic outage trips with a derated load factor in excess of 2. As shown in Figure 31, with implementation of high efficiency measures, most substation clusters in the central basin area were projected to operate with load factors below one during the worst heat wave conditions. As shown in Figure 32, in all 2060 cases, the Santa Clarita and San Fernando Valley areas were projected to have several substations exceed automatic outage tolerances. Without energy efficiency improvements both population projections result in a majority of substations being heavily overloaded. With energy efficiency improvements, the Palmdale and Lancaster areas are vulnerable to automatic outages in the Department of Finance population projections by 2060, whereas the basin area is vulnerable to automatic outages in SCAG population projections. Both result in emergency (load factor >1.2) conditions during the peak hour of a heat wave in both locations.

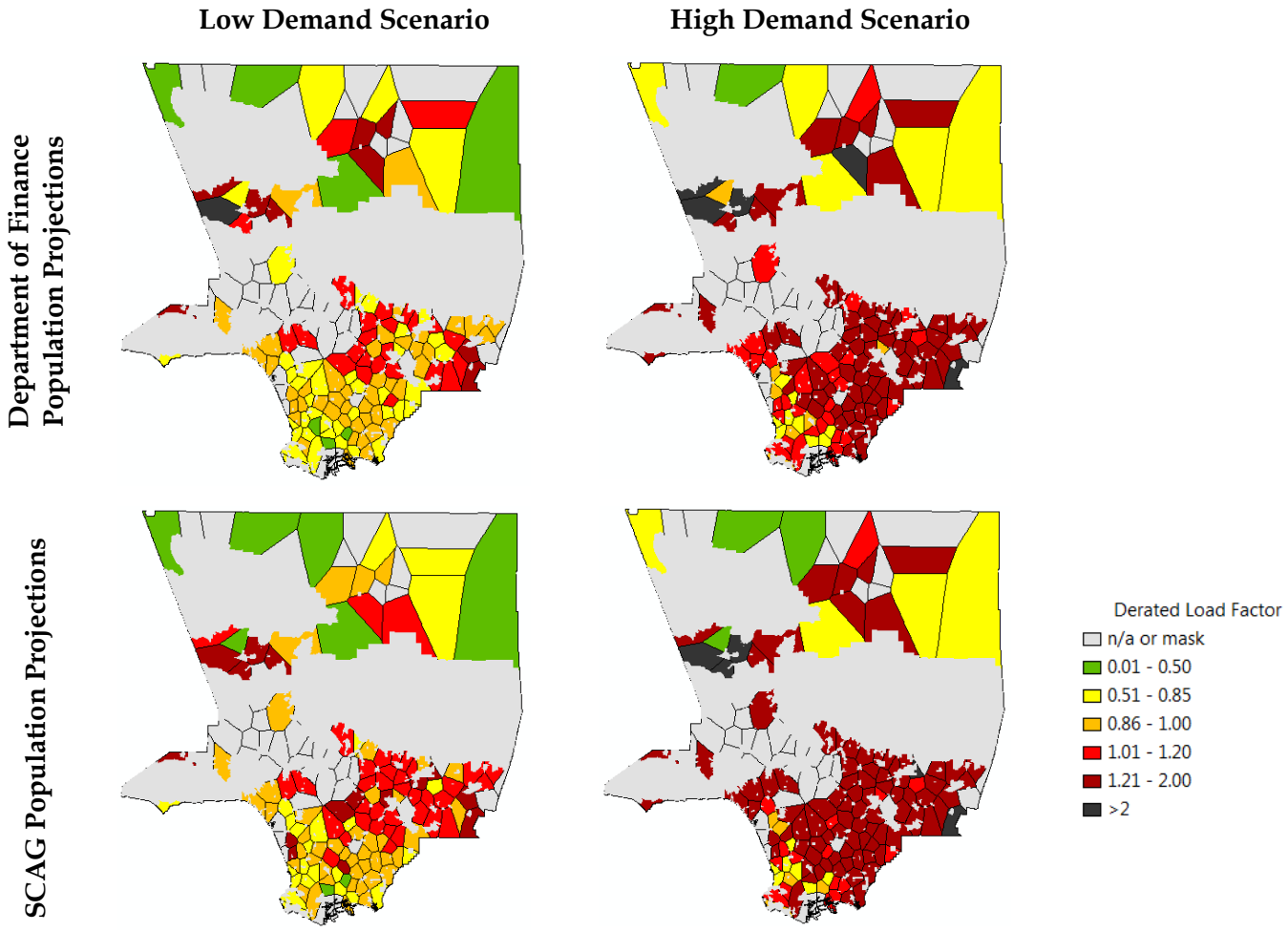

Figure 31. Maps of substation risks in 2040. Future substation load factors derated for composite worst-case 2040 heat waves. I.e., this is what the peak hour could look like during a heat wave in 2040.

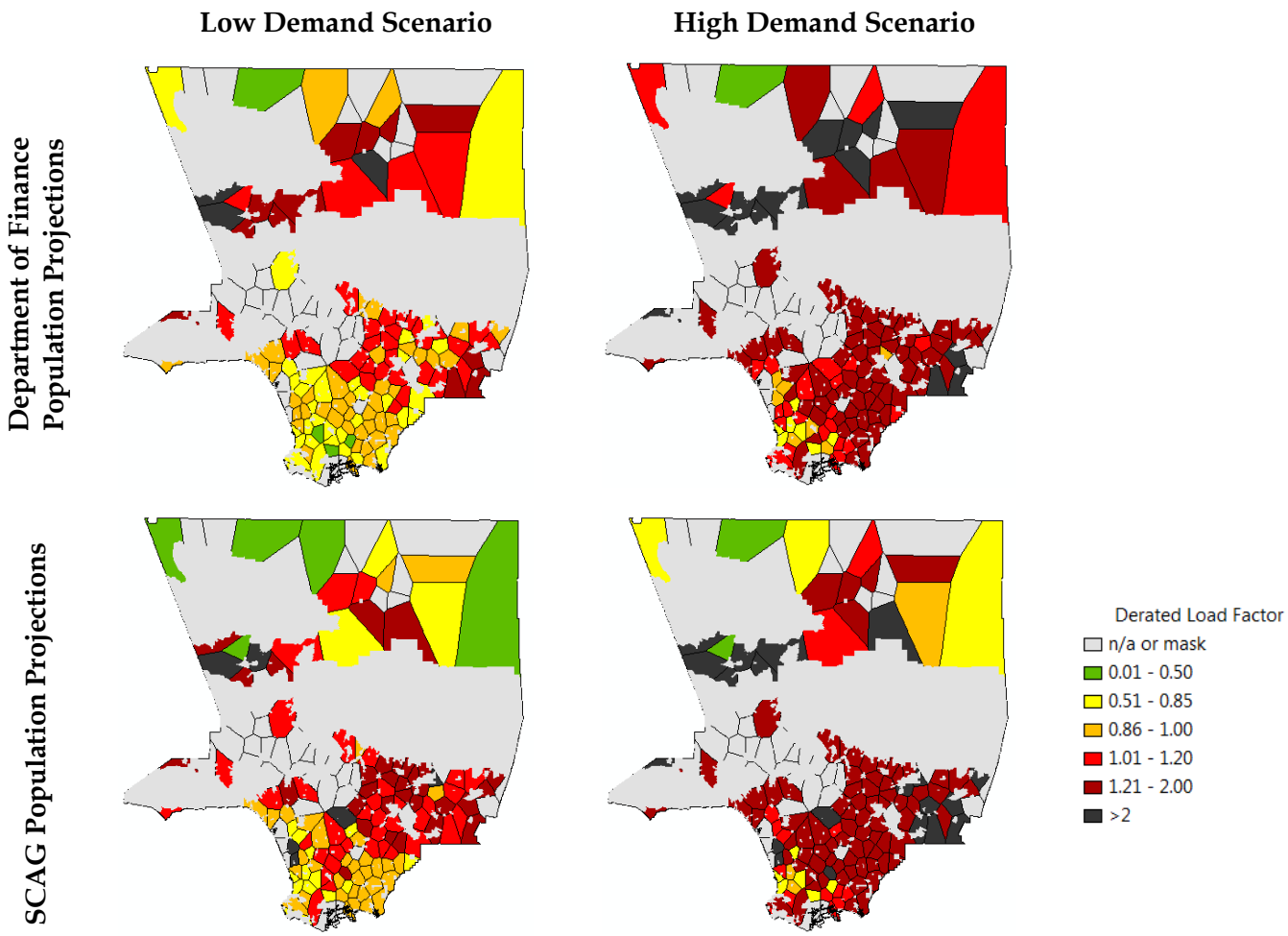

Figure 32. Maps of substation risks in 2060. Future substation load factors derated for composite worst-case 2060 heat waves. I.e., this is what the peak hour could look like during a heat wave in 2060.

4.3.3 Transmission Lines

Of LAC's 185 transmission line segments and 3.5 million meters (2,200 miles) of conductor length, 99% of conductor length, and all segments, are vulnerable to air temperatures over 40 °C (104°F), including reductions in loadability of up to 20% of ampacity ratings. As shown in Figure 33, for worst-case temperature projections, 2060 RCP 8.5, high voltage transmission lines (>200 kV) across Antelope and San Fernando Valley could experience ambient air temperatures up to 47-54 °C (117-129 °F) and be safely loadable at 4-8%±50% or 2-13% less than their summertime 40°C ampacity ratings. The lower voltage transmission lines (< 200 kV) that are most vulnerable to heat waves are located around Central and West LA, with projected ambient air temperatures up to 47-50 °C (117-122 °F), and corresponding reductions in ampacity of 10-15%±40% or 6-20%. As shown in the probability distribution function curves in Figure 34, results at different time periods and RCPs were fairly uniform with a range of loadability reductions of up to 2% of ampacity on any line. Approximately 67% of conductors by length were projected to experience average ampacity losses of 0.4-1.2% ±50% or 0.2% to 1.8% due to average warming, and 33% were projected to experience average ampacity losses of 1.5-3%

±50% or 0.8-4.5%. As much as 25% of conductor length could experience ampacity reductions of up to 15% due to some length of the segment experiencing temperatures above 47 °C (120 °F) during future heat waves.

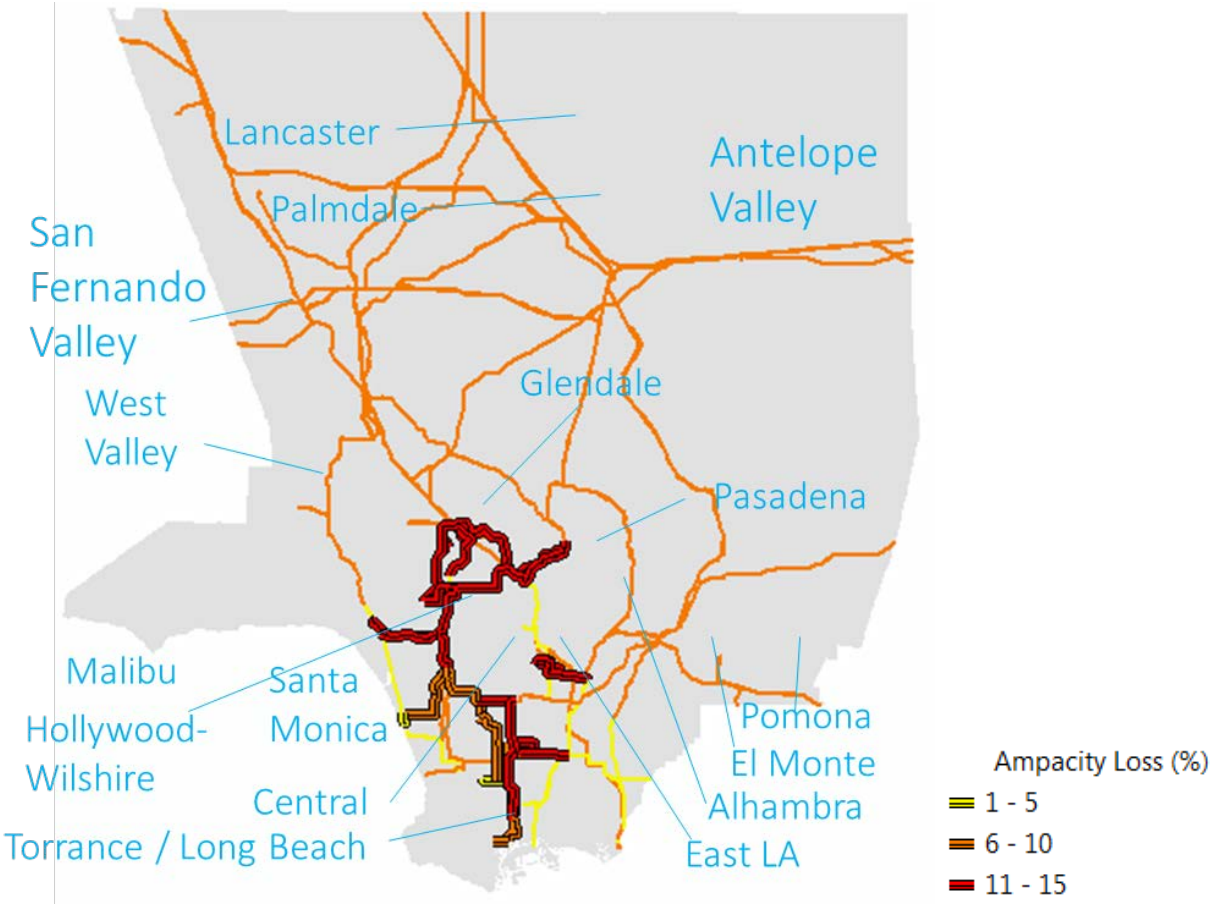

Figure 33. Map of worst-case losses of transmission line ampacity for composite temperatures in 2060 RCP 8.5. Percent loss values shown are based on average derating factors. High voltage (≥230 kV) lines' values should be considered ±50%, and low voltage (<230 kV) lines' ±33%. I.e., 6% refers to 3-9% or 4-8% accordingly. Low voltage lines are shown in bold in this figure; see Figure 20 for map of more specific line voltage ratings.

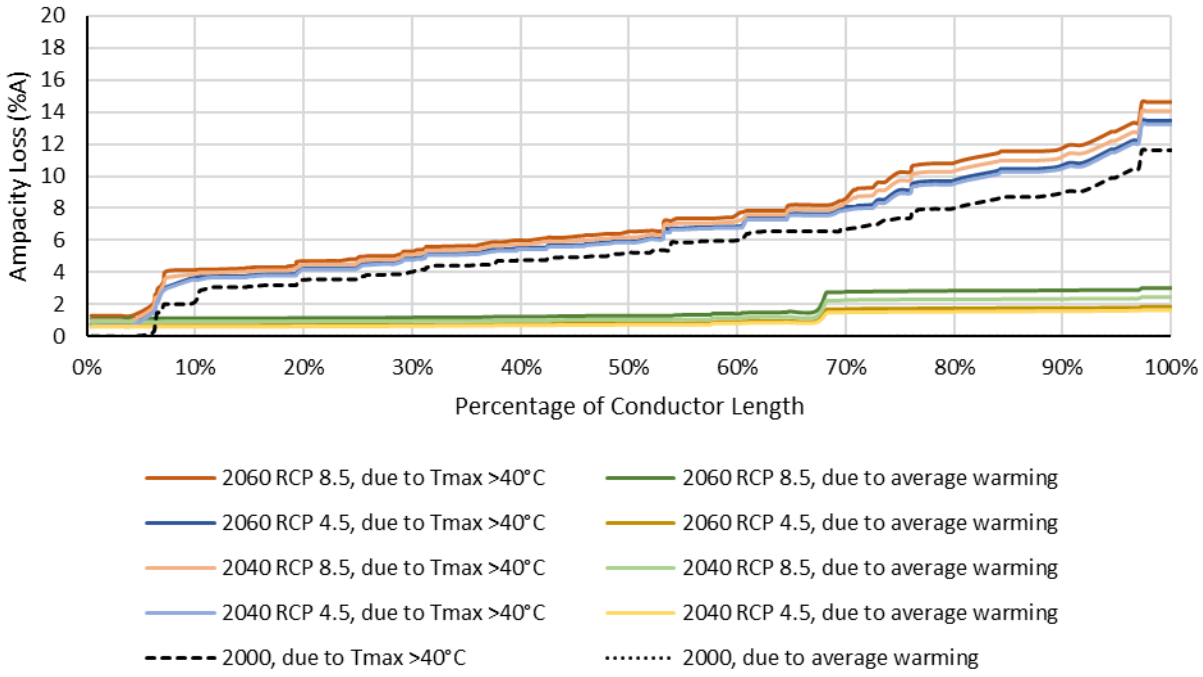

Figure 34. PDF of transmission line vulnerabilities by time period and RCP. Low voltage (<230 kV) and high voltage (≥230 kV) lines are shown together in figure. Uncertainty of ±40% and ±50% are applicable respectively. Year 2000 average warming values are all equal to zero and may not be visible.

Results for long-term forecasts for transmission line loading mirrored results closely as for substations. As shown in Figure 35, despite population growth, climate change, and warming, transmission lines in the basin can experience up to 21% lower weather-adjusted loads by 2060 if the Department of Finance population growth projections are realized with high energy efficiency gains. In all scenarios, major population growth in the northern region of the county equated to increased loading on those lines up to a factor of two.[3]

[3] Technical note: One line in Pomona had endpoints that were at the edge of the county boundary only, so the allocation method resulted in zero values. The lines values were manually updated to be equal to an adjacent line's, as it was the research team's opinion that that result was due to error in the GIS data.

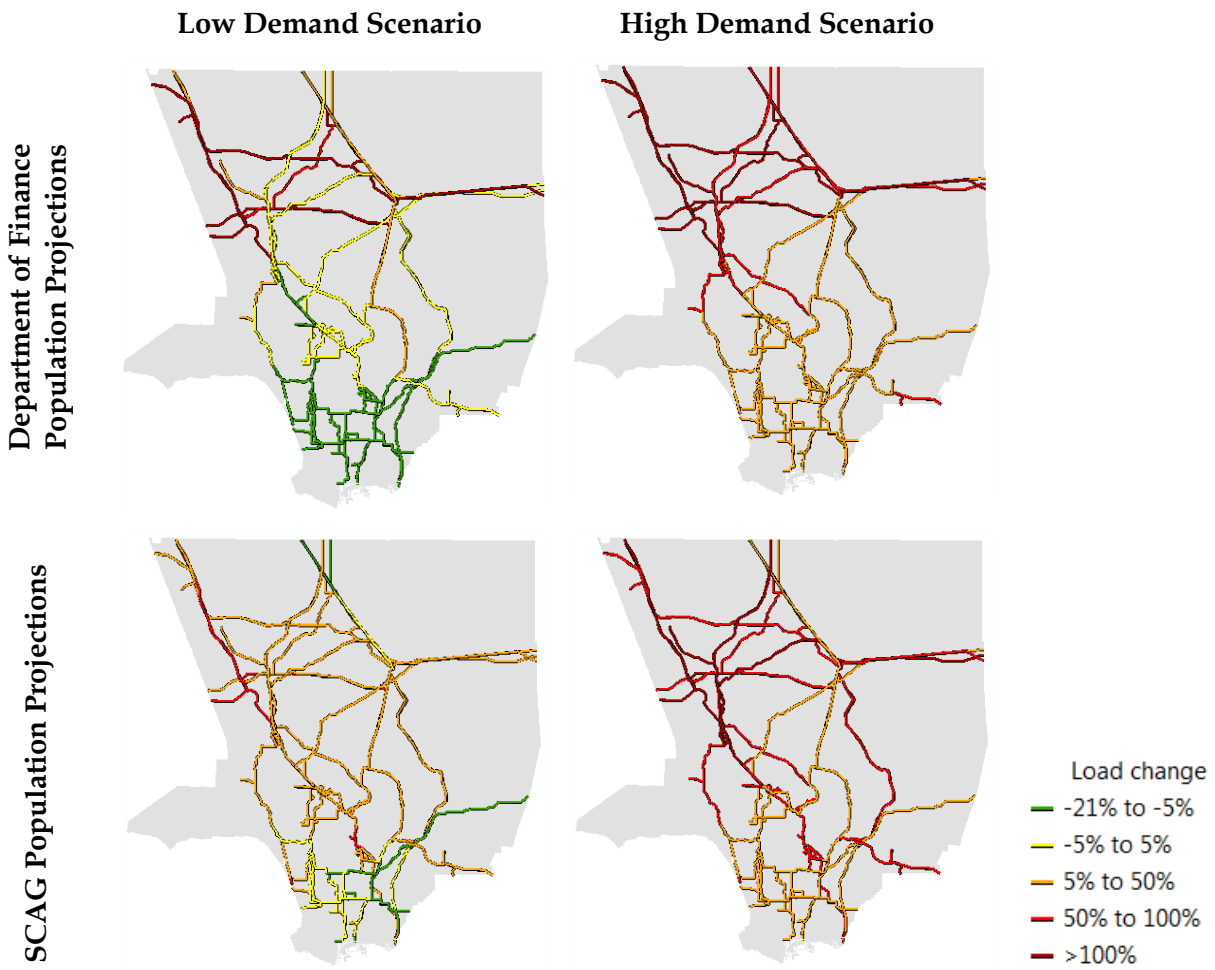

Figure 35. Percent change in transmission line temperature-adjusted loading for 2060 scenarios.

4.4 Conclusions

The overall vulnerability of Los Angeles's electricity infrastructure to rising air temperatures is 2-20% of rated capacity. The low range 2% vulnerability value is attributable to the reduction in local generation resources. Natural gas plants could lose up to 6% of their rated generation capacities, or approximately 2% of LRMs. The high range vulnerability value of 20% is attributable to reduced safe operating loads on substations and transmission lines. As shown in Figure 36, substation cluster areas around El Monte and in the northern half of the county could experience the highest temperatures during heat waves, up to 53 °C (127 °F). Based on the assessment of SCE's present substation loadings in Appendix D, there are 6 substations that are already operating with load factors over 100% in those areas at immediate risk of a heat wave. Dozens more substations are operating at or near capacity throughout the county with the potential for 10-15% loadability loss due to high ambient air temperatures in the event of a record-breaking heat wave. The only infrastructure in the region that is not at risk of heat waves are the components within a few miles of the western-facing coast of Santa Monica Bay.

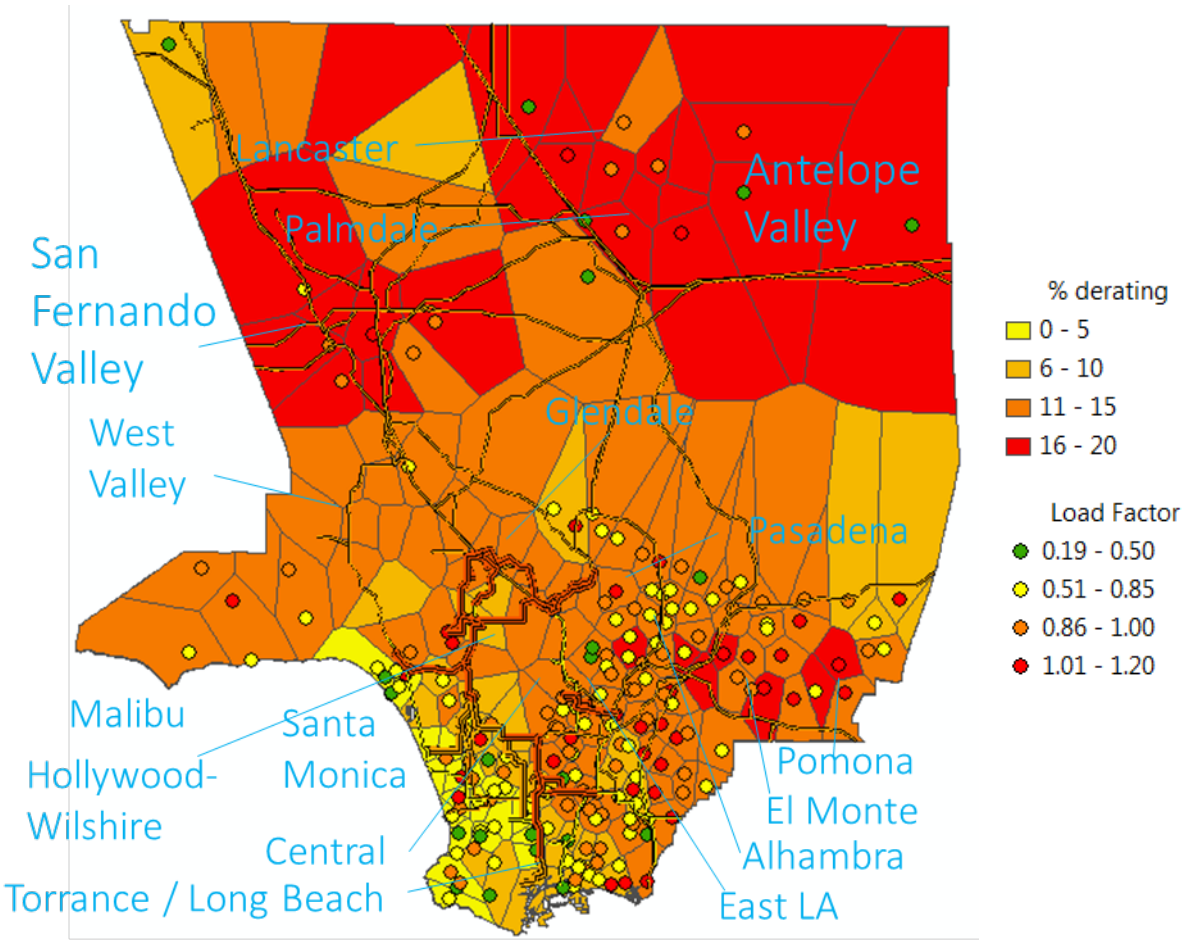

Figure 36. Map of worst-case percent derating in lines and substations from historical heat waves overlaid with present substation load factors.

Long-term loading on infrastructure components is more susceptible to population growth and changes in technology that affects peak demands than it is to rising air temperatures. As shown in Figure 37, if the Department of Finance's population projections are realized, and significant efficiency measures are implemented, then lines and substations throughout the basin could be relieved from approximately 4 GWh peak hour demand in the base period to 3.33 GWh by 2060, or by as much as 32% in certain clusters, including future temperature rise. Net peak demand in the in-basin area remained approximately the same in the SCAG projections. The northern regions of Lancaster, Palmdale, and Santa Clarita were projected for 300-900 MWh increase in peak hour load (50%-150%), as well as 110 MWh (50%) increase in the far west. The central CZ 9 region from West Valley to Pomona's peak demand was projected to decrease from 7.5 GWh in the base period to 7.2 GWh in the Department of Finance population projection, and increase to 9 GWh in the SCAG projections.

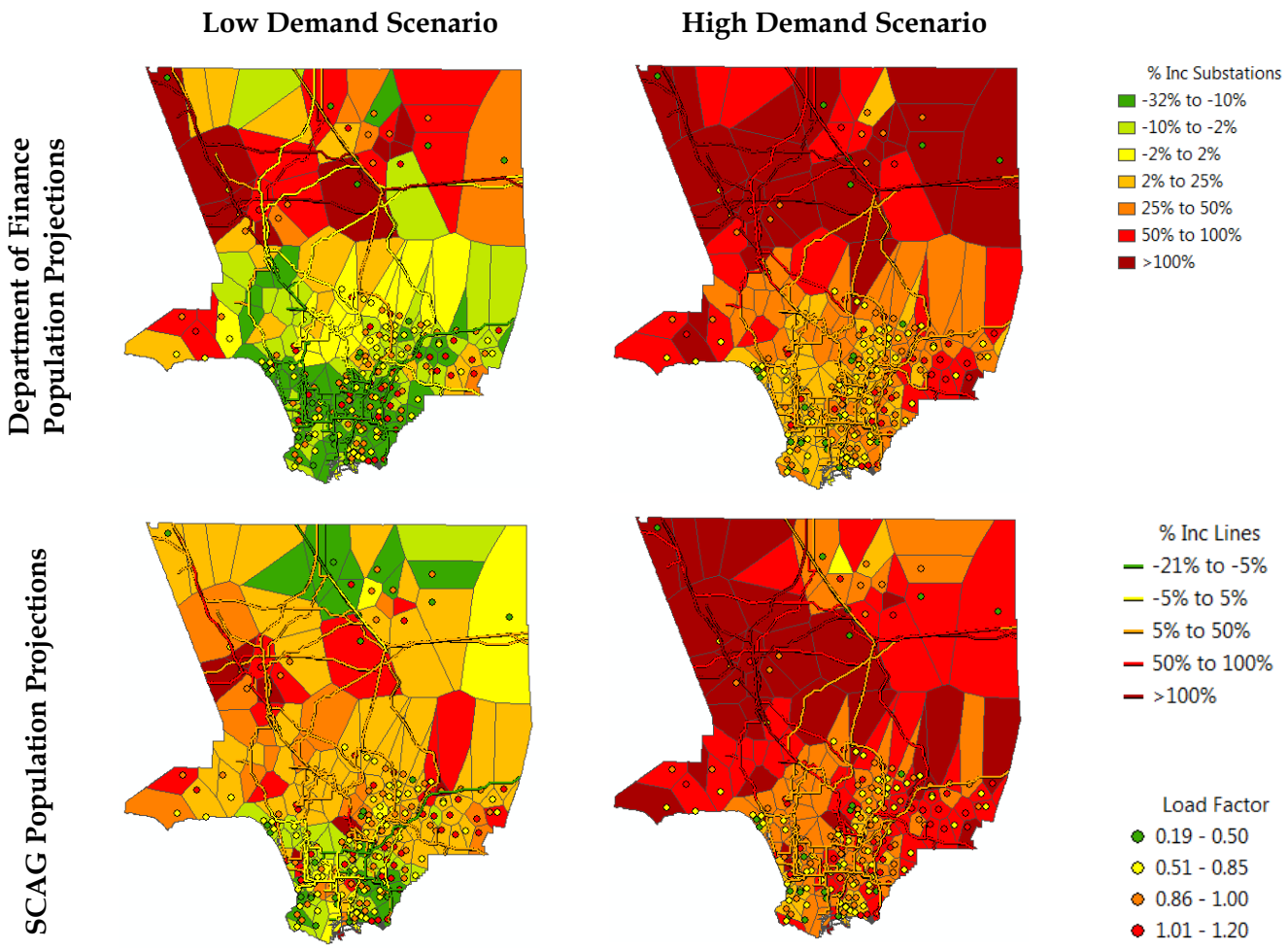

Figure 37. Maps of percent change in substation and transmission line temperature-adjusted loading for 2060, overlaid with present substation load factors.

5: Conclusions – Mitigation and Adaptation

Climate change mitigation is defined by the IPCC as activities to reduce greenhouse gas emissions or enhance sinks, and adaptation as either making system adjustments in response that moderates harm or exploits beneficial opportunities [46]. Mitigation of greenhouse gasses in the electric power sector are primarily being achieved through displacement of fossil fuel-burning as a means of electricity production with renewables or cleaner fossil fuel burning systems relative to coal plants such as natural gas plants, or by reducing demand such as by increasing energy efficiency in buildings and appliances. Adaptation may occur through increased usage and deployment of AC, and thus increase peak demand [39]. Moreover, the following may be arguably mitigation or adaptation: improved equipment cooling systems, implementation of distributed energy resources to supplement generation for increased peak demand, additional building shading, and higher building shell thermal efficiency standards [39]. All of these mitigation and adaptation activities further complicate long-term infrastructure planning.

There are many ways to maintain reserve margins in Los Angeles County, safe operating loads on the components, and reliable electric power services in general. Electricity is necessary to do work to run devices. If more work is demanded, then either more electricity must be produced, or the ability to do the work with less electricity (energy efficiency) must be improved. Several options in both categories, are listed categorically in Figure 38, both relative to electrical systems and urban form. The impacts between each of these options on reliability and other factors based on [61] are also included. The discussion in this section follows that framing of effects and trade-offs, and while several recommendations are provided for LAC specifically based on the preceding analyses, this list is not intended to be exhaustive nor advocate any particular option as a one-size fits all solution for regions that may have different constraints unique to their geographies. The aim of this discussion is to serve LAC, and California in general, to address their specific climate change-oriented policy goals and potential future challenges related to extreme heat.

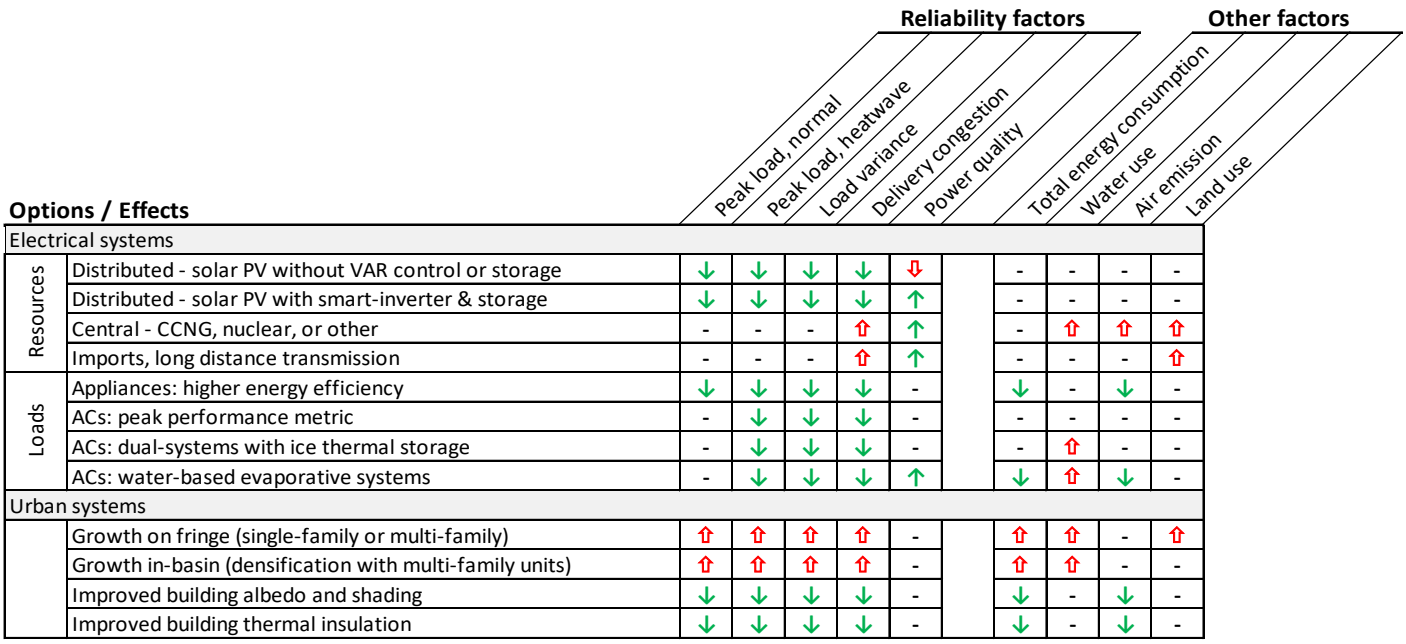

Figure 38. Climate change risk mitigation options and effects. Arrows indicate an increase or decrease in the factor. Solid green indicates higher efficiencies and or conservation of limited natural resources. Hollow red indicates the opposite.

5.1 Electrical Systems – Resources

An additional 0.2-6.5 GWh of peak hour demand was projected by 2060, dependent upon growth and efficiency factors. If new generation is to meet this demand, the major tradeoffs between generation technologies – distributed solar PV (with storage and quality controls) and centralized systems – in meeting demand are: land space requirements, delivery congestion relief, water usage, air emissions, and marginal capital costs. Solar PV can be installed on building roofs, whereas central systems require their own dedicated land space. When implemented at the distribution level, solar PV can power load directly without going through delivery components that are necessary for central systems. The net effect is a relative decrease in load from the perspective of the grid relative to demand, which will be important to monitor for reliability purposes going forward. Currently, the most prominent fast-ramping central generation technology is combined cycle natural gas plants, which consume water and emit various gasses into the atmosphere. Combustion-only natural gas plants could be implemented, which would not use water, but would be more sensitive to rising air temperatures, as well as less fuel-efficient and therefore cost more and produce more emissions per kWh. While levelized costs of solar PV are now at or below parity with bulk generation plants on a per kWh basis, the combined costs of solar PV with storage to provide 24/7 dispatchable energy and regulation services are still higher than traditional central generation plants [44]. However, in the future it is certainly possible that PV with storage becomes more competitive if EV penetration grows and as roof-top solar is deployed.

Expanding DER in existing buildings can probably be done in a more cost-effective manner in already well-developed and constrained areas. Most substations in LAC examined as part of

this study were identified as currently operating at or near capacity, and results indicated that many will have dangerously high load factors if significant population growth and/or rise in AC penetration occurs. While this study was unable to produce specific line load factors, if most lines were not constructed with significantly higher capacities than the substations operating in series with them, then the capacity expansion requirements of each are close to the other. While some substations may be able to be adapted with improved heat sinks, forced air, or water cooling systems, overhead power lines will still be vulnerable to overloading and outages.

If additional centralized generation is needed to meet additional peak demand in LAC in 2060, the cost of increasing delivery infrastructure capacity necessary to support more central generation, or long-distance imported power into the CZ9 area, could be quite significant at an estimated $10-130 million USD per substation and $1-3 million USD per mile of line length leading all the way out of the urban center [82], [83]. If SCE's DERiM load factors are correct, if the relative projected demand increases were reasonably modeled, and if increasing substation and line capacities are not readily feasible in the projected high-risk areas, then implementing DER in those areas could meet a broad range of energy policy objectives at the lowest total cost to the ratepayers.

Based on the results of this study, it appears reasonable to implement 0.9-1.1 GW of DER in LAC depending upon population growth by 2060 to supplement generation and delivery infrastructure capacity. Net peak demand in the in-basin area remained approximately the same in the SCAG projections. The northern regions of Lancaster, Palmdale, and Santa Clarita were projected to have a 300-900 MWh increase in peak hour load (50%-150%), as well as 110 MWh (50%) increase in the far west. The central CZ 9 region from West Valley to Pomona's peak demand was projected to decrease from 7.5 GWh in the base period to 7.2 GWh in the Department of Finance population projection and increase to 9 GWh in the SCAG projections. Implementation of the following DER would allow temperature-derivated load factors on SCE substations to be at or below one on the hottest days: 200-900 MW in Santa Clarita, up to 200 MW between Lancaster and Palmdale, and up to 700 MW in the SCE portion of CZ 9 from West Valley to Pomona, and 60 MW between Calabasas and Malibu.

Identification of specific site locations, total Watt-hours of necessary storage capacity to complement solar PV capacity, and considerations for network aggregation in supplying ancillary services should be the subject of follow-up implementation studies to ensure reliable service during near-peak hours. Circuits with a higher portion of commercial and industrial loads may be preferable for installation of DERs, as their load profiles may more closely match the PV generation profile (higher mid-day) allowing for more efficiency. Effective implementation of energy storage would reduce load variance by charging during off-peak hours and discharging during peak hours, resulting in a more consistent load, which is more readily manageable by system operators, and therefore has lower operation and maintenance costs [84]. This could occur through some kind of automated and networked market incentives that are now available for wholesale markets as of February 2018 [85].

Landscape-level analysis should continue to be used as part of the process to carefully consider environmental concerns, including climate change, as part of consideration of potential large-scale power plants. The most appropriate mix of centralized and DER resources may change by

2060, as new residential construction will be required to include rooftop solar by 2020 and California has a goal to require new commercial construction to include rooftop solar by 2030.

5.2 Electrical Systems – Loads

More energy efficient appliances reduce use-phase load, load variance, and are therefore generally beneficial for reliability. To mitigate risks from heat waves however, focus should be directed to improve air conditioner units. While differences in lighting and other appliance efficiencies are significant for total annual energy consumption, they accounted for less than a 2% difference in peak demand in the models. By contrast, AC units generally accounted for 60—70% of summertime peak demand within residential buildings, and higher air temperatures resulted in a 3—7% increase in demand per 1°C (1.8 °F). This is because LAC currently has only 45% AC penetration in its residential buildings, meaning that peak demand in just over half of the current building stock does not increase with air temperature. By 2060, almost all buildings in LAC could have AC.

Policies that would guide new or replacement ACs based on either different performance constraints or different technologies would aid in reducing the risk of excessive peak demand during extreme heat events. It is possible to design AC units that are more efficient under the hottest conditions or that utilize thermal storage to achieve 'flat' efficiency curves that do not degrade at the hottest temperatures [86],[87]. Developing a new 'peak performance rating' for ACs at 50 °C (122°F) could be useful to mitigate peak load during extreme heat waves. Doing so could provide incentive for ACs to be optimally engineered for more efficient performance at or near such extreme temperatures. Current standards, SEER and EER [63], are primarily for temperatures at or below 35 °C (95 °F). The current SEER standard, SEER 13, is already optimized to the point that improvements in SEER ratings in the model up to SEER 21 only affected peak demand by a few percent and were slightly counter-effective in some instances where temperatures exceeded 45 °C (113 °F) due to tradeoffs in engineering design optimization. Water-based evaporative cooling systems are another option that uses much less electric power, but requires water to operate, and are often not accepted by users as the sole-source of air conditioning due to insufficient comfort levels when the weather is both hot and humid [88], [89]. Further study may be useful to identify the practicality of hybrid designs.

5.3 Urban Systems

Population growth may not necessarily increase peak demand, as energy efficiency improvements have the potential to reduce peak demand per capita by up to 50% and the number of persons per household could theoretically increase as well. We modeled growth based on the assumption that household density will stay the same at 3 persons per household, and therefore necessitate an increase in the total number of buildings. If household density increased however, then that would mitigate the need for the construction of additional residential buildings, and residential sector peak demand would scale proportionately, i.e. 3.3 persons per household would result in 10% fewer residential buildings than 3 persons per household, and so residential sector peak demand would be approximately 10% less, minus minor variations for indoor body heat effects on the thermostat and other appliance usage. How much population growth occurs, and where, may reflect the management and land markets of urban systems.

From the 2010 base period, population was projected to increase by 1.2-3.1 million people (12-32%) by 2060, which is expected to drive construction of new commercial and residential buildings. Further research is necessary for significant insights into commercial buildings. Commercial buildings were one of the most significant sources of uncertainty in this study, including the classification of those building types in the LAC assessor database and the output of the nationally standardized commercial building energy models used. Residential building data and building energy models were much more precise, and while the original models were originally calibrated to annual energy consumption, reasonable adjustments were made in this study to calibrate building's peak demand to historical peak demand. Further research would be beneficial to specifically develop residential building energy models calibrated for all hours of the day as electrification of natural gas appliances, widespread adoption of electric vehicles, and rooftop solar PV will have significant effects on residential loads. Nevertheless, if growth occurs primarily on undeveloped land in the northern Santa Clarita and Lancaster areas, as the California Department of Finance forecasted, then housing demand can be met through either single family or multi-family dwelling units. Whereas, if growth occurs as SCAG forecasted, more so in the basin, then most of that housing demand must be met through new multi-family dwelling units. In either case, population density and total demand increase on a neighborhood-level scale, but the benefits of building new multi-family unit residential housing can result in as much as a 50% lower peak demand per capita than single-family detached units. Those benefits are due to reduced volume and shared walls, which significantly reduce exposure to extreme heat.

6: References

[1] K. Ralff-Douglas, "Climate Adaptation in the Electric Sector: Vulnerability Assessments & Resiliency Plans," 2016.

[2] J. L. Reyna and M. V. Chester, "Energy efficiency to reduce residential electricity and natural gas use under climate change," *Nat. Commun.*, vol. 8, no. May, p. 14916, 2017.

[3] J. a. Sathaye, L. L. Dale, P. H. Larsen, G. a. Fitts, K. Koy, S. M. Lewis, and A. F. P. de Lucena, "Estimating impacts of warming temperatures on California's electricity system," *Glob. Environ. Chang.*, vol. 23, no. 2, pp. 499–511, 2013.

[4] N. L. Miller, J. Jin, K. Hayhoe, and M. Auffhammer, "Climate change, extreme heat, and electricity demand in California: CEC-500-2007-023," 2007.

[5] WECC, "Loads and Resources Methods and Assumptions," Salt Lake City, Utah, 2014.

[6] NERC, "2015 Long-Term Reliability Assessment," 2015.

[7] M. Garcia-cerrutti, B. Junker, S. Bender, and M. Jones, "Revised Short - Term (2011 - 2012) Peak Demand Forecast Commission," *Energy*, 2012.

[8] IEEE, "IEEE Std C37.30.1-2011 IEEE Standard Requirements for AC High-Voltage Air Switches Rated Above 1000 V 2.00." pp. 76–81, 2012.

[9] D. B. Walton, F. Sun, A. Hall, and S. Capps, "A hybrid dynamical-statistical downscaling technique. Part I: Development and validation of the technique," *J. Clim.*, vol. 28, no. 12, pp. 4597–4617, 2015.

[10] F. Sun, D. B. Walton, and A. Hall, "A hybrid dynamical-statistical downscaling technique. Part II: End-of-Century warming projections predict a new climate state in the Los Angeles region," *J. Clim.*, vol. 28, no. 12, pp. 4618–4636, 2015.

[11] G. Purdy, "ISO 31000:2009 - Setting a new standard for risk management: Perspective," *Risk Anal.*, vol. 30, no. 6, pp. 881–886, 2010.

[12] A. M. Fraser, M. V. Chester, D. Eisenman, D. M. Hondula, S. S. Pincetl, P. English, and E. Bondank, "Household accessibility to heat refuges: Residential air conditioning, public cooled space, and walkability," *Environ. Plan. B Urban Anal. City Sci.*, vol. 44, no. 6, pp. 1036–1055, 2017.

[13] D. Burillo, M. Chester, and B. Ruddell, "Power system planning and operation across multiple coincident non-stationary temperature futures," in *International Conference on Sustainable Infrastructure 2017: Methodology - Proceedings of the International Conference on Sustainable Infrastructure 2017*, 2017.

[14] D. J. Sailor and A. A. Pavlova, "Air conditioning market saturation and long-term response of residential cooling energy demand to climate change," *Energy*, vol. 28, no. 9, pp. 941–951, 2003.

[15] U.S. Global Change Research Program (USGRCP), "National Climate Assessment," 2014.

[16] B. M. Sleeter, "USGS Land-Use and Climate Change Team," 2017. [Online]. Available:

https://geography.wr.usgs.gov/LUCC/california_landchange_projections.php. [Accessed: 08-Jun-2017].

[17] SCAG, "2016 - 2040 RTP / SCS Final Growth Forecast by Jurisdiction 2016 - 2040 RTP / SCS Final Growth Forecast by Jurisdiction," 2016.

[18] J. L. Reyna and M. V. Chester, "The Growth of Urban Building Stock: Unintended Lock-in and Embedded Environmental Effects," *J. Ind. Ecol.*, vol. 19, no. 4, pp. 524–537, 2015.

[19] Barry Fisher, "STAT OF THE WEEK: Los Angeles shatters its record for peak electric demand, twice - Opower : Opower," 2014. [Online]. Available: https://blog.opower.com/2014/09/peak-electric-demand-record-los-angeles/.

[20] CEC, "Building Energy Efficiency Standards for Residential and Nonresidential Buildings," no. June 2015, 2016.

[21] M. Taleghani, M. Tenpierik, S. Kurvers, and A. Van Den Dobbelsteen, "A review into thermal comfort in buildings," *Renew. Sustain. Energy Rev.*, vol. 26, pp. 201–215, 2013.

[22] L. Yang, H. Yan, and J. C. Lam, "Thermal comfort and building energy consumption implications - A review," *Appl. Energy*, vol. 115, pp. 164–173, 2014.

[23] S. H. Association, "Southern Historical Association The End of the Long Hot Summer : The Air Conditioner and Southern Culture Author (s): Raymond Arsenault Source : The Journal of Southern History , Vol . 50 , No . 4 (Nov ., 1984), pp . 597-628 Published by : Southern Hi," vol. 50, no. 4, pp. 597–628, 2016.

[24] M. D. Bartos and M. V. Chester, "Impacts of climate change on electric power supply in the Western United States," *Nat. Clim. Chang.*, vol. 5, no. 8, pp. 748–752, 2015.

[25] FERC, "The August 14 Blackout Compared With Previous Major North American Outages," 2003.

[26] J. Sathaye, L. Dale, P. Larsen, G. Fitts, K. Koy, S. Lewis, and A. Lucena, "Estimating Risk To California Energy Infrastructure From Projected Climate Change," Publication number: CEC-500-2012-057, 2012.

[27] M. E. Mann and P. H. Gleick, "Climate change and California drought in the 21st century," *Proc. Natl. Acad. Sci.*, vol. 112, no. 13, p. 201503667, 2015.

[28] M. T. H. van Vliet, D. Wiberg, S. Leduc, and K. Riahi, "Power-generation system vulnerability and adaptation to changes in climate and water resources," *Nat. Clim. Chang.*, vol. IN PRESS, no. January, 2016.

[29] M. T. H. van Vliet, J. R. Yearsley, F. Ludwig, S. Vögele, D. P. Lettenmaier, and P. Kabat, "Vulnerability of US and European electricity supply to climate change," *Nat. Clim. Chang.*, vol. 2, no. 9, pp. 676–681, 2012.

[30] IEEE Standards Association, "IEEE Std C57.91™-2011 (Revision of IEEE Std C57.91-1995) Guide for Loading Mineral- Oil-Immersed Transformers and Step-Voltage Regulators," 2012.

[31] M. Bartos, M. Chester, N. Johnson, B. Gorman, D. Eisenberg, I. Linkov, and M. Bates,

"Impacts of rising air temperatures on electric transmission ampacity and peak electricity load in the United States," *Environ. Res. Lett.*, 2016.

[32] D. Committee, I. Power, and E. Society, *IEEE Standard for Calculating the Current-Temperature Relationship of Bare Overhead Conductors*. 2013.

[33] Ferc and Nerc, "Arizona-Southern California Outages on September 8 2011," 2012.

[34] D. Burillo, M. Chester, and B. Ruddell, "Electric Grid Vulnerabilities to Rising Air Temperatures in Arizona," in *Procedia Engineering*, 2016, vol. 145.

[35] S. M. Rinaldi, J. P. Peerenboom, and T. K. Kelly, "Identifying, understanding, and analyzing critical infrastructure interdependencies," *IEEE Control Syst. Mag.*, vol. 21, no. 6, pp. 11–25, 2001.

[36] "California's Zero Net Energy Action Plan | Latest on ZNE," 2018. [Online]. Available: https://www.capath2zne.org/latest-on-zne. [Accessed: 26-Feb-2018].

[37] "Community GHG Inventories For Cities In LA County." [Online]. Available: http://www.laregionalcollaborative.com/la-county-ghg-inventory/. [Accessed: 11-Oct-2017].

[38] Los Angeles County Department of Regional Planning, "Community Climate Action Plan." [Online]. Available: http://planning.lacounty.gov/CCAP. [Accessed: 11-Oct-2017].

[39] E. Vine, "Adaptation of California's electricity sector to climate change," *Clim. Change*, vol. 111, no. 1, pp. 75–99, 2012.

[40] California Energy Commission, "Renewables Portfolio Standard (RPS)." [Online]. Available: http://www.energy.ca.gov/portfolio/. [Accessed: 11-Feb-2018].

[41] California Energy Commission, "Tracking Progress Renewable Energy," 2017.

[42] LADWP, "Power Integrated Resource Plan," 2016.

[43] SCE, "APPLICATION OF SOUTHERN CALIFORNIA EDISON COMPANY (U 338-E) FOR APPROVAL OF ITS DISTRIBUTION RESOURCES PLAN," 2015.

[44] I. Penn, "California invested heavily in solar power. Now there's so much that other states are sometimes paid to take it - Los Angeles Times," 2017. [Online]. Available: http://www.latimes.com/projects/la-fi-electricity-solar/. [Accessed: 15-Feb-2018].

[45] E. J. Toll, "California pays APS to take surplus solar power -," *Phoenix Business Journal*, 2016. [Online]. Available: https://www.bizjournals.com/phoenix/news/2016/10/05/california-pays-aps-to-take-surplus-solar-power.html. [Accessed: 15-Feb-2018].

[46] IPCC, "Fifth Assessment Report - Climate Change 2013," 2013. [Online]. Available: https://www.ipcc.ch/report/ar5/wg1/. [Accessed: 22-Jan-2018].

[47] W. C. Skamarock, J. B. Klemp, J. Dudhi, D. O. Gill, D. M. Barker, M. G. Duda, X.-Y. Huang, W. Wang, and J. G. Powers, "A Description of the Advanced Research WRF Version 3," *Tech. Rep.*, no. June, p. 113, 2008.

[48] F. Mesinger, G. DiMego, E. Kalnay, K. Mitchell, P. C. Shafran, W. Ebisuzaki, D. Jović, J. Woollen, E. Rogers, E. H. Berbery, M. B. Ek, Y. Fan, R. Grumbine, W. Higgins, H. Li, Y. Lin, G. Manikin, D. Parrish, and W. Shi, "North American regional reanalysis," *Bull. Am. Meteorol. Soc.*, vol. 87, no. 3, pp. 343–360, 2006.

[49] DOE, "Program for Climate Model Diagnosis & Intercomparison." [Online]. Available: https://pcmdi.llnl.gov/?cmip5/. [Accessed: 22-Jan-2018].

[50] D. Walton, "Personal Communication." 2017.

[51] "U.S. Census Bureau QuickFacts: Los Angeles County, California; California." [Online]. Available: https://www.census.gov/quickfacts/fact/table/losangelescountycalifornia,CA/PST045216. [Accessed: 20-Jun-2018].

[52] LADWP, "Electric Rate Schedules." [Online]. Available: https://ladwp.com/ladwp/faces/ladwp/aboutus/a-financesandreports/a-fr-electricrates/a-fr-er-electricrateschedules;jsessionid=v7vPYKqTKr3hMPFJps1Y8hGyTXvcLLmKQyhK3L2MMbJNgRQJ5Khy!545368516?_adf.ctrl-state=cs0kc1rp1_4&_afrLoop=268583008846984&_afrWindowMode. [Accessed: 15-Mar-2017].

[53] SCE, "Residential Rates | Rates & Pricing Choices | SCE Tariff Books | Regulatory Information | Home - SCE." [Online]. Available: https://www.sce.com/wps/portal/home/regulatory/tariff-books/rates-pricing-choices/residential-rates/!ut/p/b1/tVJNU8IwEP01PYYsbemHtw44WBxUBEbaC5OGtI22SUmDqL_ewHDQEUQO5pRs3r7d93Zxihc4FeSVF0RzKUi1e6fechQPou7QteOhPxpA9DDwB_NHr-vedg0gMQA4cSI4l_-EU5xSoRtd4qSlbE. [Accessed: 15-Mar-2017].

[54] M. Deru, K. Field, D. Studer, K. Benne, B. Griffith, P. Torcellini, B. Liu, M. Halverson, D. Winiarski, M. Rosenberg, M. Yazdanian, J. Huang, and D. Crawley, "U.S. Department of Energy commercial reference building models of the national building stock," *Publ.*, no. February 2011, pp. 1–118, 2011.

[55] SCAG, "The 2016-2040 Regional Transportation Plan/Sustainable Communities Strategy," 2016.

[56] S. Pincetl and LA Energy Atlas Development Team, "LA Energy Atlas," *California Center for Sustainable Communities. UCLA*. Los Angeles, CA, 2017.

[57] A. H. Whittemore, "Zoning Los Angeles: a brief history of four regimes," *Plan. Perspect.*, vol. 27, no. 3, pp. 393–415, 2012.

[58] B. M. Sleeter, T. S. Wilson, E. Sharygin, and J. Sherba, "Future scenarios of land change based on empirical data and demographic trends," *Earth's Futur.*, pp. 1–16, 2017.

[59] SCAG, "RTPSCS Appendix - Demographics & Growth Forecast," 2016.

[60] "US Census Bureau 2010 Census Interactive Population Map." [Online]. Available: https://www.census.gov/2010census/popmap/. [Accessed: 14-Jun-2017].

[61] D. Burillo, M. V. Chester, B. Ruddell, and N. Johnson, "Electricity demand planning forecasts should consider climate non-stationarity to maintain reserve margins during heat waves," *Appl. Energy*, vol. 206, 2017.

[62] CEC, "Energy Maps of California." [Online]. Available: http://www.energy.ca.gov/maps/renewable/building_climate_zones.html. [Accessed: 03-Nov-2017].

[63] SCE, "EER & SEER As Predictors of Seasonal Cooling Performance," 2003.

[64] GreenInfo Network, "California Protected Areas Data Portal," 2018. [Online]. Available: http://www.calands.org/. [Accessed: 31-May-2018].

[65] EIA, "U.S. Electric System Operating Data - Hourly," 2016. [Online]. Available: http://www.eia.gov/beta/realtime_grid/#/data/graphs?end=20160916T00&start=20160909T00.

[66] EIA, "Electric Power Annual 2014," *Eia.Doe.Gov*, vol. 0348, no. January, p. 2, 2016.

[67] California Energy Commission, "California Energy Demand Updated Forecast, 2017-2027," 2014.

[68] R. Faramarzi, B. Coburn, R. Sarhadian, S. Mitchell, and R. A. Pierce, "Performance Evaluation of Rooftop Air Conditioning Units At High Ambient Temperatures," 2004.

[69] CA ISO, "Electricity 2030 - Trends and Tasks for the Coming Years," 2017.

[70] Southern California Edison (SCE), "The Interconnection Handbook," 2016.

[71] US Energy Information Administration, "Layer Information for Interactive State Maps," 2017. [Online]. Available: https://www.eia.gov/maps/layer_info-m.php. [Accessed: 01-Oct-2017].

[72] C. L. Henry and L. F. Pratson, "Effects of Environmental Temperature Change on the Efficiency of Coal- and Natural Gas-Fired Power Plants," *Environ. Sci. Technol.*, p. acs.est.6b01503, 2016.

[73] F. J. Brooks, "GE Gas Turbine Performance Characteristics."

[74] J. S. Maulbetsch and M. N. DiFilippo, "Cost and value of water use at combined-cycle power plants," 2006.

[75] S. Dubey, J. N. Sarvaiya, and B. Seshadri, "Temperature dependent photovoltaic (PV) efficiency and its effect on PV production in the world - A review," *Energy Procedia*, vol. 33, pp. 311–321, 2013.

[76] Homeland Infrastructure Foundation-Level Data (HIFLD Open), "Electric Substations," 2017. [Online]. Available: https://hifld-geoplatform.opendata.arcgis.com/datasets/ec5ecb9e8fec448fa0de73d37cbd74c3_0?geometry=-231.133%2C14.675%2C35.878%2C60.45. [Accessed: 04-Nov-2017].

[77] Southern California Edison (SCE), "Distributed Energy Resource Interconnection Map (DERiM)," 2016.

[78] Homeland Infrastructure Foundation-Level Data (HIFLD Open), "Electric Power Transmission Lines," 2017. [Online]. Available: https://hifld-dhs-gii.opendata.arcgis.com/datasets/37654d07acfc45689b82fbfc64031d40_0. [Accessed: 11-Nov-2017].

[79] US Department of Agriculture, "Design Manual for High Voltage Transmission Lines," 2009.

[80] Nexans, "Bare Overhead Conductors AAC, ACSR, ACSR II," 2014. [Online]. Available: http://www.nexans.us/eservice/US-en_US/fileLibrary/Download_540190082/US/files/BareOverhead. [Accessed: 01-Dec-2017].

[81] D. Burillo, M. Chester, and B. Ruddell, "Electric Grid Vulnerabilities to Rising Air Temperatures in Arizona," in *Procedia Engineering*, 2016, vol. 145, pp. 1346–1353.

[82] CA ISO, "Final PG&E Generator Interconnection Unit Cost Guide," 2012. [Online]. Available: https://www.caiso.com/Documents/PGE_2012FinalPerUnitCostGuide.xls.

[83] T. Mason, T. Curry, and D. Wilson, "Capital Costs for Transmission and Substation Recommendations for WECC Transmission Expansion Planning," 2012.

[84] H. L. Willis, G. V. Welch, and R. R. Schrieber, *Aging Power Delivery Infrastructures*. Marcel Dekker, Inc., 2001.

[85] J. St. John, "FERC Allows Energy Storage to Play in Nationwide Wholesale Markets," 2018. [Online]. Available: https://www.greentechmedia.com/amp/article/ferc-energy-storage-wholesale-markets?__twitter_impression=true. [Accessed: 21-Feb-2018].

[86] B. L. Ruddell, F. Salamanca, and A. Mahalov, "Reducing a semiarid city's peak electrical demand using distributed cold thermal energy storage," *Appl. Energy*, vol. 134, pp. 35–44, 2014.

[87] J. Bush and B. Ruddell, "Field Testing an Ice Storage Air Conditioner in Phoenix, Arizona," *EPRI*, no. September, 2015.

[88] S. Kumar, J. Mathur, S. Mathur, M. K. Singh, and V. Loftness, "An adaptive approach to define thermal comfort zones on psychrometric chart for naturally ventilated buildings in composite climate of India," *Build. Environ.*, vol. 109, pp. 135–153, 2016.

[89] K. Parsons, *Human thermal environments - The effects of hot, moderate, and cold environments on human health, comfort and performance*, Second Edi. Taylor and Francis, 2003.

[90] CEC, "Residential Appliance Saturation Study," 2009. [Online]. Available: http://www.energy.ca.gov/appliances/rass/. [Accessed: 01-Oct-2016].

[91] Department of Energy, "Commercial Reference Buildings," 2017. [Online]. Available: https://energy.gov/eere/buildings/commercial-reference-buildings. [Accessed: 02-Feb-2017].

[92] B. M. Sleeter, T. S. Wilson, E. Sharygin, and J. Sherba, "(In Submission) Land use, land cover, and population scenarios to support California's Fourth Climate Change Assessment," *Geophys. Res. Lett.*, pp. 1–12, 2017.

[93] Desert Renewable Energy Conservation Plan (DRECP), "Los Angeles County Renewable Energy Fact Sheet," no. March. 2017.

[94] Southern California Edison (SCE), "Guide to Going Solar," 2009. [Online]. Available: https://www.sce.com/wps/wcm/connect/f6f873d6-1e99-4f1d-9cd7-4a309c6c9800/CSI_Guide_To_Going_Solar_lo-res.pdf?MOD=AJPERES.

APPENDIX A: Energy Simulation Weather Files

Two sets of weather file data were created to conduct the building peak electricity demand assessment:

1. Spatial images of T_{max} for LAC. These images were of daily maximum air temperatures throughout LAC at 2x2 km resolution as described in Chapter 2: Climate Modeling for Heat Events. These images were transformed into CBG resolution for data processing with minor difference (up to 1°C effect on summary statistics) as shown in Figure A1.
2. Weather profiles used in building energy simulation software. These weather profiles represent the hourly weather conditions at any building throughout a daily, and were developed specifically for individual building energy simulation purposes with considerations for limitations in software as follows.

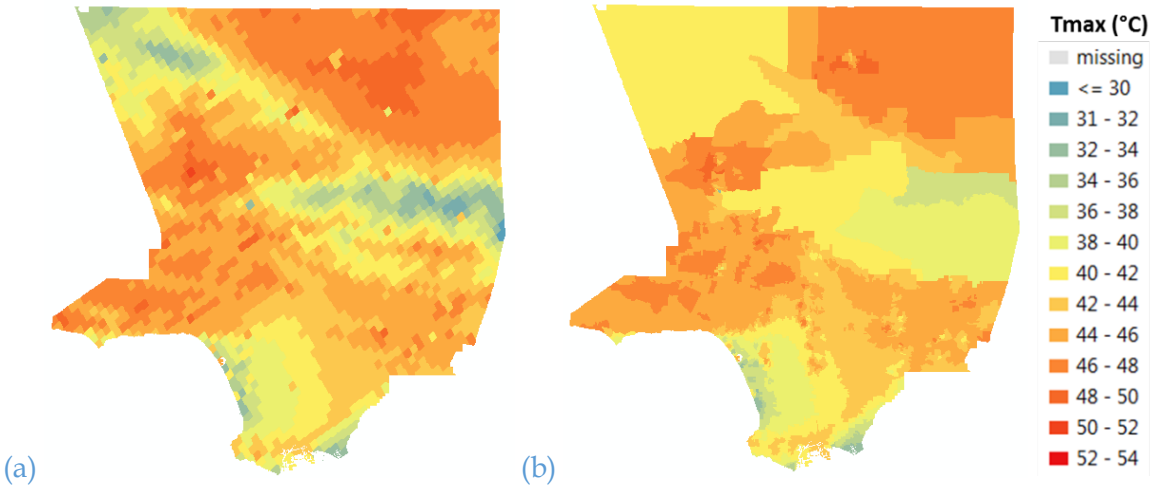

Figure A1. Sample image processing from (a) grid cell to (b) CBG resolution for base period hottest day.

Building energy simulations were conducted using EIA's Energy Plus and BEOpt software, which both require "EPW" weather files. These files require 8,760 inputs, one set of 12 parameters for each hour of the year. EIA sample historical weather data from Los Angeles was modified to simulate a range of hourly dry bulb temperatures such that daily T_{max} ranged from 20°C to 60°C in order to characterize building peak electricity consumption respectively. EPW input variables are listed in **Table A1**, and hourly parameter values used are list in **Table A2**. The dry bulb temperature was increased by 1°C for each hour each day up to T_{max} = 60°C, then decreased back to T_{max} = 20°C, and so on as shown in **Figure A2** for a sample of 82 days. The dew point was recalculated for the same relative humidity and atmospheric pressure as listed in the sample. This artificial raising and lowering of the input weather data was repeated four times throughout the 8,760 EPW file such that multiple simulations output data were created for each T_{max}, and error due to day of week or holiday usage patterns coded into the building models would be minimized.

Table A1. Energy Plus Weather (EWP) file input parameters.

ID	Description	Units	Function in this study
N1-N5	Year, month, day, hour, minute	-	Used as index for T_{max}
A1	Uncertainty Flags	-	N/A
N6	Dry bulb temperature	°C	Control variable for T_{max}
N7	Dew point temperature	°C	Constant
N8	Relative humidity	%	Constant
N9	Atmospheric pressure	Pa	Constant
N10	Extraterrestrial horizontal radiation	Wh/m^2	N/A
N11	Extraterrestrial direct normal radiation	Wh/m^2	N/A
N12	Horizontal infrared radiation from sky	Wh/m^2	Constant
N13	Global horizontal radiation	Wh/m^2	N/A
N14	Direct normal radiation	Wh/m^2	Constant
N15	Diffuse horizontal radiation	Wh/m^2	Constant
N16	Global horizontal illuminance	lux	N/A
N17	Direct normal illuminance	lux	N/A
N18	Diffuse horizontal illuminance	lux	N/A
N19	Zenith luminance	Cd/m^2	N/A
N20	Wind direction	Degrees	Constant
N21	Wind speed	m/s	Constant
N22	Total sky cover	Tenths of sky	N/A
N23	Opaque sky cover	Tenths of sky	N/A
N24	Visibility	km	Constant
N25	Ceiling height	-	N/A
N26	Present weather observation	-	Constant

N27	Present weather codes	-	N/A
N28	Precipitable water	mm	N/A
N29	Aerosol optical depth	1/1000	N/A
N30	Snow depth	cm	N/A
N31	Days since last snowfall	days	N/A
N32	Albedo	%	N/A
N33	Liquid Precipitation Depth	m	N/A
N34	Liquid Precipitation Quantity	-	N/A

Table A2. EPW weather file data for one 24-hour period @T_{max} = 20°C.
The column N4 represents hour of the day.

N4	N6	N7	N8	N9	N12	N14	N15	N20	N21	N24	N26
1	10.4	-6.4	16	96900	406	0	0	320	4.1	56.3	9
2	9.3	-7.5	16	97000	400	0	0	280	3.6	56.3	9
3	8.8	-8	16	97000	396	0	0	250	4.1	56.3	9
4	7.1	-8.9	20	97000	390	0	0	100	2.1	56.3	9
5	6.6	-9	22	97100	389	0	0	80	2.6	80.5	9
6	6	-9	25	97100	387	49	5	120	3.1	80.5	9
7	6	-9.2	24	97200	386	439	41	100	2.6	80.5	9
8	8.8	-6.8	22	97200	402	678	63	0	0	112.7	9
9	11.6	-5.2	16	97300	414	778	87	10	1	112.7	9
10	12.7	-4.7	13	97200	426	825	120	290	2.1	112.7	9
11	14.9	-2.9	11	97200	437	862	148	210	3.1	112.7	9
12	16.6	-1.4	10	97200	445	895	159	230	3.1	112.7	9
13	18.2	0.2	10	97100	462	897	180	290	6.7	96.6	9
14	19.3	1.3	10	97000	470	886	175	280	6.7	96.6	9
15	20	1.8	9	96900	478	868	168	270	5.7	96.6	9
16	20	1.8	9	96900	472	838	146	270	5.7	80.5	9
17	20	2	10	96800	479	769	108	260	6.7	80.5	9

18	20	1.8	9	96800	486	508	167	260	6.2	80.5	9
19	19.3	1.3	10	96800	479	144	114	240	5.7	80.5	9
20	17.1	-0.7	11	96900	467	10	13	250	4.1	56.3	9
21	15.4	-2	13	96900	457	0	0	280	2.6	56.3	9
22	14.3	-2.9	14	97000	455	0	0	270	3.6	56.3	9
23	14.3	-2.9	14	97000	444	0	0	290	3.6	56.3	9
24	13.2	-3.4	17	97000	444	0	0	250	1.5	56.3	9

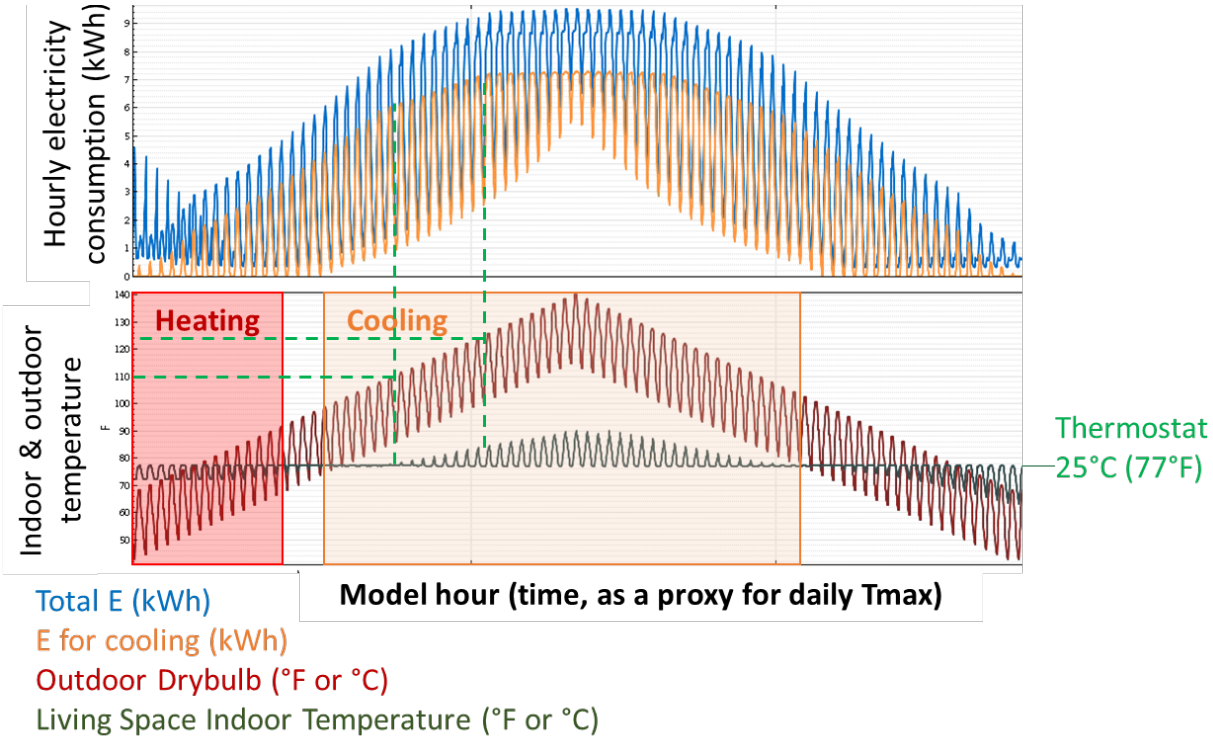

Figure A2. Sample BEOpt hourly simulation output for 82 days.

APPENDIX B: Building Energy Modeling

Building peak electricity performance was characterized for commercial and residential buildings using the US DOE's EnergyPlus and BEOpt simulation software. A total of 45 commercial building models (EnergyPlus files), and 153 residential building models (BEOpt files) were used. Peak hour electricity consumption (kWh) was estimated for all building models using the weather profile EPW files created. Building peak demand performances were characterized over a range of daily T_{max}, from 20°C to 60°C, as the average of the noon-6pm hourly profiles observed in the simulation results for the respective T_{max}.

B.1 Residential buildings

Previous work conducted by Reyna and Chester in [2] developed 1,071 residential building models (using BEOpt and Energy Plus) calibrated specifically for LAC to estimate change in electricity use for various climate and urban infrastructure future scenarios. Those models were developed categorically for 4 types of building dwellings: single family detached (SFDD), single family attached (SFAD), small multifamily (MFSD), and large multifamily (MFLD); 5 CEC climate zones (6, 8, 9, 14, 16); 7 construction time-periods based on the county assessor's database; and 21 appliance configurations for heating, cooling, and lighting efficiency. The consolidated 51 "archetypes" of different building shell properties are listed in Table B1. All appliance usage patterns were kept at the default settings, including thermostat set point equal to 25°C (77°F). The 21 appliance configurations were defined as closely as possible with the options available in the software to fit the California Residential Appliance Saturation Survey (RASS), and were allocated by climate zone, building type and vintage [90]. The 51 archetypes were then calibrated for LAC specifically by adjusting building shell parameters such that when the total 51 x 21 = 1,071 models were run, simulation results were within 10% of total annual electricity sales for several recent years – aggregated by building count and or square footage for the LADWP service territory.

Table B1. Residential Simulation Archetype Divisions and Names. Note: CZ = climate zone.

Multifamily Small (MFS), apartment or condo (2-4 units)						Multifamily Large (MFL), apartment or condo (5+units)				
	CZ 6	CZ 8	CZ 9	CZ 14	CZ 16	CZ 6	CZ 8	CZ 9	CZ 14	CZ 16
<1940	6MFSD-5	8MFSD-4	9MFSD-5	14MFSD-5	16MFSD-4	6MFLD-5	8MFLD-5	9MFLD-5	14MFLD-5	16MFLD-4
1940-1949	6MFSD-5	8MFSD-5	9MFSD-5	14MFSD-5	16MFSD-4	6MFLD-5	8MFLD-5	9MFLD-5	14MFLD-5	16MFLD-4
1950-1959	6MFSD-5	8MFSD-5	9MFSD-5	14MFSD-5	16MFSD-4	6MFLD-5	8MFLD-5	9MFLD-6	14MFLD-5	16MFLD-4
1960-1969	6MFSD-5	8MFSD-5	9MFSD-6	14MFSD-5	16MFSD-4	6MFLD-6	8MFLD-6	9MFLD-6	14MFLD-5	16MFLD-4
1970-1982	6MFSD-6	8MFSD-6	9MFSD-6	14MFSD-5	16MFSD-6	6MFLD-6	8MFLD-6	9MFLD-6	14MFLD-5	16MFLD-4
1983-1997	6MFSD-6	8MFSD-6	9MFSD-6	14MFSD-5	16MFSD-6	6MFLD-6	8MFLD-6	9MFLD-6	14MFLD-6	16MFLD-4
1998-2008	6MFSD-6	8MFSD-6	9MFSD-6	14MFSD-5	16MFSD-6	6MFLD-7	8MFLD-6	9MFLD-7	14MFLD-6	16MFLD-4
Single family detached (SFD)						**Single family attached (SFA), townhouse, duplex, etc.**				
	CZ 6	CZ 8	CZ 9	CZ 14	CZ 16	CZ 6	CZ 8	CZ 9	CZ 14	CZ 16
<1940	6SFDD-5C	8SFDD-5C	9SFDD-5C	14SFDD-5C	16SFDD-7	6SFAD-6C	8SFAD-6C	9SFAD-6C	14SFAD-6M	16SFAD-7
1940-1949	6SFDD-5C	8SFDD-6C	9SFDD-6C	14SFDD-5C	16SFDD-7	6SFAD-6C	8SFAD-6C	9SFAD-6C	14SFAD-6M	16SFAD-7
1950-1959	6SFDD-5M	8SFDD-6M	9SFDD-6M	14SFDD-5C	16SFDD-7	6SFAD-6C	8SFAD-8M	9SFAD-7M	14SFAD-6M	16SFAD-7
1960-1969	6SFDD-7M	8SFDD-7M	9SFDD-7M	14SFDD-7M	16SFDD-7	6SFAD-6C	8SFAD-8M	9SFAD-7M	14SFAD-6M	16SFAD-7
1970-1982	6SFDD-7M	8SFDD-7M	9SFDD-7M	14SFDD-7M	16SFDD-7	6SFAD-7M	8SFAD-7M+	9SFAD-7M	14SFAD-6M	16SFAD-7
1983-1997	6SFDD-8M+	8SFDD-7M+	9SFDD-7M	14SFDD-7M	16SFDD-7	6SFAD-6M+	8SFAD-7M+	9SFAD-7M	14SFAD-6M	16SFAD-7
1998-2008	6SFDD-8M+	8SFDD-7M+	9SFDD-8M+	14SFDD-8M+	16SFDD-8	6SFAD-6M+	8SFAD-7M+	9SFAD-8M+	14SFAD-6M	16SFAD-7

This study used the 51 core building archetypes (in BEOpt) with four AC configurations, to characterize peak demand. This consolidation was done for both technical reasons to reduce computational time, and for practical purposes to define urban infrastructure scenarios. The original 21 appliance configurations included 20 different AC types, and no AC. AC unit efficiency effects on peak demand were characterized for AC types as shown in Figure B1. The AC technology comparison showed approximately 2x energy efficiency gains from SEER 8 to SEER 16, and diminishing returns at higher SEER ratings with the most efficient being the central AC (CAC) SEER 21. Minor efficiency trade-offs were inconsistent between 2-stage & variable-speed motors, as well as CAC to air source heat pump (ASHP). Peak demand from room air conditioners (RACs) saturated between T_{max} = 30 and 35 °C. AC technologies were accordingly labeled as low-, medium-, and high-efficiency (SEER 8, 16, 21) in the residential building models for each archetype for a total of 51x3= 153 simulation models. Peak demand for the 51 archetypes with no AC was calculated post simulation, with the same peak demand value for all T_{max}. The AC technology categorization is summarized in Table B2 with high-level statistics of the base case allocation for LAC at large.

Relative differences in AC performance were consistent when tested in other residential building types as well, as shown in Figure B2. Note: MFLD buildings include 12 DUs, and MFSD and SFAD buildings include 4 DUs. Spikes at low T_{max} are due to indoor heating. All models assumed 34% CFLs and 66% incandescent lighting, and a thermostat set point of 25°C (77°F) in the software. This assumption is maintained as the difference is not significant to peak demand. Relative to 34% CFL, BEOpt lists 100% CFL using ~1/3rd less power, and 100% LEDs as using another ~1/7th less power. Dwelling units with the base 34% CFL penetration were listed at ~1,000 kWh/unit/year, Therefore, ~3kWh/day over ~10 hours, makes for ~0.3kWh contribution to peak load, or ~0.1kWh difference in lighting efficiency. For peak demand of

approximately 6 to 25kWh per residential dwelling unit, this is ~1% effect on peak demand. Therefore, a reduction of 1% for peak demand can be included post processing as a source of uncertainty for potential improvements in lighting efficiency.

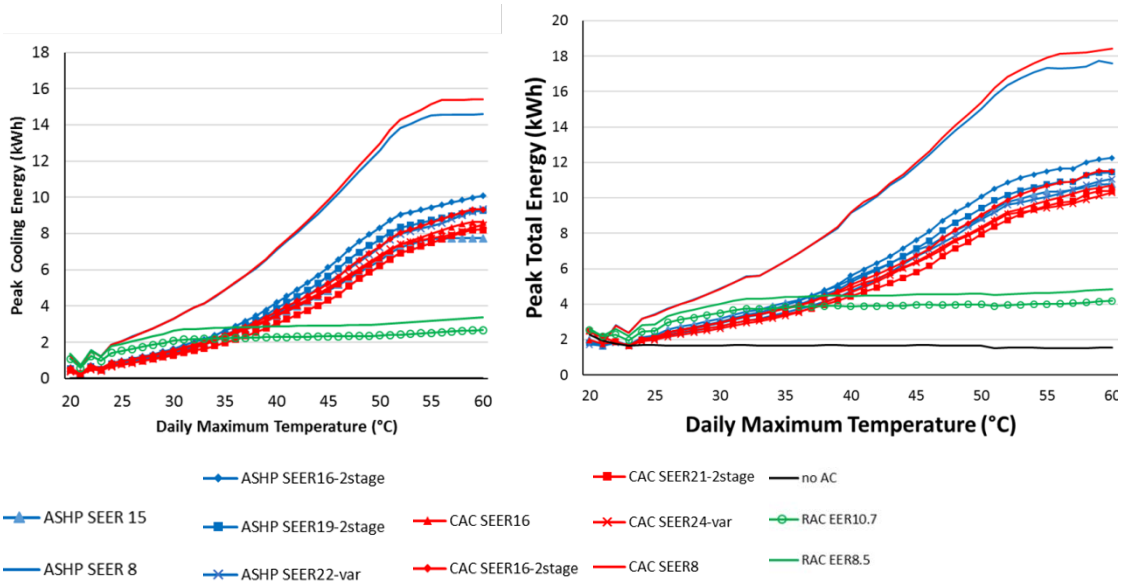

Figure B1. Comparison of AC technologies on building peak demand performance for 6SFDD-8M+. Abbreviations: ASHP – air source heat pump, CAC – central air conditioner, RAC – room air conditioner.

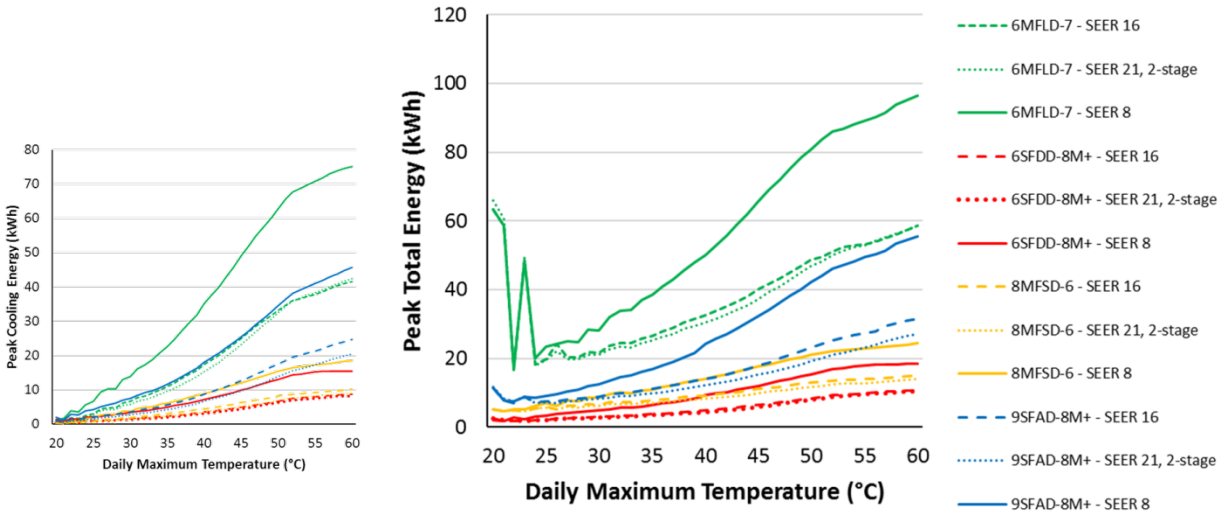

Figure B2. Comparison of AC technology on residential cooling and total peak demand for 4 major building types.

Table B2. AC technology categorization.

AC type	Definition	Clustering of (Reyna & Chester)	Base case allocation
No AC	No AC	No AC	44%
Low efficiency	SEER 8	All SEER 10 or less + ½ of all RACs	26%
Medium efficiency	SEER 16	All SEER >10 + ½ of all RACs	30%
High efficiency	SEER 21	n/a	0%

Technical Procedures

Input files

1. Building prototypes (x3 for SEER 8, SEER 16, SEER 21)
    a. MFL.BEOpt
    b. MFS.BEOpt
    c. SFA.BEOpt
    d. SFD.BEOpt
2. Weather files
    a. 2_ResidentialartificialWeatherDiurnal20to60degC.EPW

Output Files

1. Results - Residential Building Energy Simulations.xls
2. Post processed
    a. Residential AC comparison.xlsx
    b. Results Figures - Residential Building Energy Simulations.xls
    c. Results Figures - Residential AC comparison.xls
    d. PeakDemand_Residential.xls
    e. PeakDemand_Residential2.xls

General procedures

1. Open a ".BEOpt" file, e.g. SEER 16 SFD.BEOpt
    a. Note: Residential building energy simulations were performed in BEOpt, based on four ".BEOpt" files from [2] MFL.BEOpt, MFS.BEOpt, SFA.BEOpt, and SFD.BEOpt. These 4 files contain the 51 building shell designs. The building attributes (located in the "options screen") were adjusted in the BEOpt software for 3 air conditioner efficiency cases: SEER 8, SEER 16, and SEER 21, and 3 sets of BEOpt files exist in corresponding named folders in the same location.
2. Click on a tab for a building type, e.g. 6SFDD-5C
3. Load weather file on the "Site Screen" tab under "Building", "EPW Location."
    a. Note: Weather data were created as described in the Appendix A.

4. Click "Run"
5. On the Output tab, click "Generate Hourly Output"
6. Select boxes on right for desired features to display, e.g. Total (kWh), Cooling (kWh), Living Space Indoor Temperature (F), Outdoor Drybulb (F)
7. Right click on graph area, and select copy data to clipboard
3. Paste data in Excel file, e.g. "Results - Residential Building Energy Simulations.xls"
    a. Note: data will be large (446,760 rows), so one tab for each AC type recommended
    b. Note: create additional columns for coding building types and formatting
8. Repeat 1-8 for all files and building types

AC comparison

9. Repeat general procedures, modifying the "Space Conditioning" options on the "Options Screen" tab as desired. E.g. None, SEER 8, SEER 14, SEER 16, SEER 21, etc.

Post Process Summary Tables

10. Select data from "Results Figures - Residential Building Energy Simulations.xls" and create a pivot table to obtain minimum peak demand (kWh) for all building types by daily Tmax.
    a. Note: the average of the 6 hourly electricity consumptions from the noon-6 pm peak period was used.
11. Paste pivot tables' data into a new single tab workbook "PeakDemand_Residential.xls"
    a. Note: follow column header formatting
12. Copy-paste data from "PeakDemand_Residential.xls" into "PeakDemand_Residential2.xls"
    a. Note: numerical column/row header formatting for Matlab

Characterization Results

In most cases, the building energy simulation results show the newest vintage building consumes the most energy for each building type within each CAZ. This is primarily due to the increase in square footage of buildings over time, i.e. more efficient per square foot, but more square feet, as listed in Table B3.

Table B3. Residential building prototypes square footage.

Code	ft^2	Beds	Units	New
Single Family Detached				
6SDFDD-5C	1200	3	1	0
6SFDD-5M	1360	3	1	0
6SFDD-7M	2065	3	1	0
6SFDD-8M+	1940	3	1	1
8SFDD-5C	1260	2	1	0

8SFDD-6C	1300	3	1	0
8SFDD-6M	1402	3	1	0
8SFDD-7M	1775	3	1	0
8SFDD-7M+	1820	3	1	1
9SFDD-5C	1694	3	1	0
9SFDD-6C	1411	3	1	0
9SFDD-6M	1505	3	1	0
9SFDD-7M	2135	3	1	0
9SFDD-8M+	3010	4	1	1
14SFDD-5C	1175	3	1	0
14SFDD-7M	1720	3	1	0
14SFDD-8M+	2600	4	1	1
MtnSFDD-7C	1930	3	1	0
MtnSFDD-8	3615	4	1	1
Single Family Attached				
6SFAD-6C	840	2	4	0
6SFAD-7M	1228	2	4	0
6SFAD-6M+	1196	3	4	1
8SFAD-6C	924	2	4	0
8SFAD-8M	1200	2	4	0
8SFAD-7M+	1200	2	4	1
9SFAD-6C	1040	3	4	0
9SFAD-7M	1250	2	4	0
9SFAD-8M+	1496	3	4	1
14FAD-6M	1196	3	4	1
MtnSFAD-7	1092	4	4	1
Multi-family small				
6MFSD-5	870	2	4	0
6MFSD-6	910	2	4	1
8MFSD-4	840	1	4	0
8MFSD-5	800	1	4	0
8MFSD-6	1050	2	4	1
9MFSD-5	928	1	4	0
9MFSD-6	918	2	4	1
14MFSD-5	896	2	4	1
16MFSD-4	1020	1	4	0
16MFSD-6	1800	1	4	1
Multi-family large				
6MFLD-5	625	2	12	0
6MFLD-6	750	2	12	0
6MFLD-7	1435	2	12	1
8MFLD-5	675	1	12	0
8MFLD-6	840	2	12	1

9MFLD-5	725	2	12	0
9MFLD-6	812	1	12	0
9MFLD-7	1200	2	12	1
14MFLD-5	775	2	12	0
14MFLD-6	775	2	12	1
16MFLD-4	870	1	12	1

Simulation results are shown below grouped by CAZ and building type for SEER 8 efficiency ACs.

CAZ 6

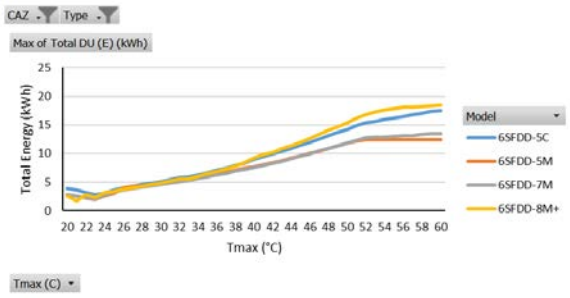

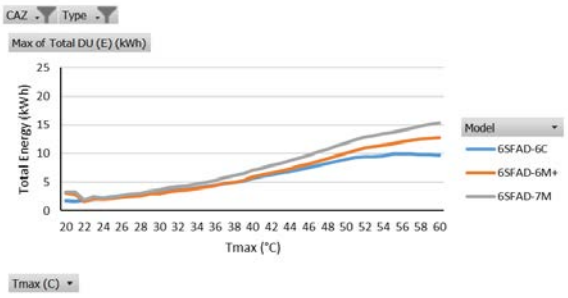

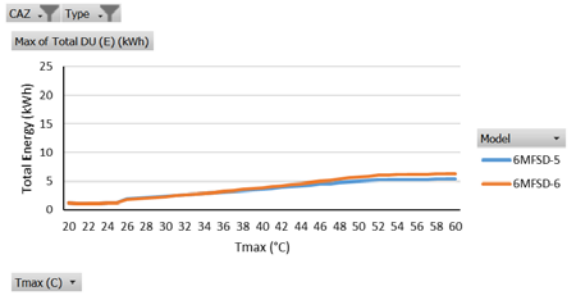

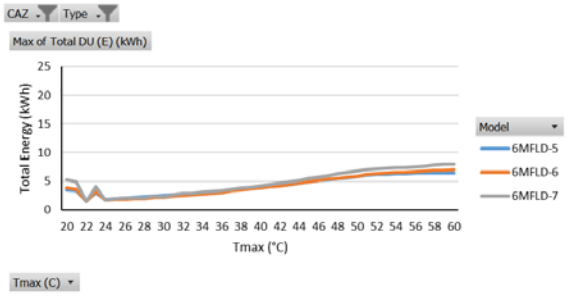

CAZ 8

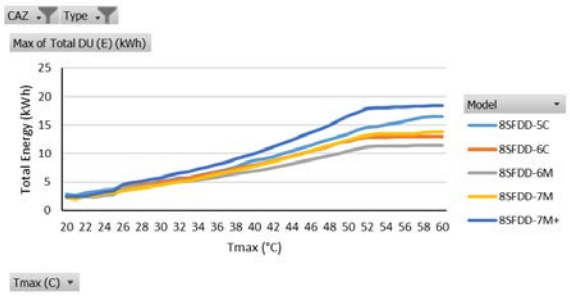

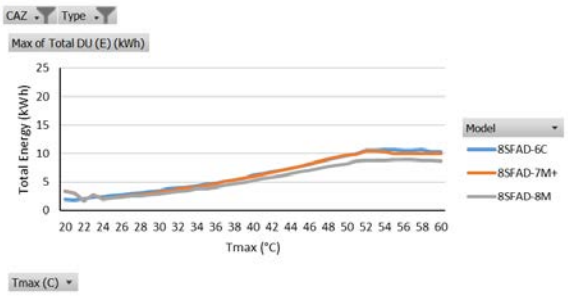

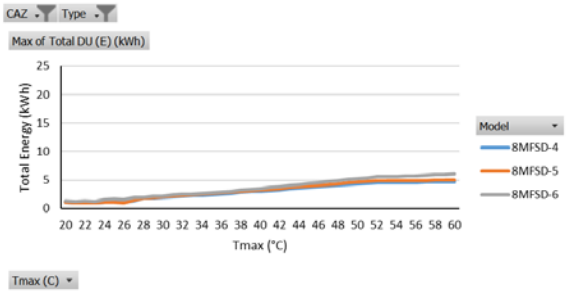
CAZ
Type
Max of Total DU (E) (kWh)
Total Energy (kWh)
Tmax (°C)
Model
8MFSD-4
8MFSD-5
8MFSD-6
Tmax (C)

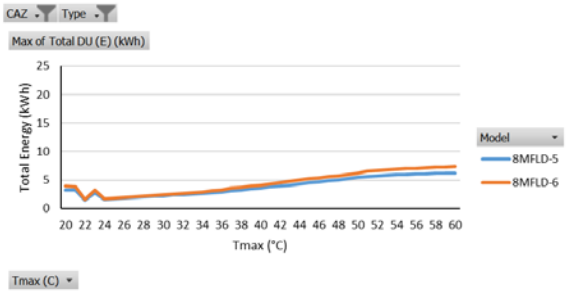
CAZ
Type
Max of Total DU (E) (kWh)
Total Energy (kWh)
Tmax (°C)
Model
8MFLD-5
8MFLD-6
Tmax (C)

CAZ 9

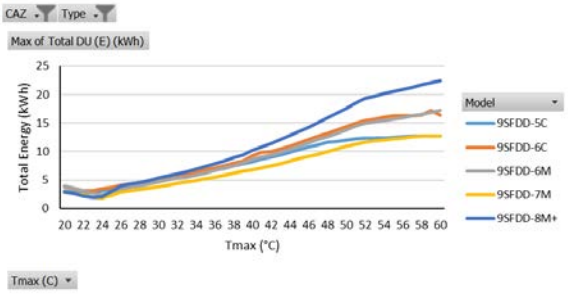
CAZ
Type
Max of Total DU (E) (kWh)
Total Energy (kWh)
Tmax (°C)
Model
9SFDD-5C
9SFDD-6C
9SFDD-6M
9SFDD-7M
9SFDD-8M+
Tmax (C)

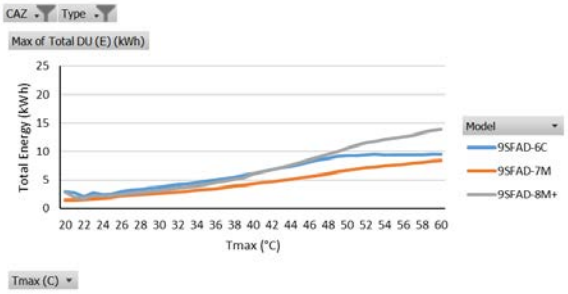
CAZ
Type
Max of Total DU (E) (kWh)
Total Energy (kWh)
Tmax (°C)
Model
9SFAD-6C
9SFAD-7M
9SFAD-8M+
Tmax (C)

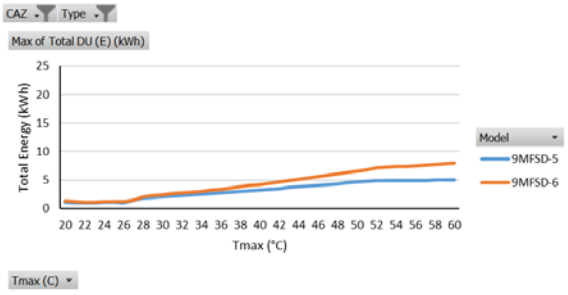
CAZ
Type
Max of Total DU (E) (kWh)
Total Energy (kWh)
Tmax (°C)
Model
9MFSD-5
9MFSD-6
Tmax (C)

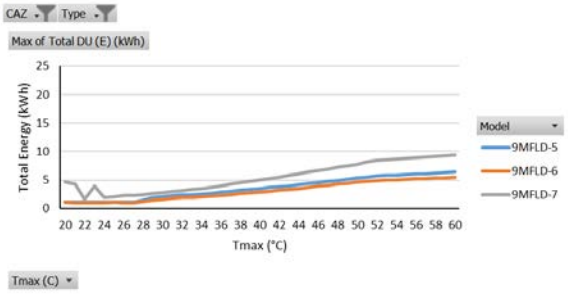
CAZ
Type
Max of Total DU (E) (kWh)
Total Energy (kWh)
Tmax (°C)
Model
9MFLD-5
9MFLD-6
9MFLD-7
Tmax (C)

CAZ 14

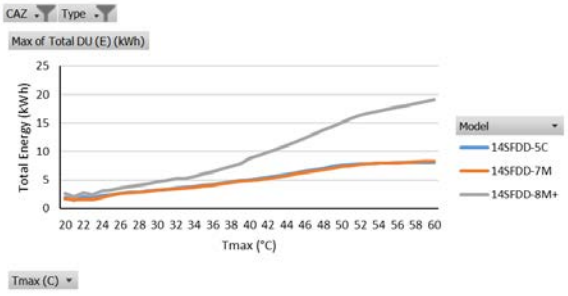
CAZ
Type
Max of Total DU (E) (kWh)
Total Energy (kWh)
Tmax (°C)
Model
14SFDD-5C
14SFDD-7M
14SFDD-8M+
Tmax (C)

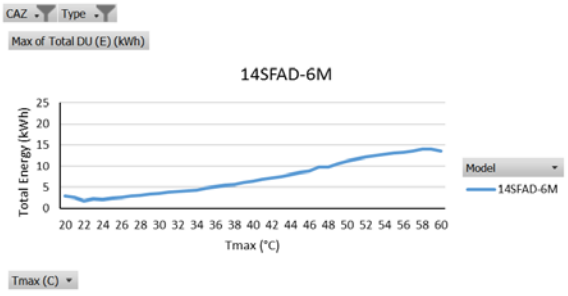
CAZ
Type
Max of Total DU (E) (kWh)
14SFAD-6M
Total Energy (kWh)
Tmax (°C)
Model
14SFAD-6M
Tmax (C)

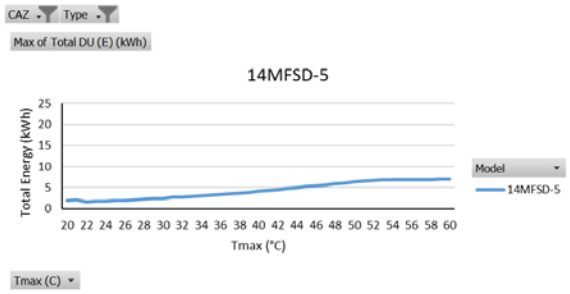

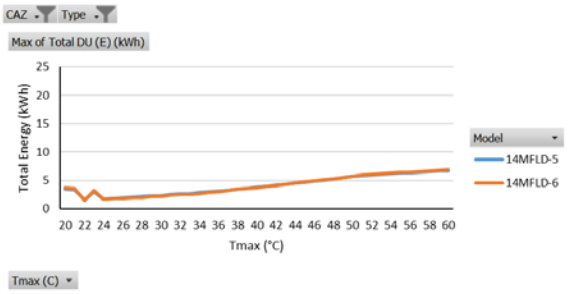

CAZ 16

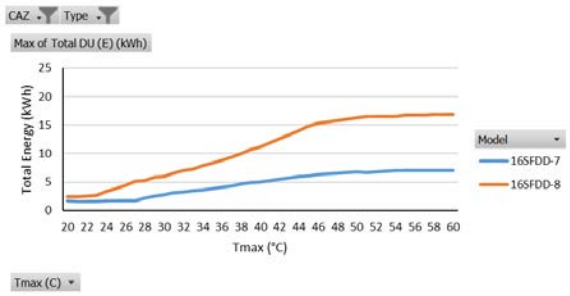

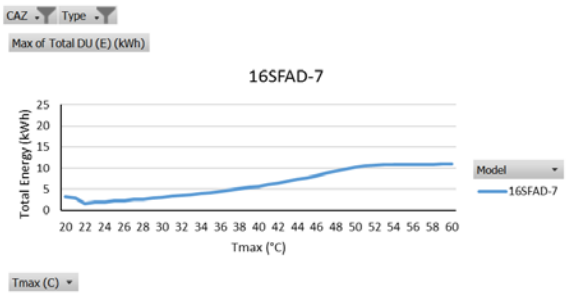

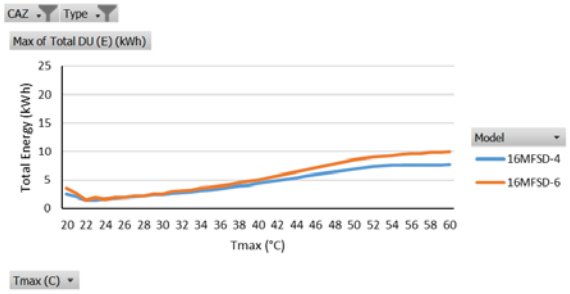

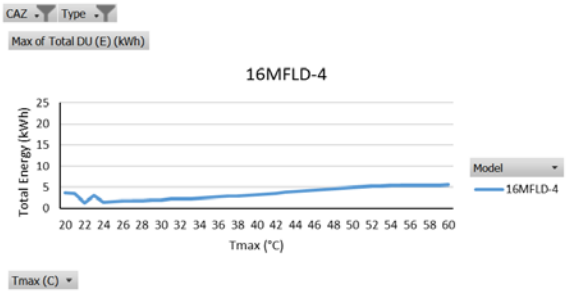

Comparing the newest vintage of buildings for SEER 8 and SEER 21, in all cases the SFDD type has higher peak demand per dwelling unit than any form of attached unit. In most cases SFAD consumes the next most energy per dwelling unit. In some cases, the MFSD consumes the least, and in some cases the MFLD consumes the least per dwelling unit.

SEER 8

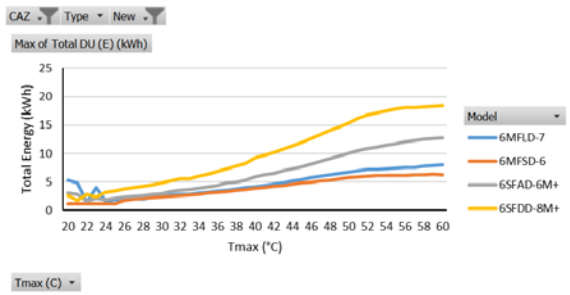

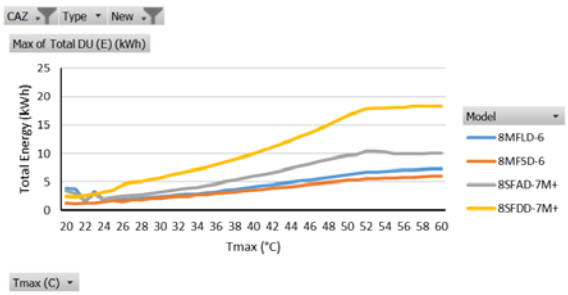

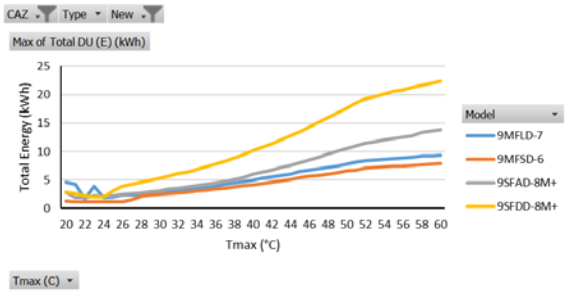
CAZ
Type
New
Max of Total DU (E) (kWh)
Total Energy (kWh)
Tmax (°C)
Model
9MFLD-7
9MFSD-6
9SFAD-8M+
9SFDD-8M+
Tmax (C)

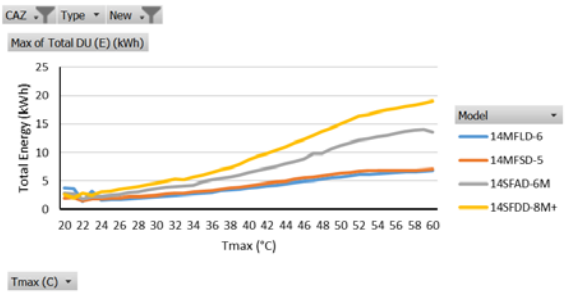
CAZ
Type
New
Max of Total DU (E) (kWh)
Total Energy (kWh)
Tmax (°C)
Model
14MFLD-6
14MFSD-5
14SFAD-6M
14SFDD-8M+
Tmax (C)

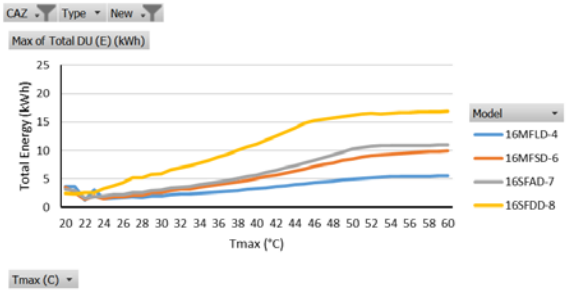
CAZ
Type
New
Max of Total DU (E) (kWh)
Total Energy (kWh)
Tmax (°C)
Model
16MFLD-4
16MFSD-6
16SFAD-7
16SFDD-8
Tmax (C)

SEER 21

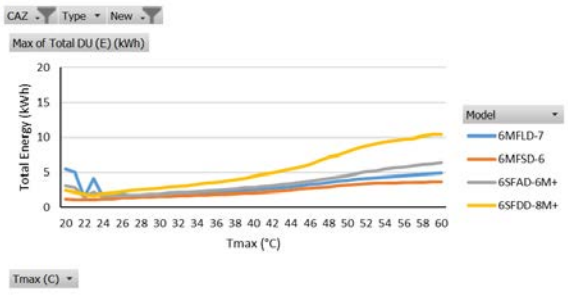
CAZ
Type
New
Max of Total DU (E) (kWh)
Total Energy (kWh)
Tmax (°C)
Model
6MFLD-7
6MFSD-6
6SFAD-6M+
6SFDD-8M+
Tmax (C)

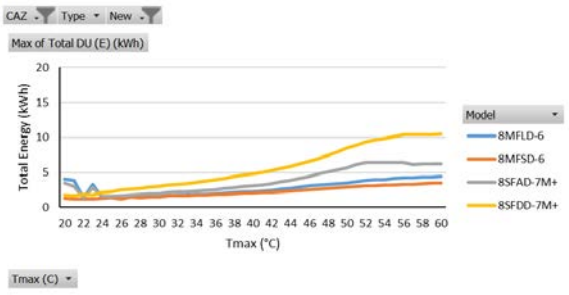
CAZ
Type
New
Max of Total DU (E) (kWh)
Total Energy (kWh)
Tmax (°C)
Model
8MFLD-6
8MFSD-6
8SFAD-7M+
8SFDD-7M+
Tmax (C)

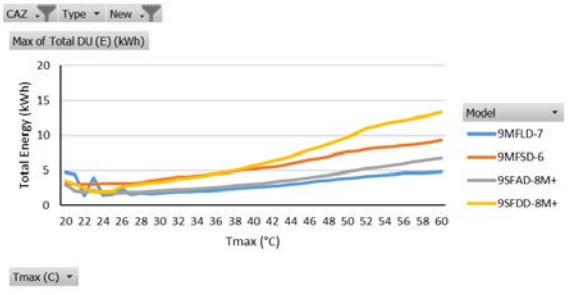
CAZ
Type
New
Max of Total DU (E) (kWh)
Total Energy (kWh)
Tmax (°C)
Model
9MFLD-7
9MFSD-6
9SFAD-8M+
9SFDD-8M+
Tmax (C)

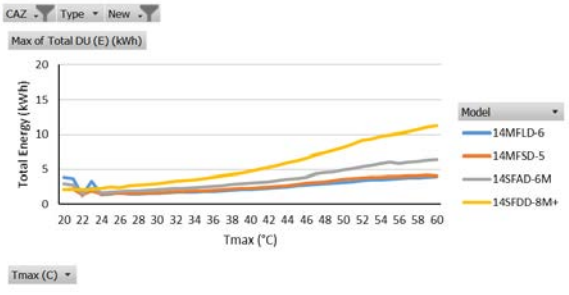
CAZ
Type
New
Max of Total DU (E) (kWh)
Total Energy (kWh)
Tmax (°C)
Model
14MFLD-6
14MFSD-5
14SFAD-6M
14SFDD-8M+
Tmax (C)

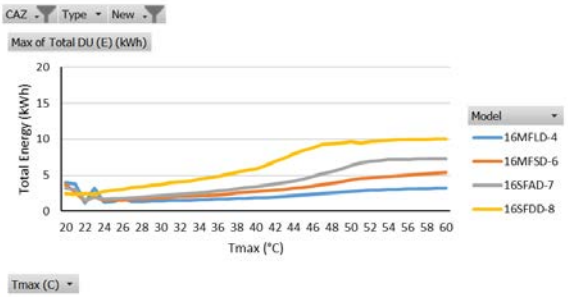
CAZ
Type
New
Max of Total DU (E) (kWh)
Total Energy (kWh)
Tmax (°C)
Model
16MFLD-4
16MFSD-6
16SFAD-7
16SFDD-8
Tmax (C)

B2. Commercial Buildings

The commercial building models used in this study were produced by NREL and published by DOE [91] for use in Energy Plus. The 15 types of commercial building models used are listed in Table B4. DOE has published models with building performance characteristics calibrated for several regions. The models calibrated for Los Angeles specifically were used; however, the details of those calibrations are not for the purposes of this report. These models were used as they were the best-known models available at the time. Moreover, DOE has published three versions of these models based on vintage for: pre-1980, post-1980, and post 2004. Thus, a total of 45 models (EnergyPlus files) were used. Characterization figures for peak demand in each commercial building type are shown in Appendix B.1. No patterns were particularly identified other than that electricity demand generally increased with daily maximum temperature. Inconsistencies in peak demand between building vintage may be explained by differences in appliance technologies and use profiles. To best calibrate the results to the validation data for commercial buildings, the lowest peak demand values were used in this assessment for any of the 3 vintages of the 15 building types at any temperature.

As stated in the documentation [54],

> ***Intended uses***
>
> *"The reference building models will be used for DOE commercial buildings research to assess new technologies; optimize designs; analyze advanced controls; develop energy codes and standards; and to conduct lighting, daylighting, ventilation, and indoor air quality studies."*
>
> *"They also provide a common starting point to measure the progress of DOE energy efficiency goals for commercial buildings."*
>
> ***Uses not intended***
>
> *"These reference building models are not intended to represent energy use in any particular building. Rather, they are hypothetical models with ideal operations that meet certain minimum requirements."*
>
> *"The reference building model definitions are not intended to act as targets to rate the energy performance of single existing or proposed buildings. The models and weighting factors are not appropriate for analysis at the state level, as the datasets used to generate the models and the weighting factors are too small to form a valid statistical model at this level. Variations of these models and weighting factors could be created for such purposes, but that is not the objective of this project."*

Thus, the use of these models in this research, and the decisions made by staff as to how to use these models consistently with historical data, is both insightful in terms of the climate change assessment, as well as the DOE research community in advancement of the models themselves. A detailed audit of the plug and process load characterization in the source models is beyond the scope of this work.

Table B4. Commercial building types.

Type	Description	Floor Area (ft^2)	Number of Floors
1	Large Office	498,588	12
2	Medium Office	53,628	3
3	Small Office	5,500	1
4	Warehouse	52,045	1
5	Stand-alone Retail	24,962	1
6	Strip Mall	22,500	1
7	Primary School	73,960	1
8	Secondary School	210,887	2
9	Supermarket	45,000	1
10	Quick Service Restaurant	2,500	1
11	Full Service Restaurant	5,500	1
12	Hospital	241,351	5
13	Outpatient Health Care	40,946	3
14	Small Hotel	43,200	4
15	Large Hotel	122,120	6

*Midrise Apartment excluded from analysis due to redundancy with residential category large multifamily unit (MFL)

Characterization Results

Commercial building model performance was characterized for a range of daily high temperatures from 20°C to 60°C.

Table B5 lists descriptive statistics of the area, stories, and count of building types in the historical base period. The following figures show the daily peak electricity consumption for building cooling only as well as the entire facility for each building type for New (2004+), Post 1980, and Pre 1980 models.

Table B5. Commercial buildings.

Index	Building Type	Area (m2)	Stories	Historic Count Pre 1980	Historic Count Post 1980	Historic Count Post 2004	Historic Count Total
0	Midrise Apt. (not used)	3,135	4	528	514	79	1,121
1	Large Office	46,320	12	2,719	1,350	265	4,334
2	Medium Office	4,982	3	5,247	1,414	657	7,318
3	Small Office	511	1	6,553	4,303	1,444	12,300
4	Warehouse	4,835	1	16,221	2,409	1,332	19,962
5	Stand-alone Retail	2,294	1	1,415	1,374	392	3,181
6	Strip Mall	2,090	1	2	2	0	4
7	Primary School	6,871	1	478	126	42	646
8	Secondary School	19,592	2	144	175	99	418
9	Super Market	4,181	1	4,086	759	241	5,086
10	Quick Service Restaurant	232	1	363	22	14	399
11	Full Service Restaurant	511	1	104	12	2	118
12	Hospital	22,422	5	386	64	8	458
13	Out Patient	3,804	3	185	162	173	520
14	Small Hotel	4,014	4	528	514	79	1,121
15	Large Hotel	11,345	6	2,719	1,350	265	4,334

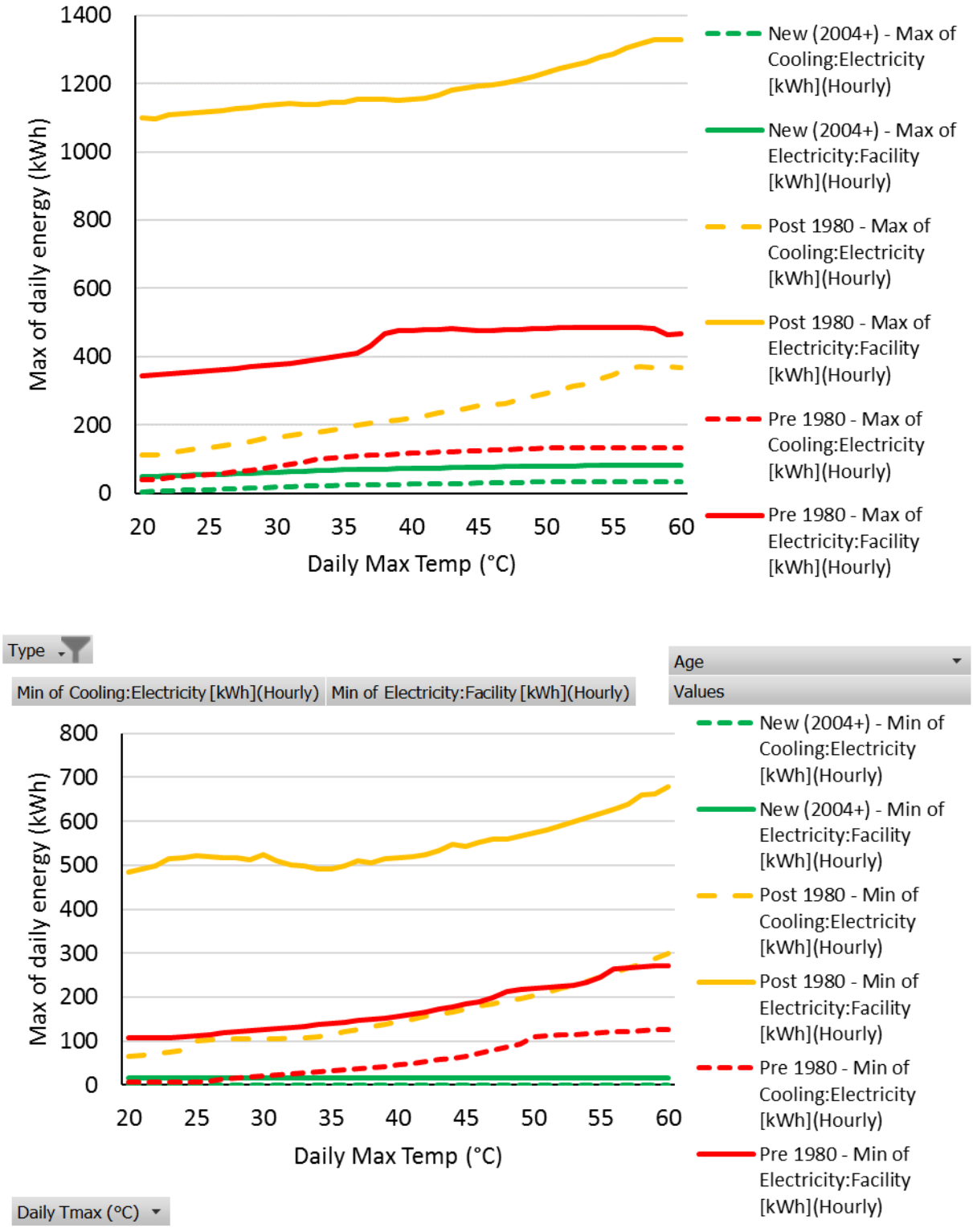

Figure B3. Full Service Restaurant.

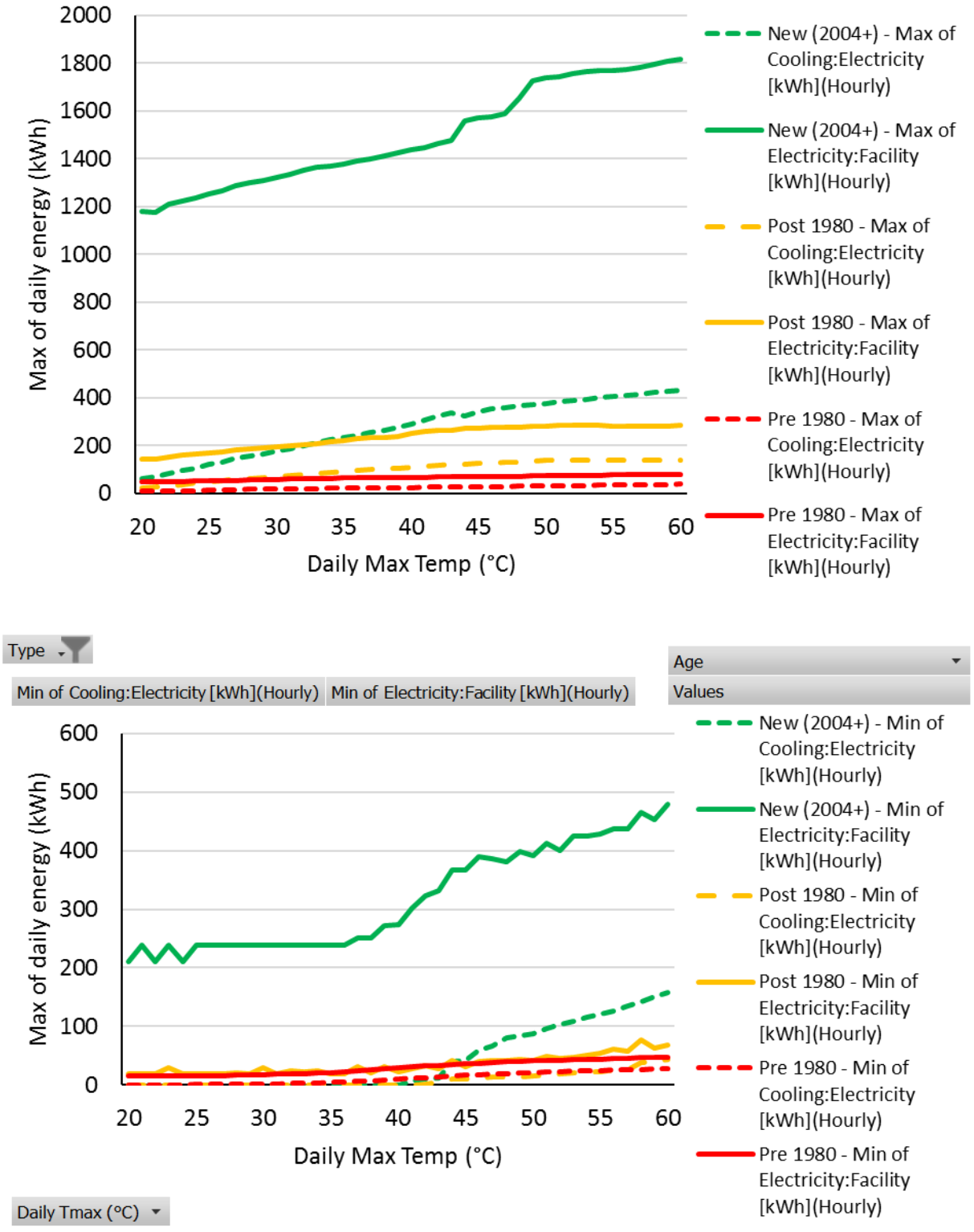

Figure B4. Hospital.

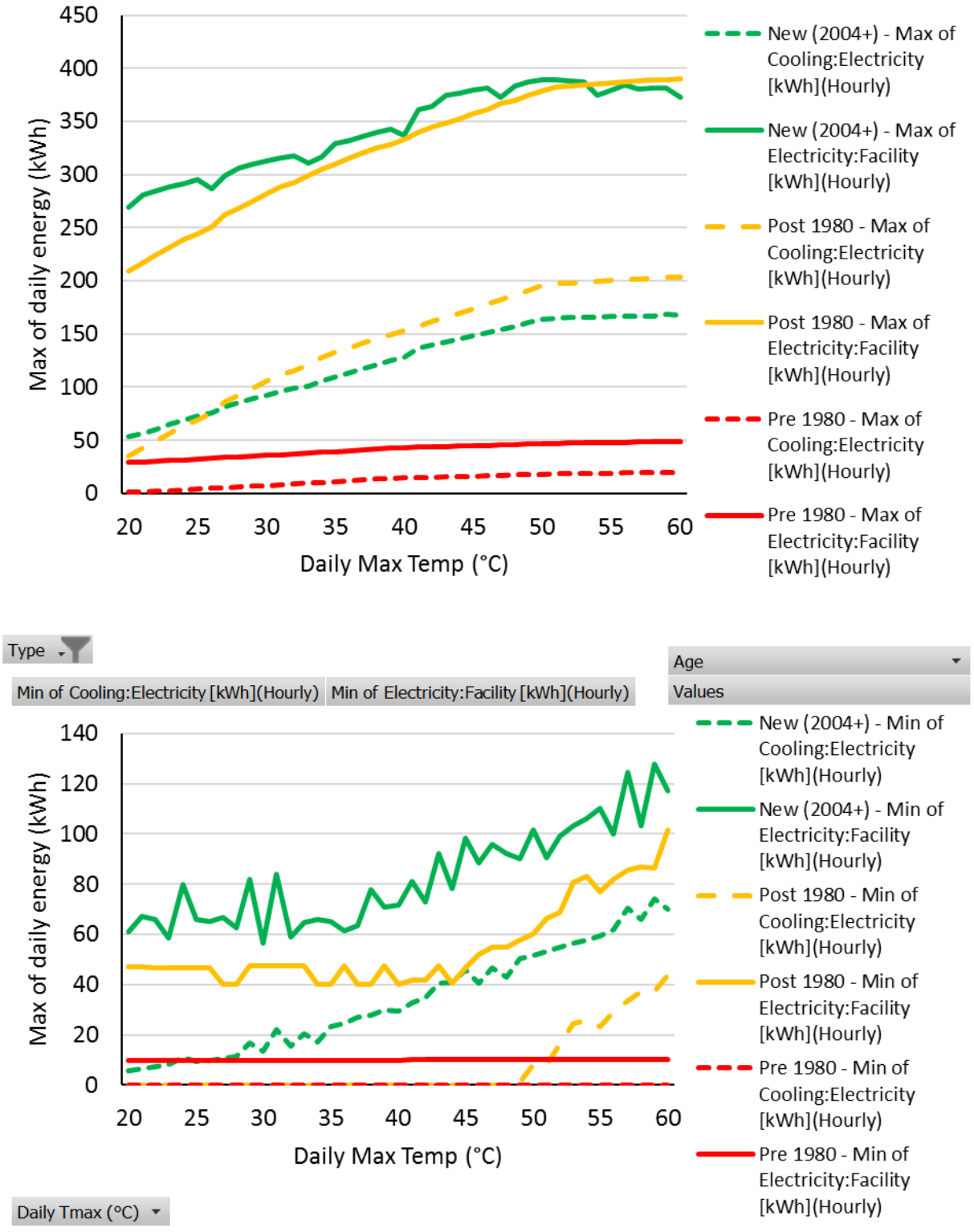

Figure B5. Large Hotel.

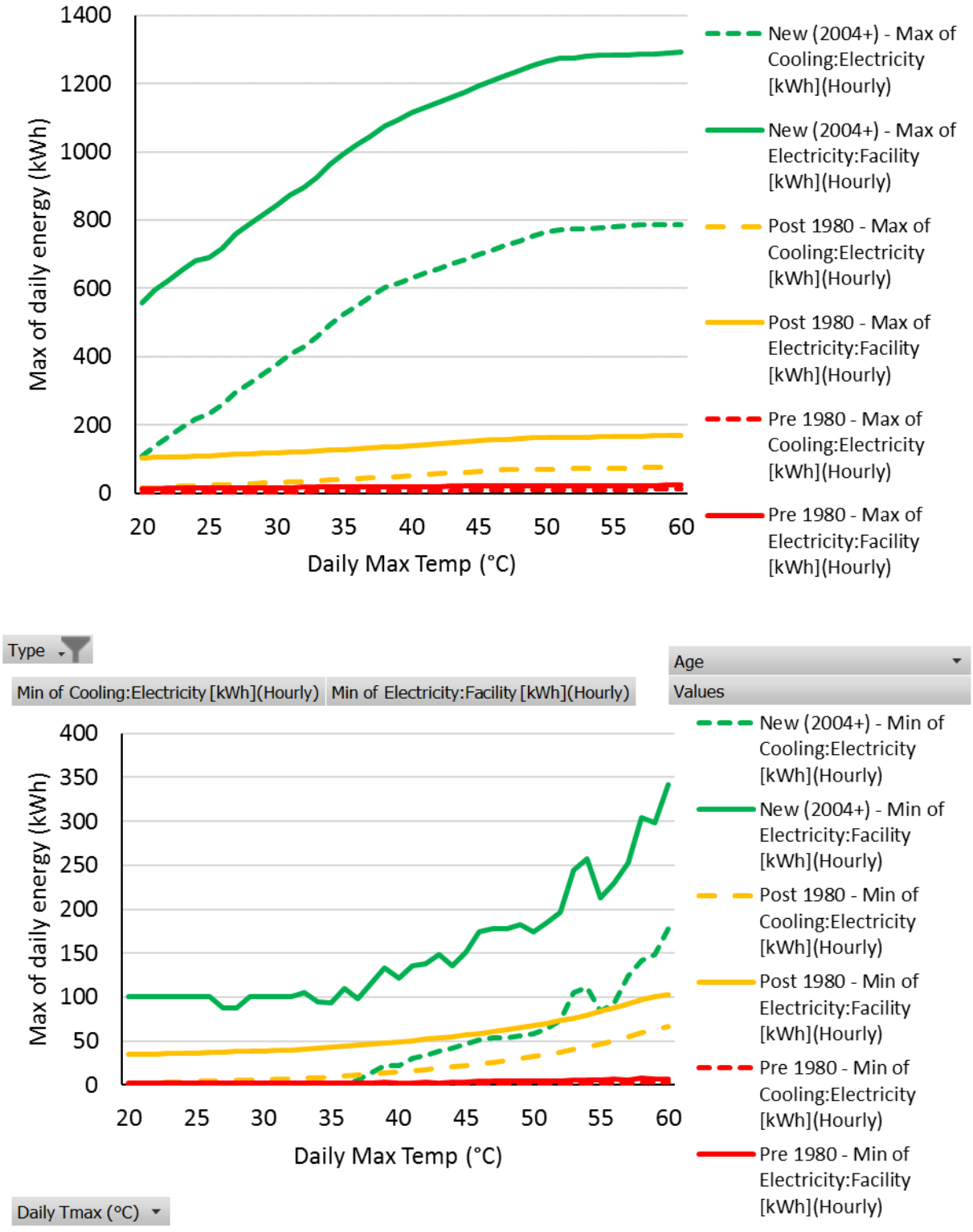

Figure B6. Large Office.

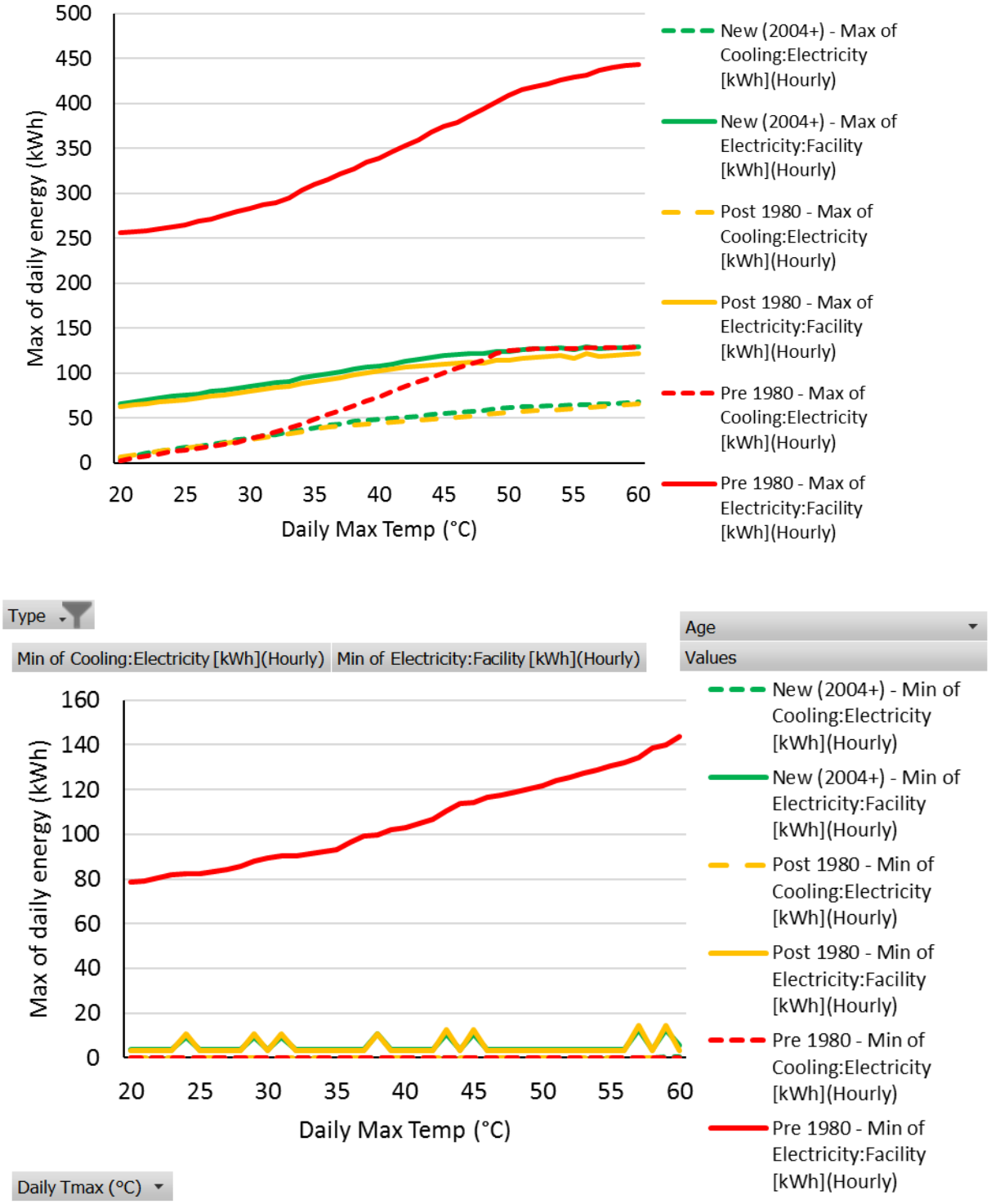

Figure B7. Medium Office.

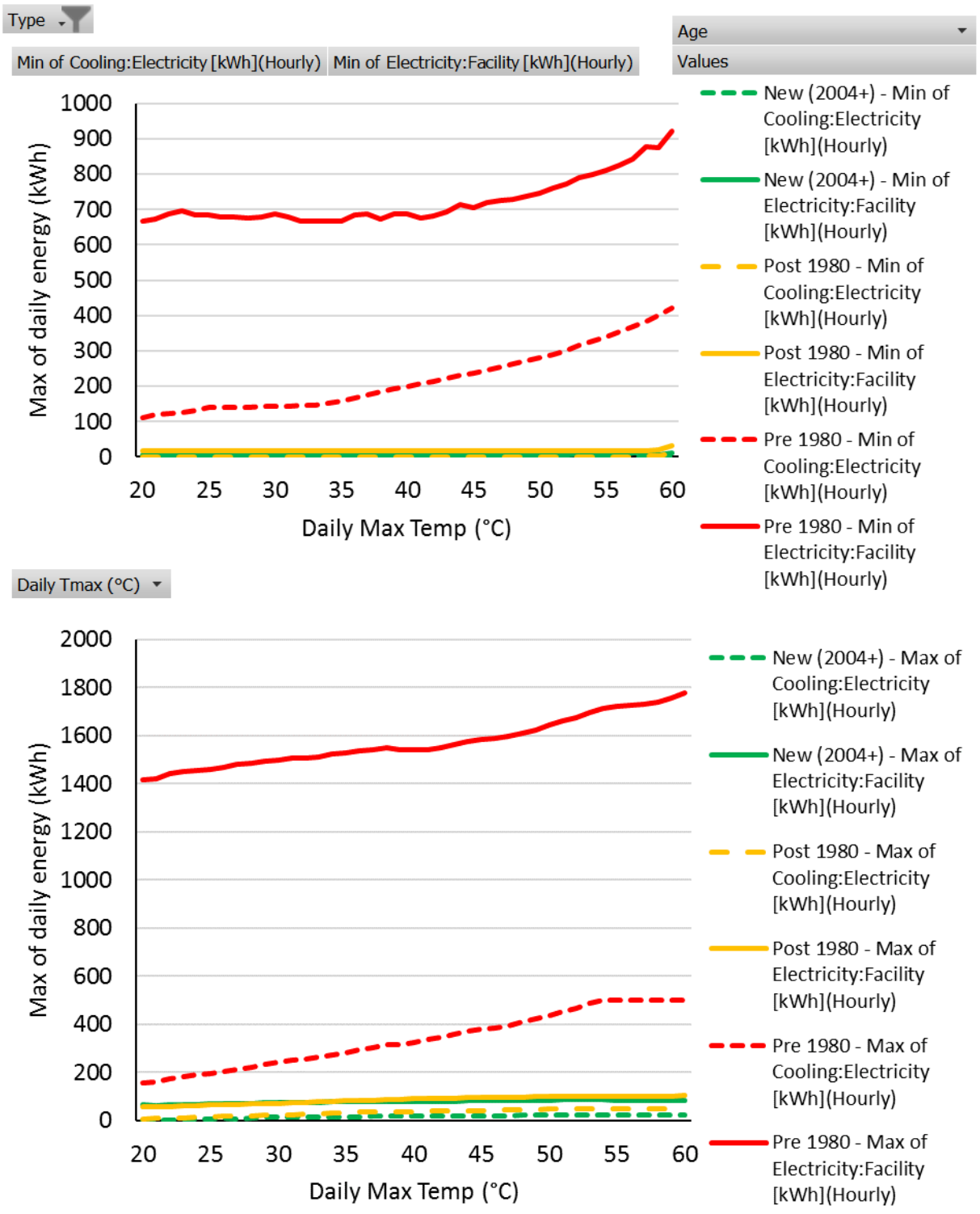

Figure B8. Midrise Apartment.

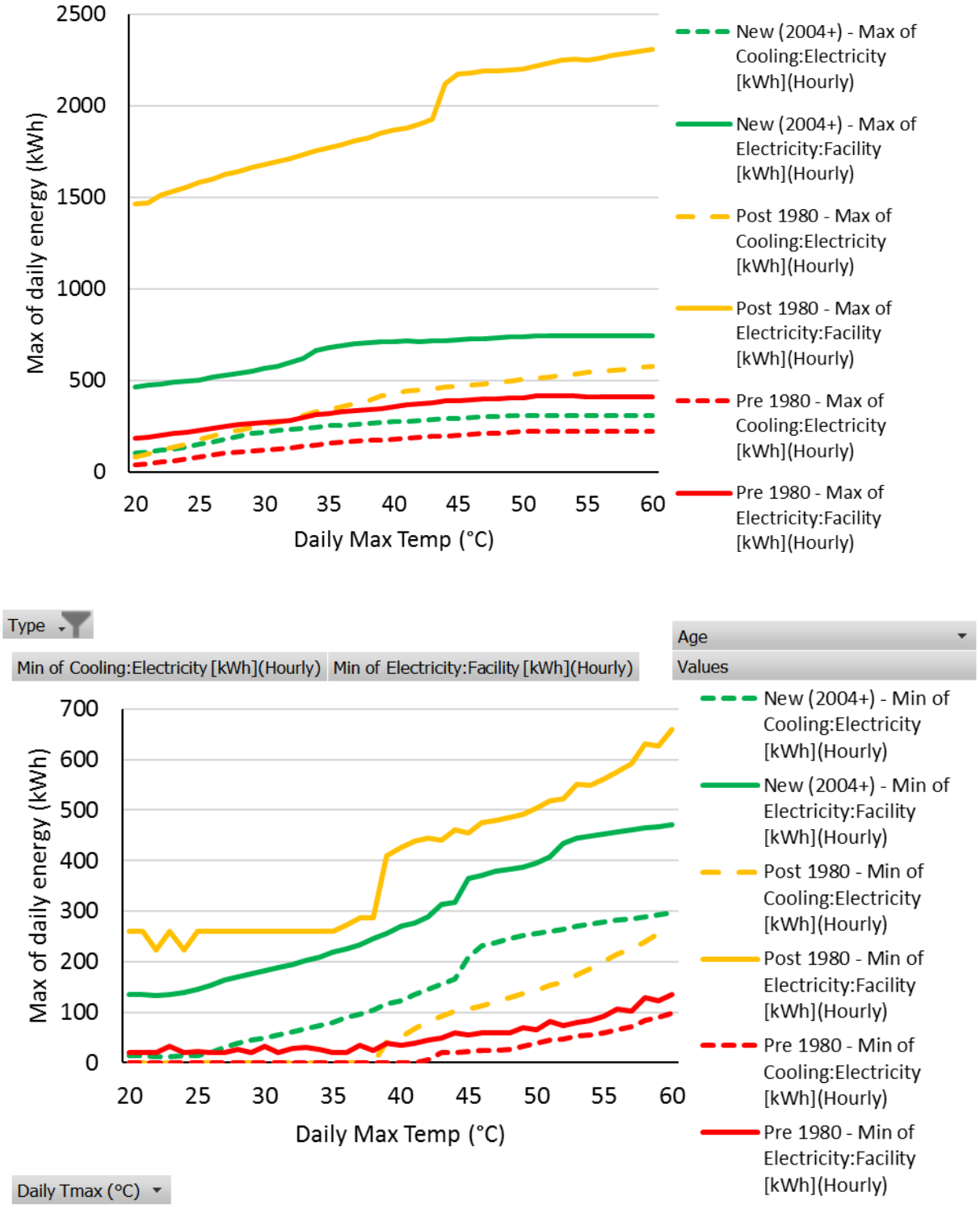

Figure B9. Out Patient.

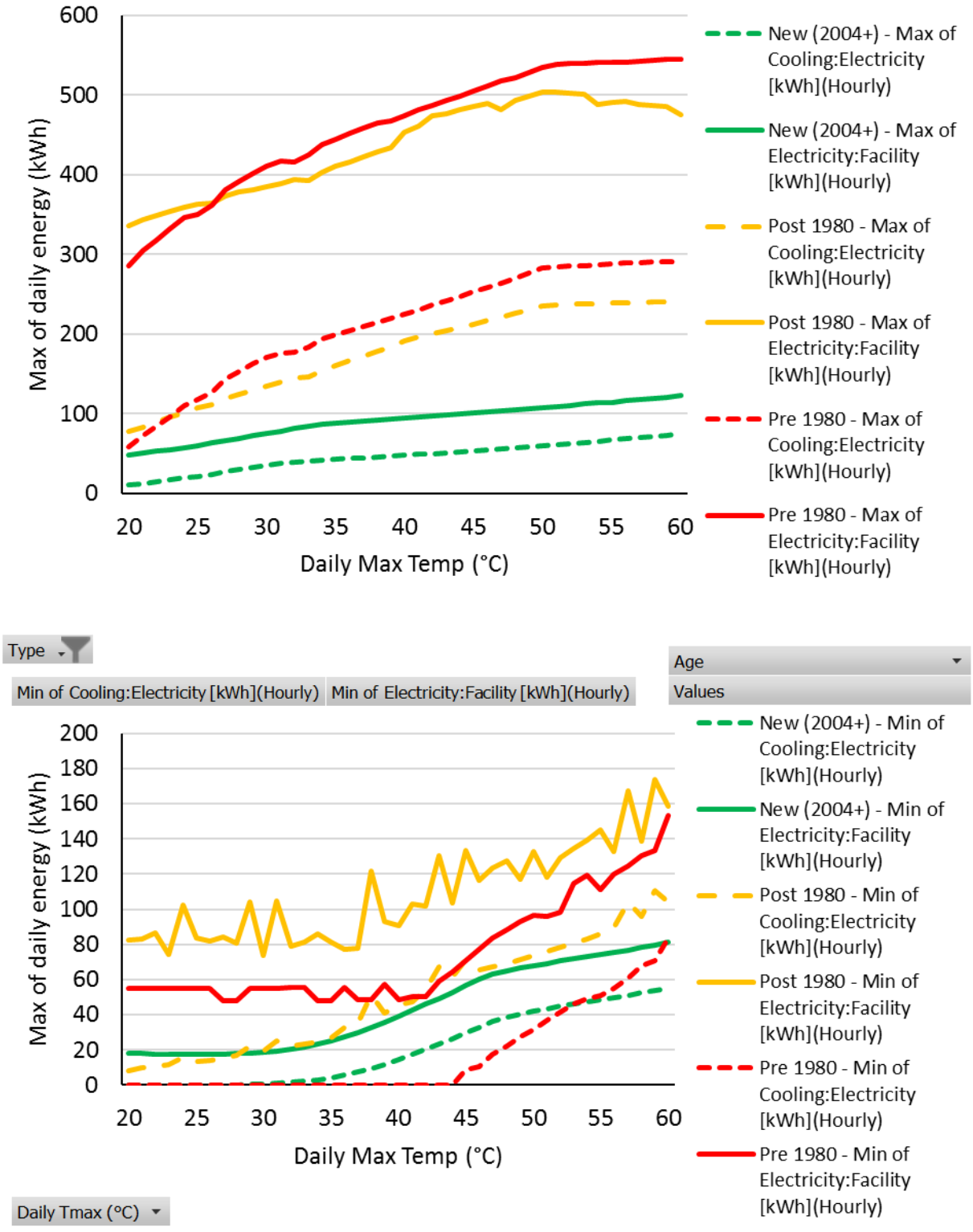

Figure B10. Primary School.

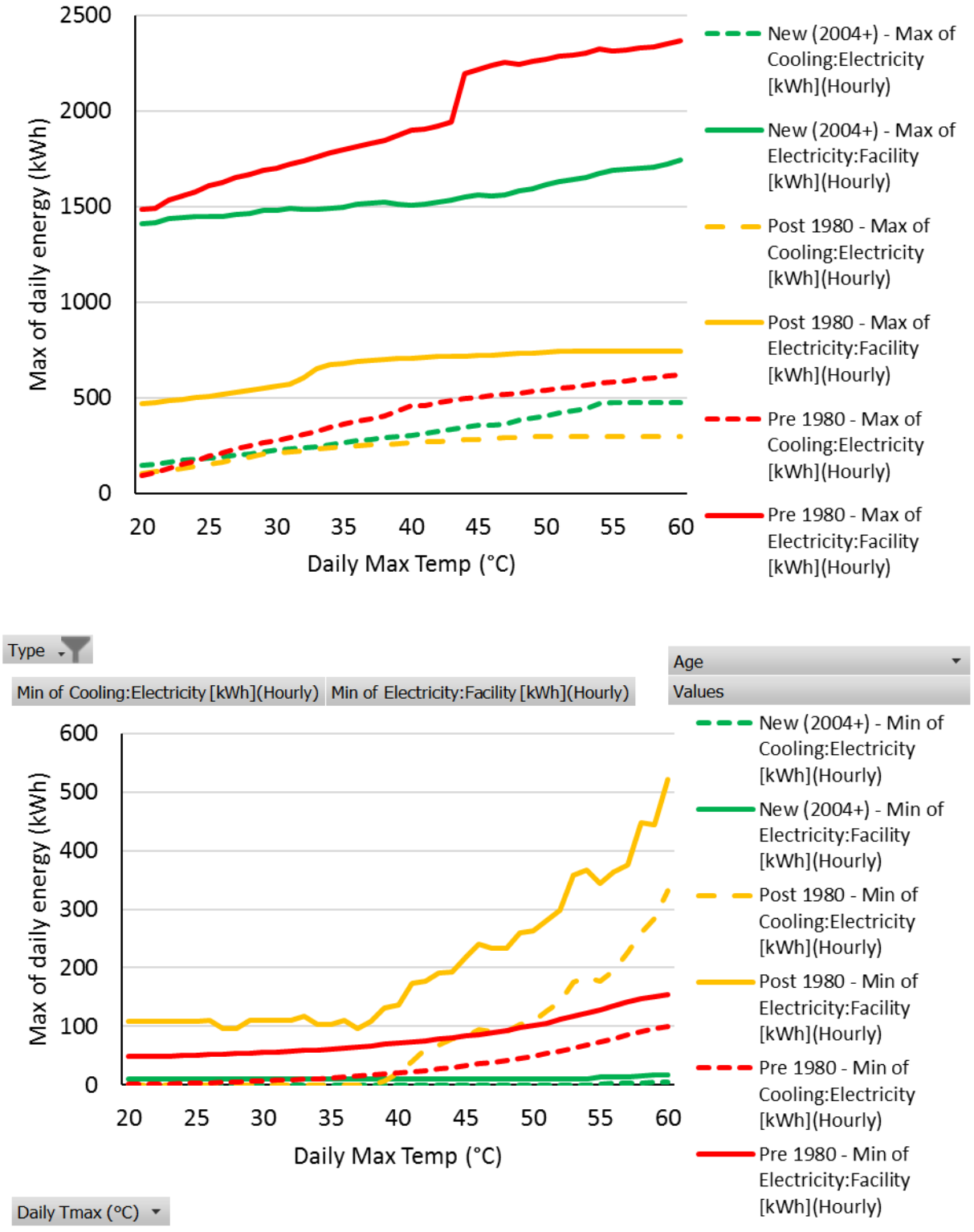

Figure B11. Quick Service Restaurant.

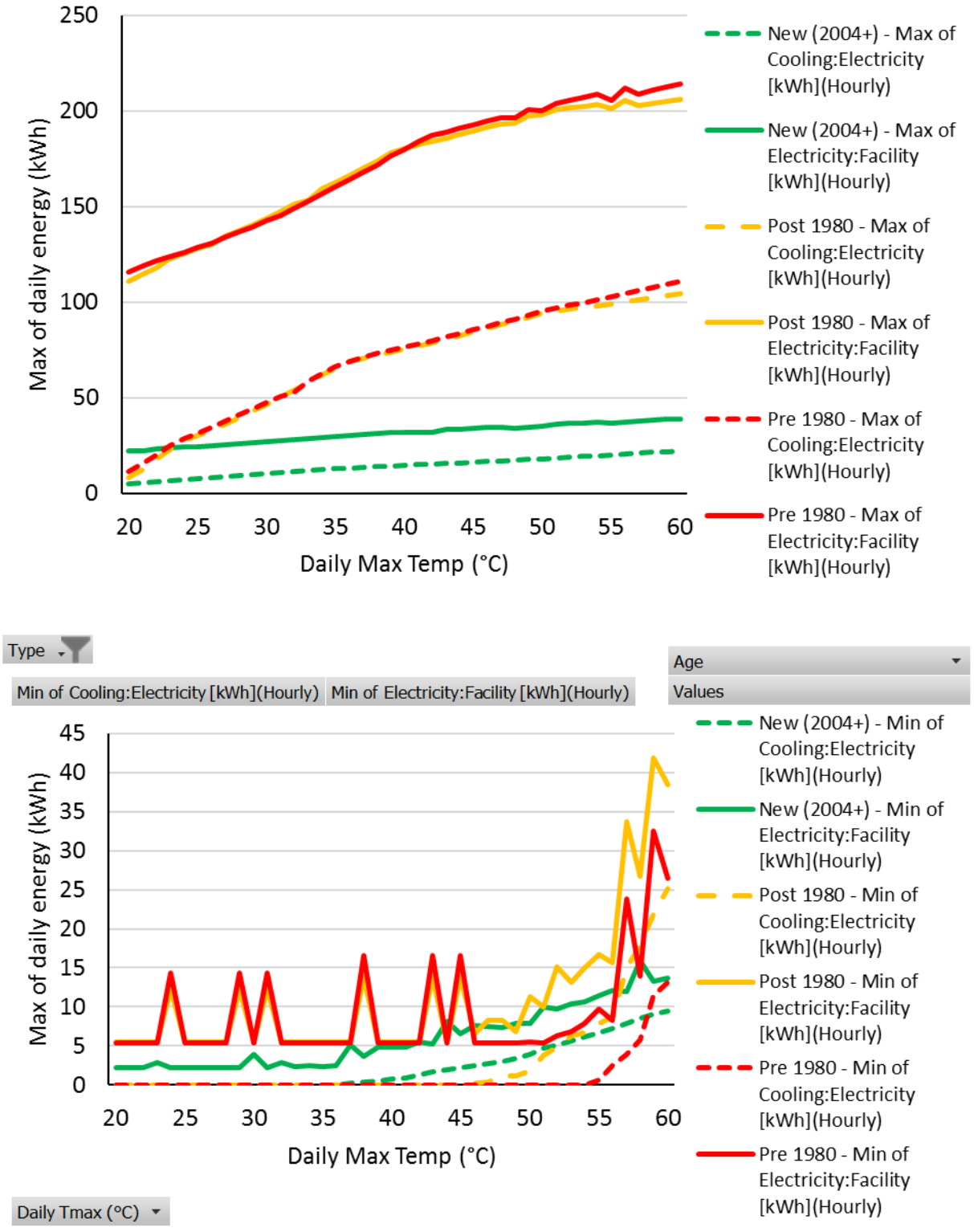

Figure B12. Secondary School.

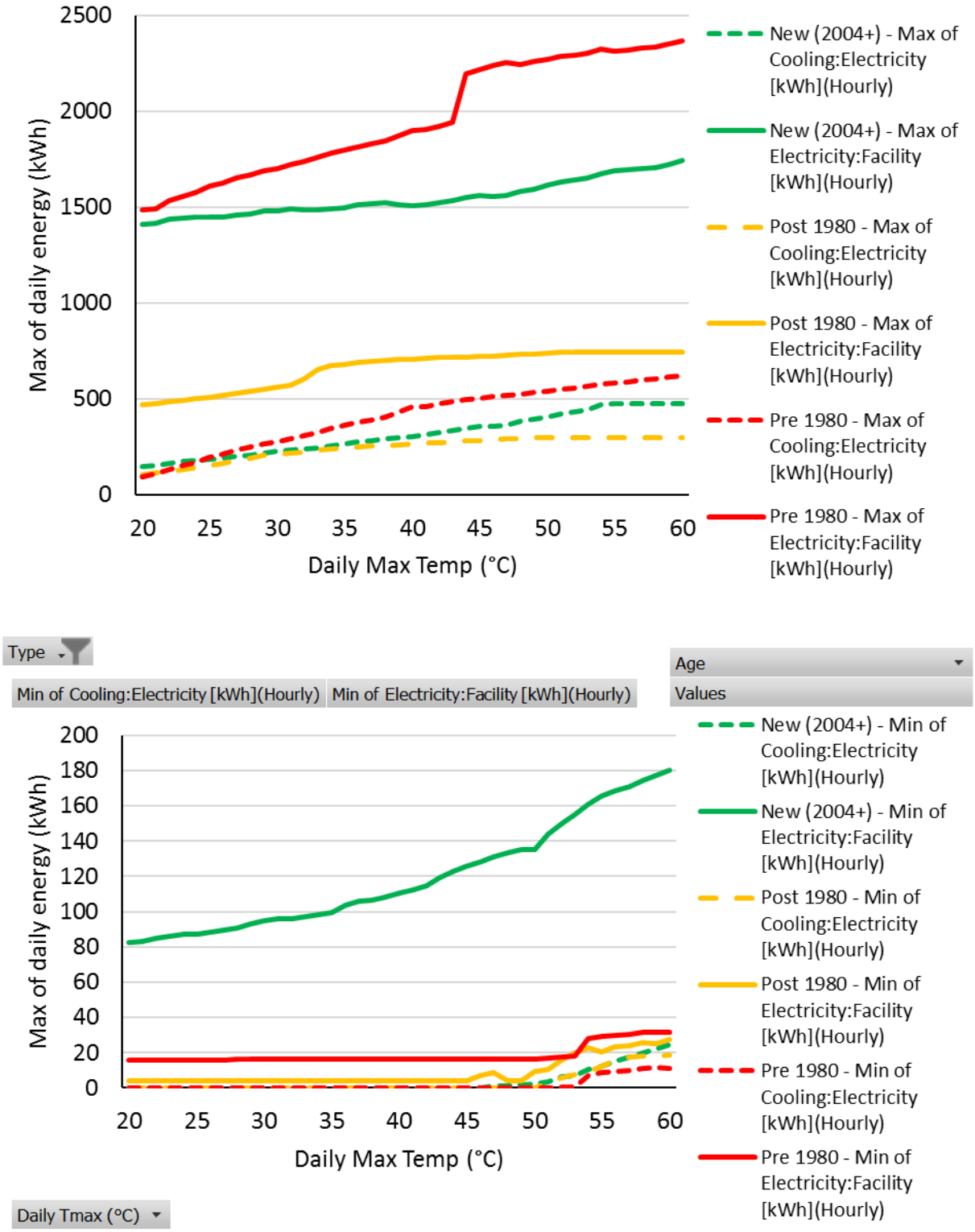

Figure B13. Small Hotel.

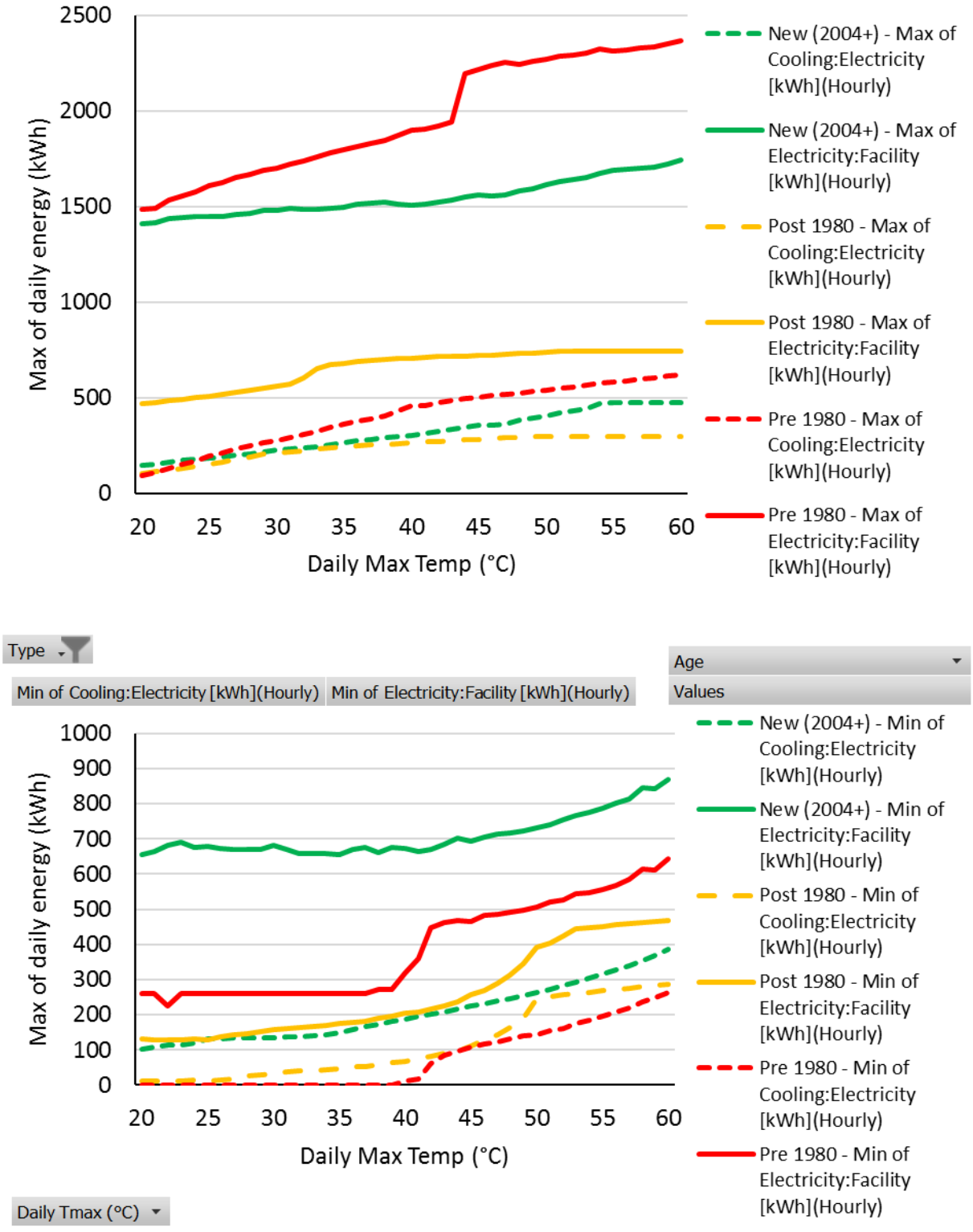

Figure B14. Small Office.

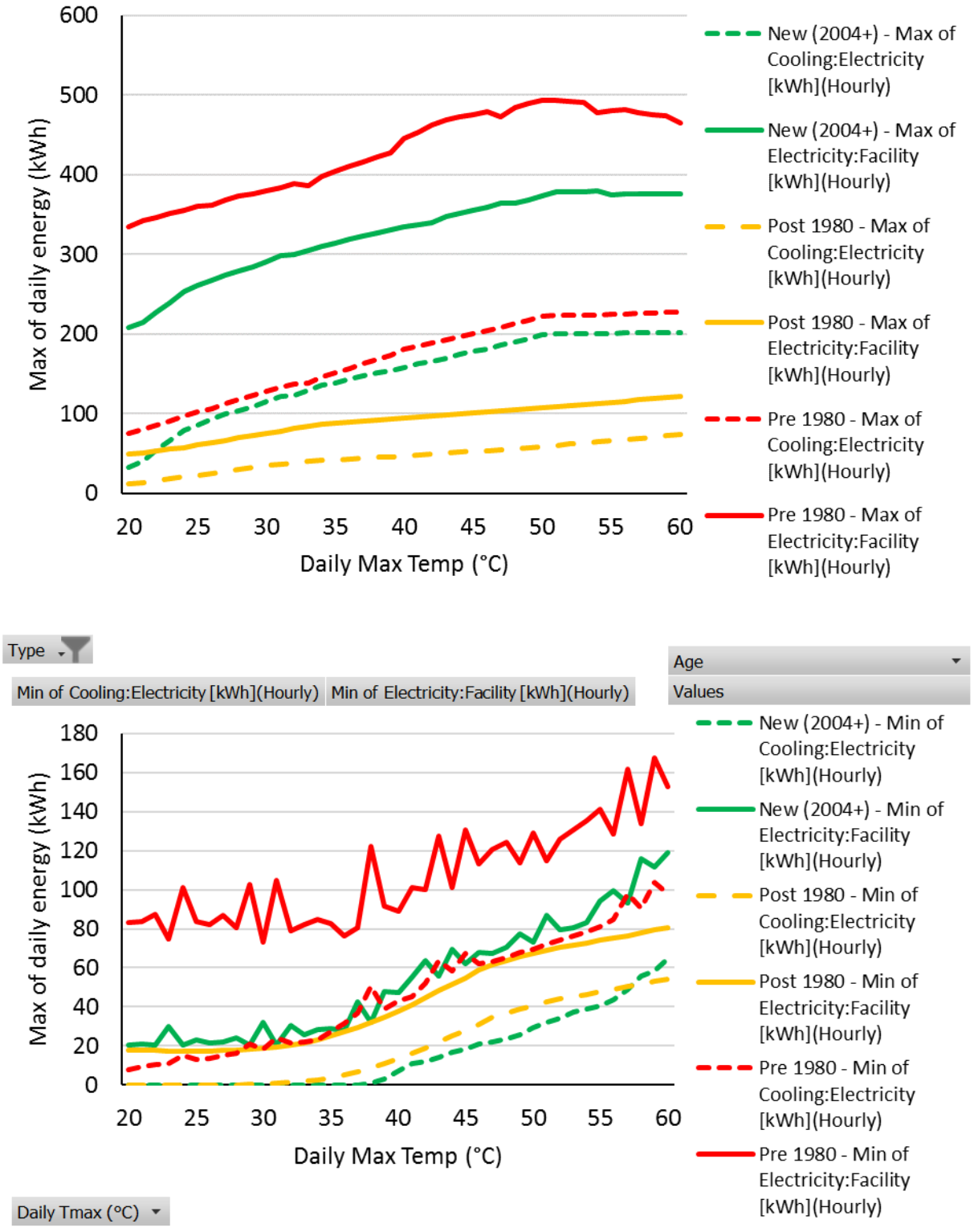

Figure B15. Stand-alone Retail.

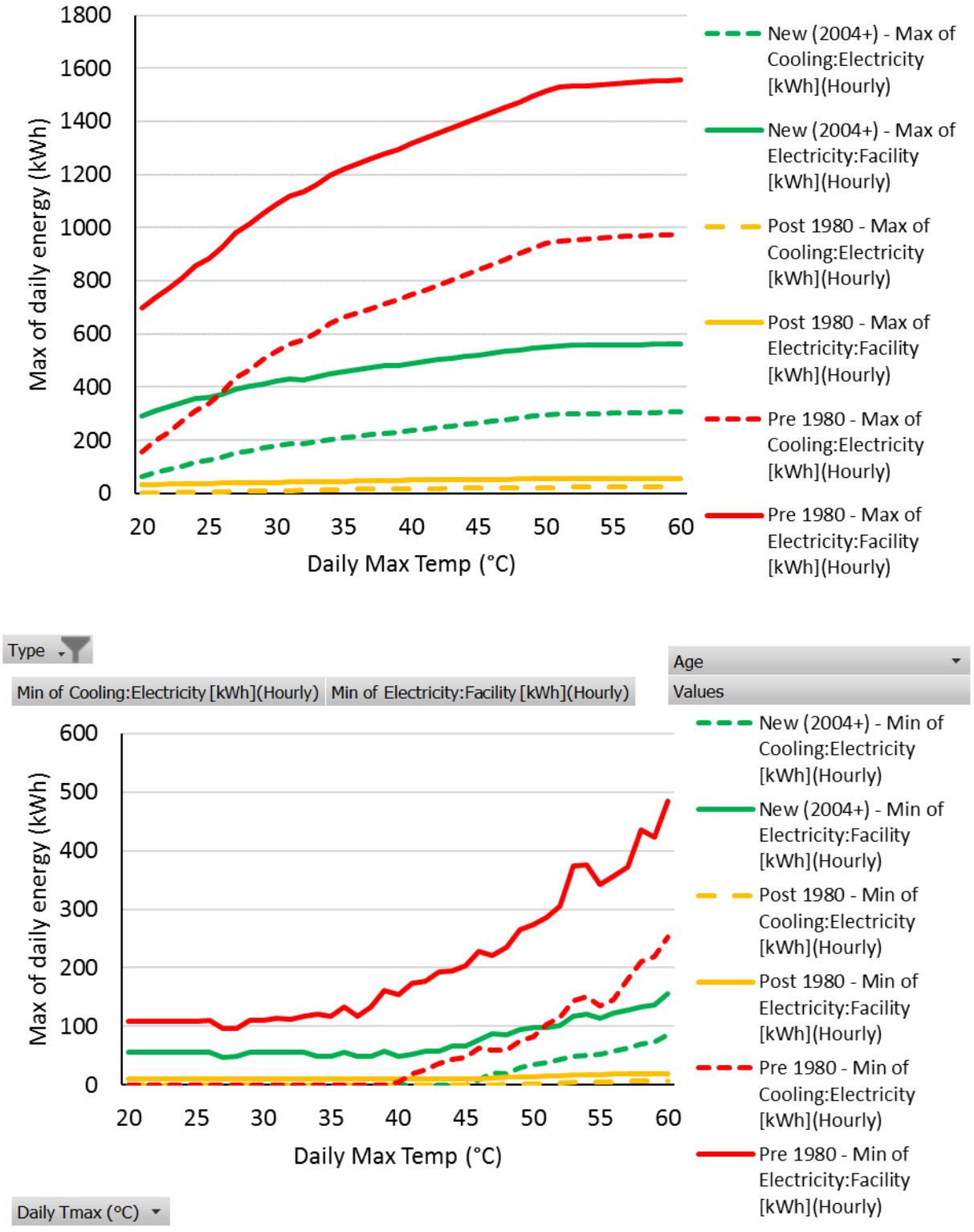

Figure B16. Strip Mall.

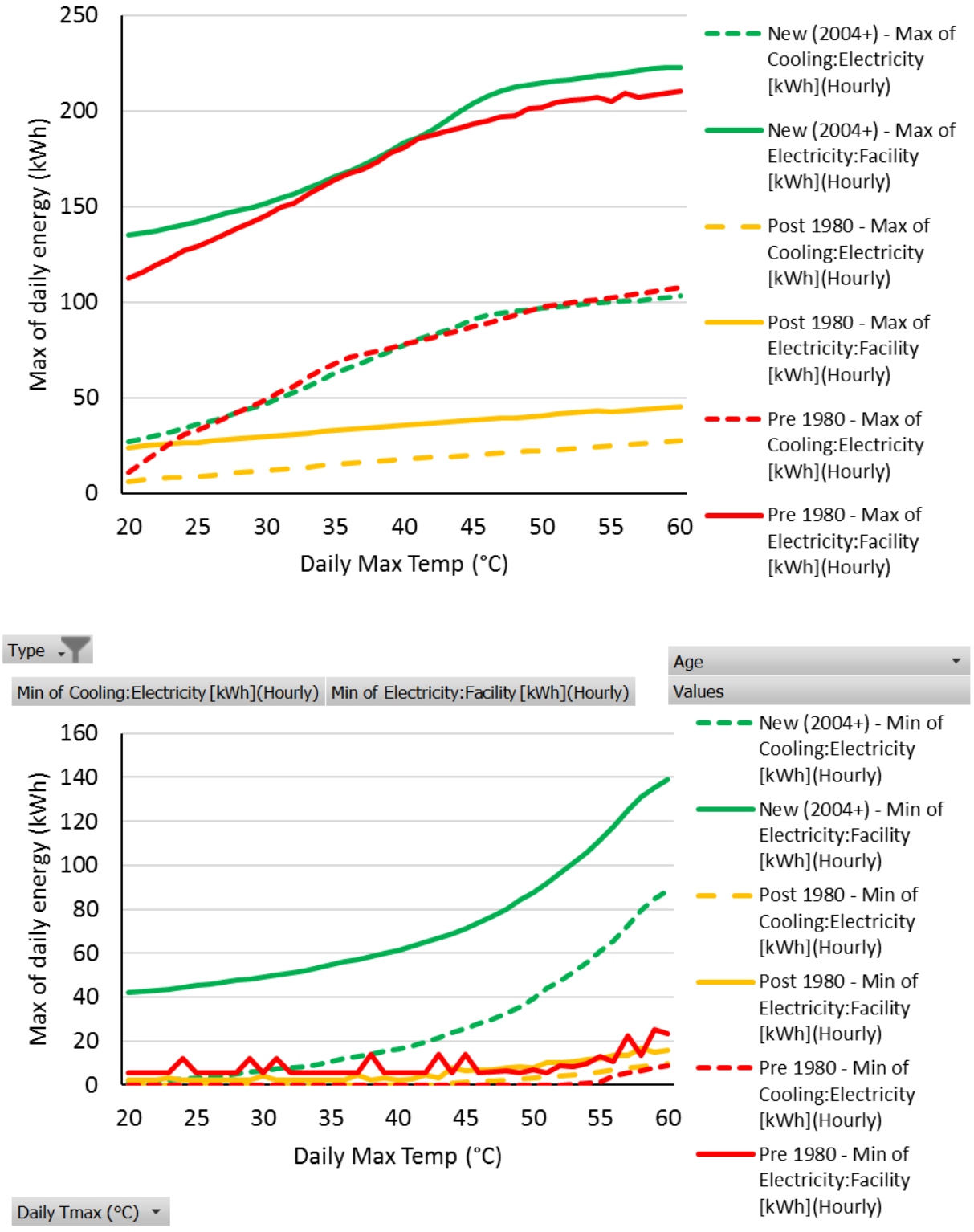

Figure B17. Super Market.

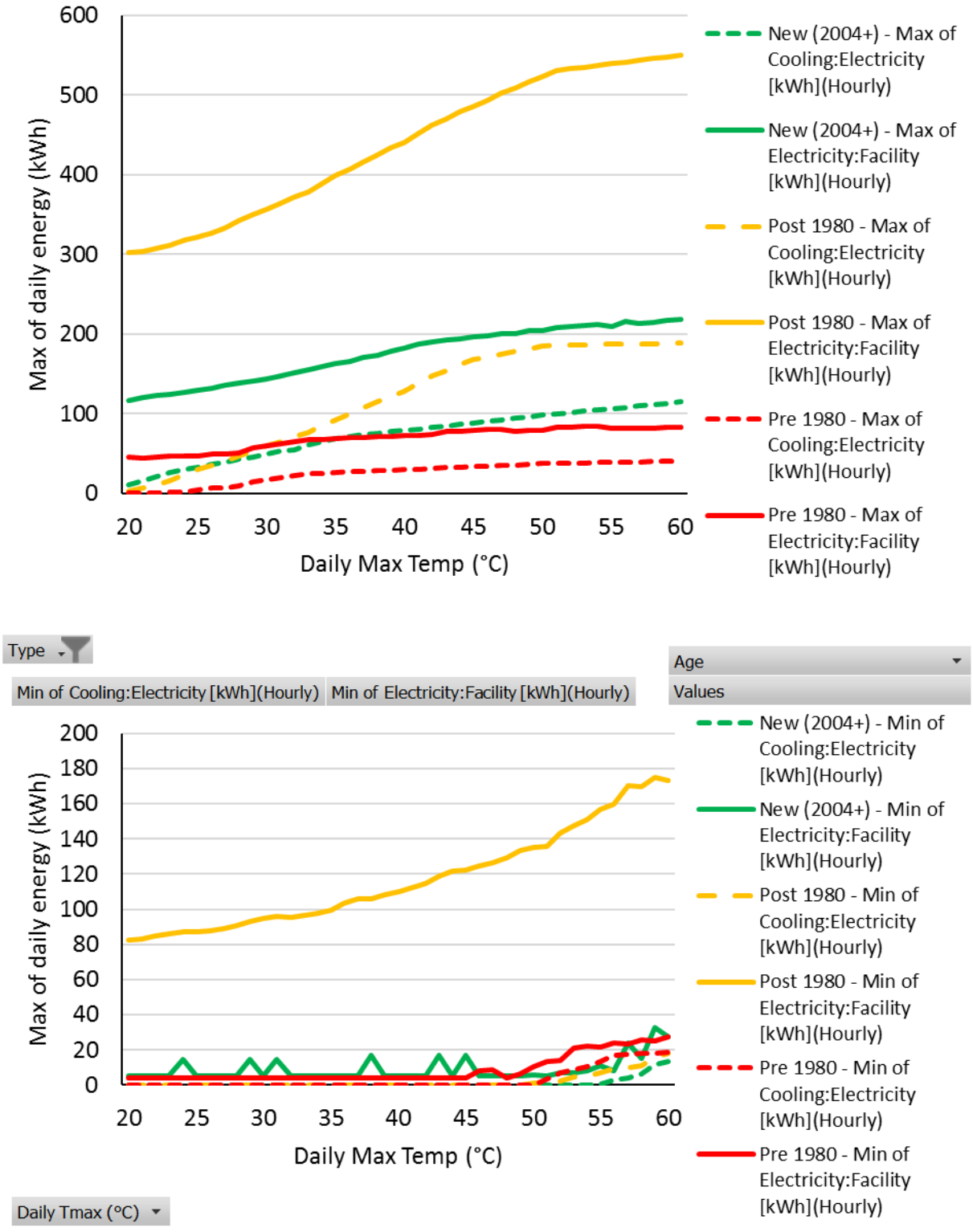

Figure B18. Warehouse.

APPENDIX C: Population Projections

C.1 Low - Finance / USGS

We used the Department of Finance population projections (published by the USGS) from [16] as described in [92]. All population projections assumed constant population density (people per km^2) for all pixels by county. This value is equal to 2897.112 persons per km^2 for Los Angeles. Increase in population is accounted for by additional pixels at 1x1 km^2 resolution. Those population data were assigned to census block groups weighted by area to create the base and future low- scenario population values for each CBG. Note: while there are 10 "iteration" results of the probabilistic forecast model, the differences are very minor (tested within 1% between iteration 1 and 10), and only one iteration was used. Also, the low- med- high- scenario population projections are the same out to 2060.

Inputs

- Sc1120-It0001-Ts2010-Sa-Population.tif
- Sc1120-It0001-Ts2040-Sa-Population.tif
- Sc1120-It0001-Ts2060-Sa-Population.tif

Process to allocate population to census block groups
Note: Make sure all maps have areas calculated before combining with other maps

1. Import the 3 population files into ArcMap
2. GEOPROCESSING: run raster to point conversion tool
3. JOIN point files to 2x2km grid of LAC "LAC_GCM_Grid_Cells_mainland"
4. ADD FIELD for population
5. CALCULATE FIELD: multiply "Join_Count" by "GRID_CODE" to get population in each grid cell
6. REPEAT 3-5 and into one new shape file with all population projections by grid cell
7. GEOPRECESSING: UNION the grid cell with population file to a map of LA CBGs
8. ADD FIELD for area of union
9. ADD FIELD for BG population
10. CALCULATE FIELD (BG population):
    = (population in GC) / (Area GC) * (area union)
    Note: if (Area GC==0): pop=0, else ..
11. GEOPROCESSING: DISSOLVE by CBG GEOID, sum population
12. MANUALLY correct for error as described below.

Outputs

Shape file, indexed by CBG, with population for 2010, 2040, 2060; population density per land mass area; absolute increase in population from 2010; and relative percent increase in population from 2010.

Descriptive statistics

- Area = 10,237 km^2
- Population in 2010 = 9.7 million
- Population in 2040 = 10.3 million
- Population in 2060 = 10.9 million
- Largest percent increase in population in any CBG = 460%

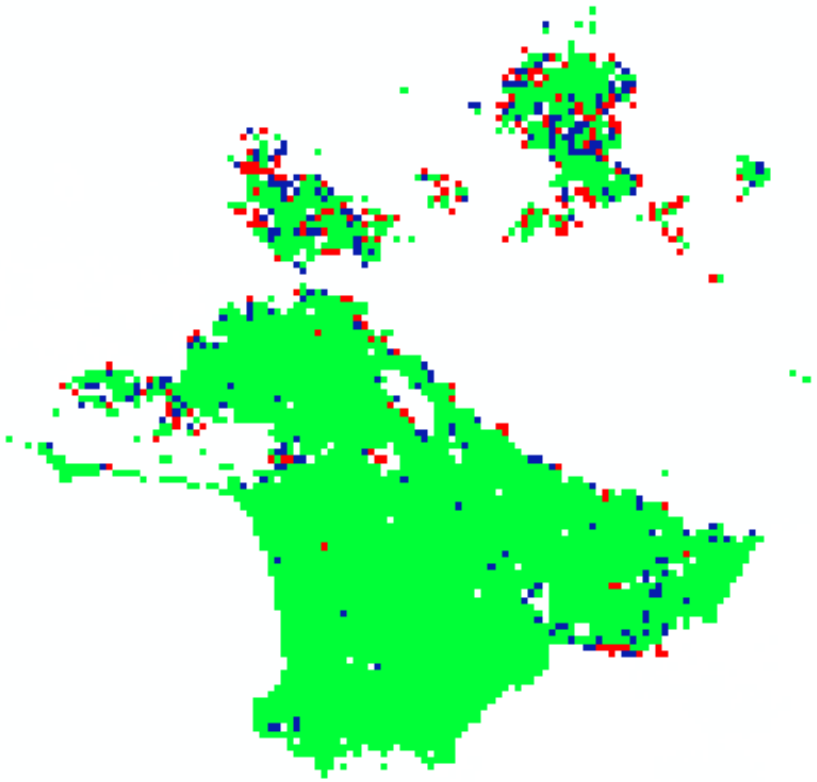

Figure C1. Input population projections. For Los Angeles County, all pixels represent 2897.112 persons.
Colors correspond to years as follows: green = 2010, blue = 2040, and red = 2060.

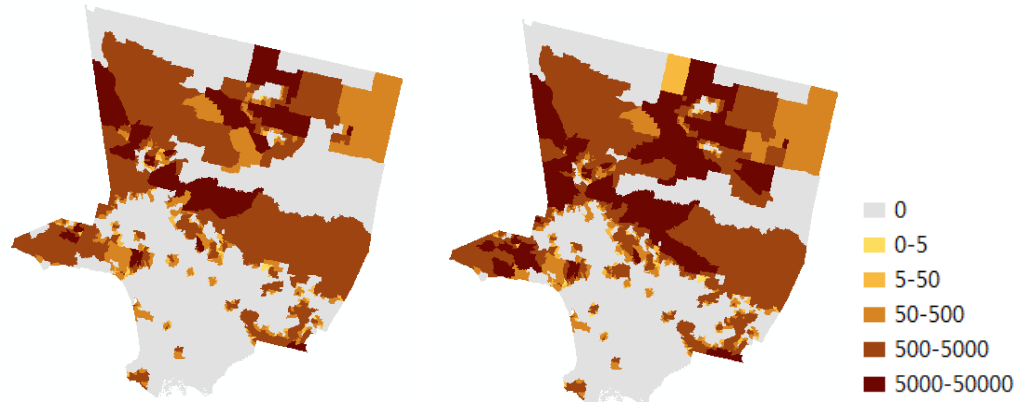

Figure C2. Department of Finance population increase projections from 2010 to 2040 (left) and 2060 (right) by census block group.

Error

Total error was not significant: ~0.05% of population was lost

C.2 High – SCAG

SCAG population projections were based on the city-level population projections listed from [17] as described in [55] and [59], for 88 cities and the unincorporated area. Because those projections were only available at the (relatively low-resolution) city-level, the annual growth rate for each city was calculated relative to the SCAG base 2012 values, and then applied to the corresponding CBG using the same 2010 population values as in the low-case method. The resulting total population was 11,435,479 for 2040 (within 1% of SCAG reported projection of 11,514,800) and 12,814,475 for 2060. The resulting population increase from 2010 to 2040 and 2060 are shown in Figure C3 below.

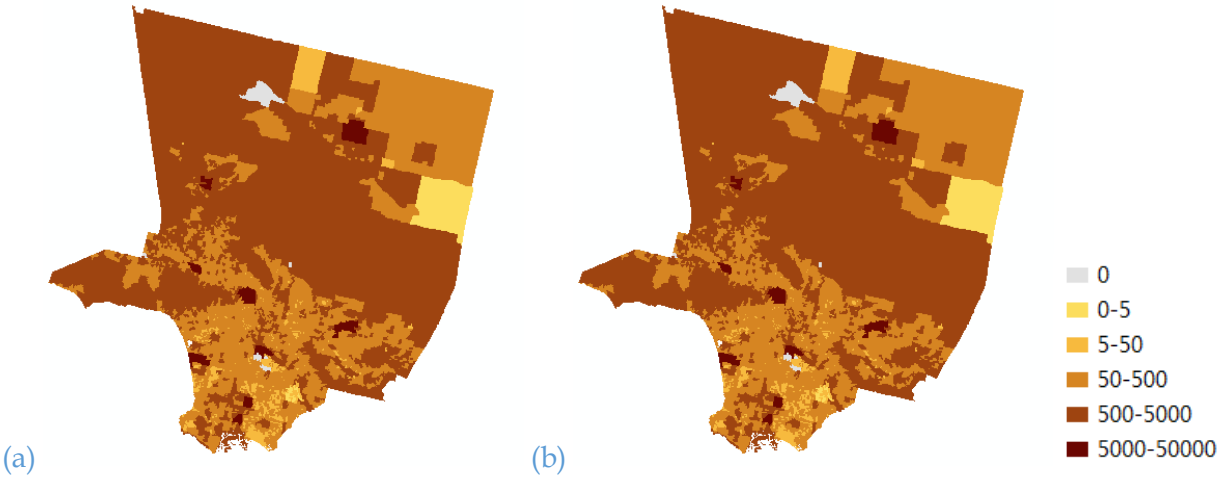

Figure C3. Modeled SCAG population projection increases from 2010 to 2040 (a) and 2060 (b) by census block group.

The range of differences in population projections in 2060 from low to high scenarios are shown in Figure C4 below. The major difference is that the SCAG projections include more infill in already developed central and downtown areas, and less growth in less developed areas.

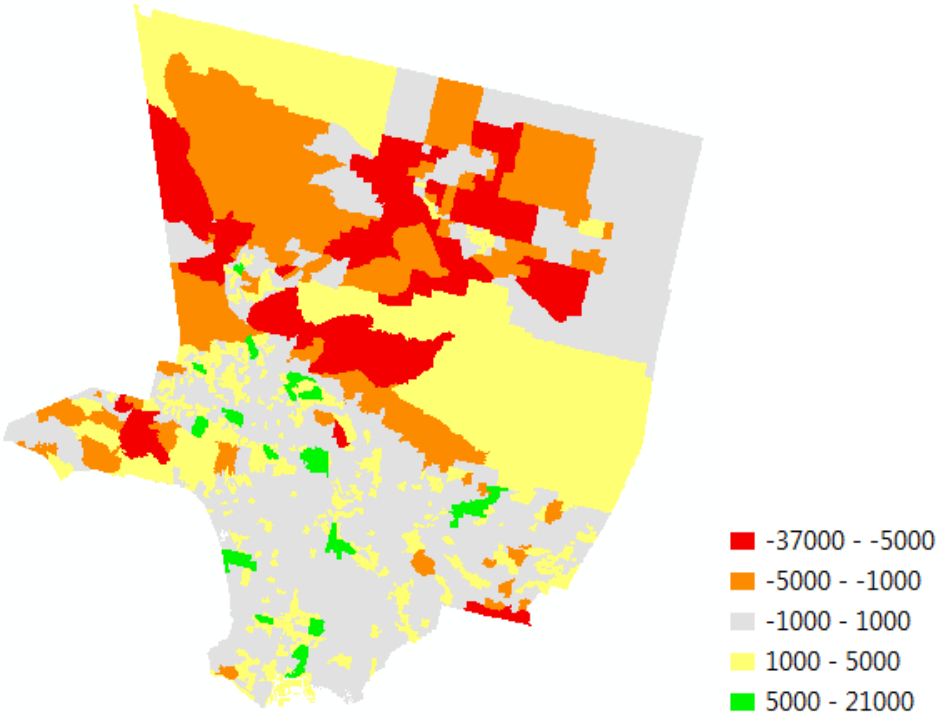

Figure C4. Difference between low and high population projection increase in 2060 by census block group.

APPENDIX D: Substation Demand Allocations with Voronoi Tessellations

Instructions are for ArcMap Desktop 10.5.

Start with EIA / homeland security data set [76], as shown in Figure below. Notice transmission lines from [78] are overlaid in the figure.

- 410 substations total
- 102 have voltage ratings
    - 66-69 kV, count = 25, all but 9 are listed with connections to one or more lines
    - 115-138 kV, count = 18, all but 7 are listed with connections to one or more lines
    - 230-500 kV, count = 59, all but 5 are listed with connections to one or more lines
- 308 unknown are assumed to be medium to low voltage, i.e. <=138 kV

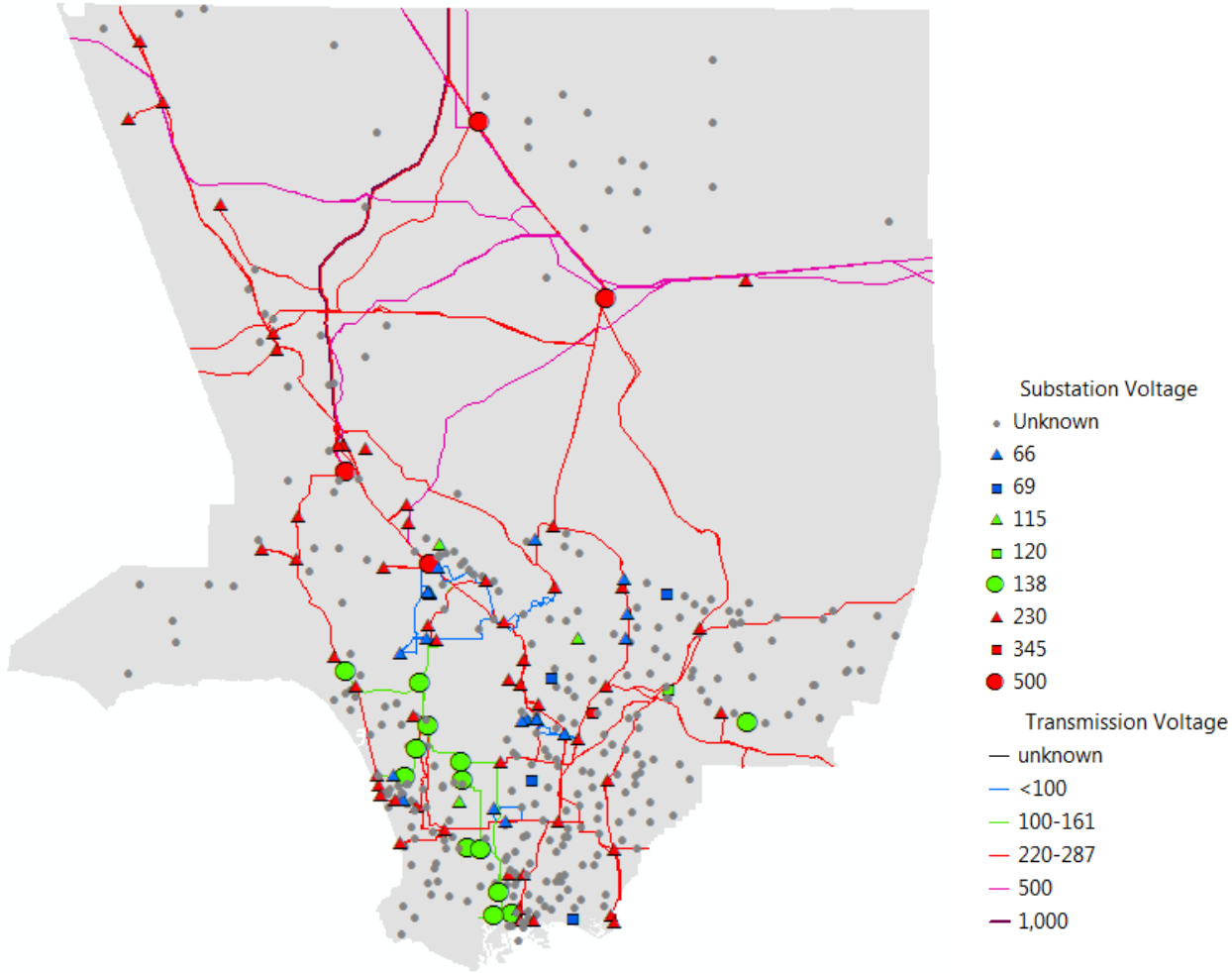

Figure D1. LAC substations with transmission line overlay. Note: not all components may be visibly identifiable due to close proximity.

Separate substations into two layers, high voltage and low voltage per the Preliminary Analysis of Substation Loading.

- High voltage: 230kV and up
- Medium and low voltage: rest including unknown

D.1 High Voltage

1. Use "Integrate" tool on high voltage layer with 2km tolerance, and then "collect" to produce new layer as shown in Figure 39. The 59 substations will be consolidated into 36 clusters. Substations are grouped together in this manner to prevent creation of nonsensically small polygon areas in the following step.

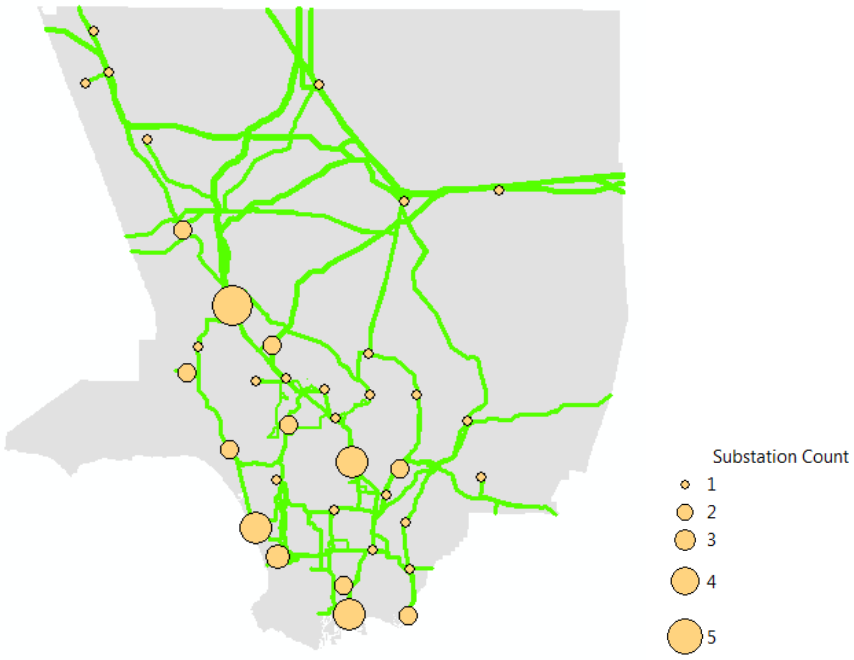

Figure 39. Clustered high voltage substations only with transmission line overlay

2. Use "Create Theissen polygon" to run Voronoi Tessellations and allocate substations to land area coverage, and then "clip" to LAC as shown in Figure 40. Add the attribute of Area for square meters.

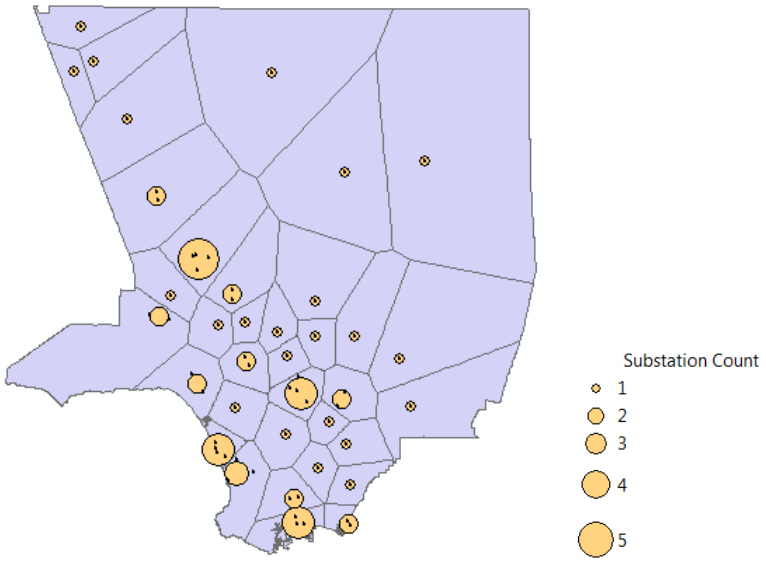

Figure 40. Clustered high voltage substations with Voronoi polygons.

3. Use the "intersect" tool assign the CBG peak demand composite image for the base period. Make sure peak demand is available in terms of Wh and that the areas of the CBGs are in that shape file.
4. Create a new column for area of the intersected space in terms of square meters.
5. Create a new column for the peak demand (Wh) to allocate to the Voronoi polygon. Calculate it as the product of peak demand (Wh) in the CBG and the ratio of intersection area to CBG area.
6. "Dissolve" the layer by the FID of the Voronoi polygons, and sum the peak demand (Wh). Base case shown in Figure 41 for 13.5 GWh.

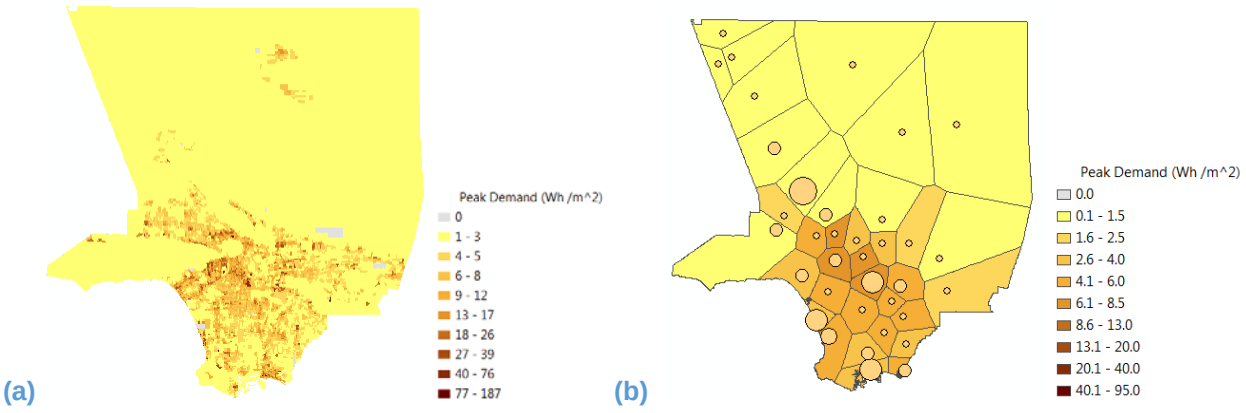

Figure 41. Sample transform of peak demand from CBGs to high voltage substation Voronoi areas.

Comparison of substation allocations with SCE DERiM data is shown in Figure 42. Total peak demand estimated in the model at substations corresponding to the same geographic locations

was 10% less than values estimated from the DERiM data, 6,388 MWh versus 7,098 MW. The majority of that difference was 250MW at the three clustered substations in the southwest LA Fresa (x2) and El Nido substations, and 180MW at the Antelope substation in the north.

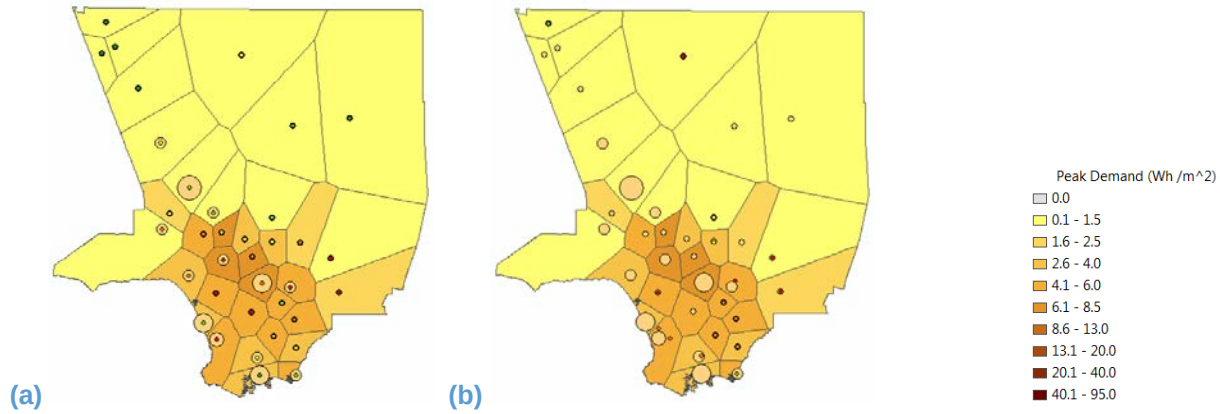

Figure 42. Overlay of substation clustering, Voronoi polygons with base period demand allocation (Wh/m^2), to (a) model estimated peak load, and (b) SCE DERiM peak load estimates.

D.2 Medium and Low Voltage

Repeat steps for high voltage.

Cluster 351 substations into 173 Voronoi polygons by grouping within 1km proximity, Figure 43.

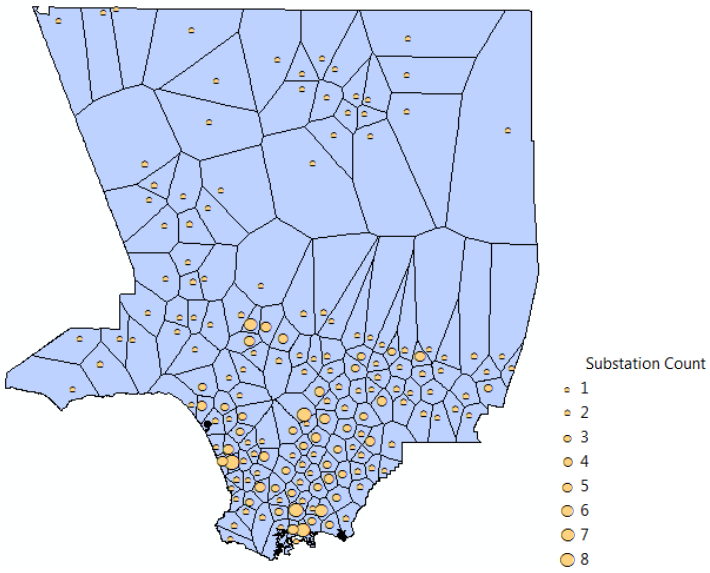

Figure 43. Clustered low voltage substations with Voronoi polygons.

Comparison of demand allocation shown in Figure 44.

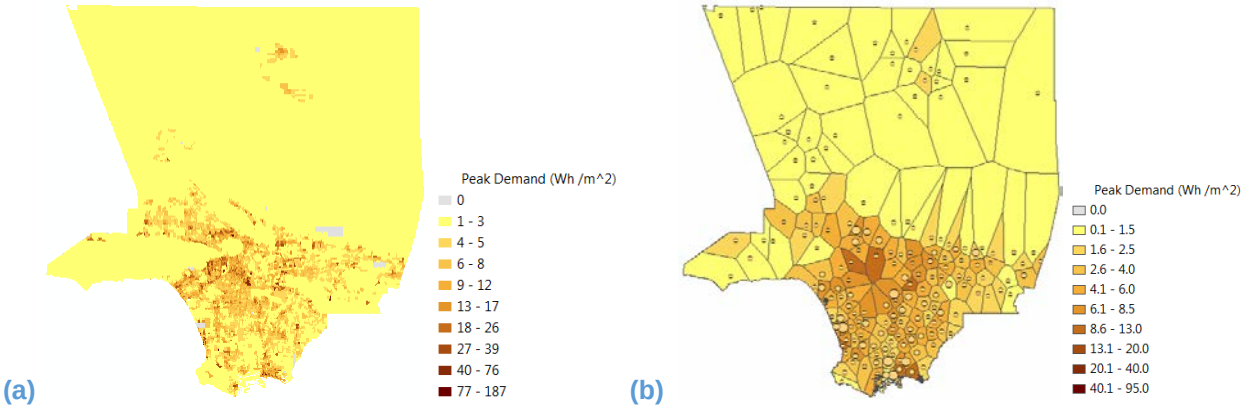

Figure 44. Sample transform of peak demand from CBGs to high voltage substation Voronoi areas.

Of the 173 substation clusters, 133 overlapped with the SCE DERiM's distribution substations, with a combined model peak demand of 9.94 GWh, 15% higher than the DERiM's 8.62 GW. Comparison of loads on substations and substation clusters is shown in Figure 45. Most of that difference was due to Voronoi polygons that included LADWP substations in the clustering.

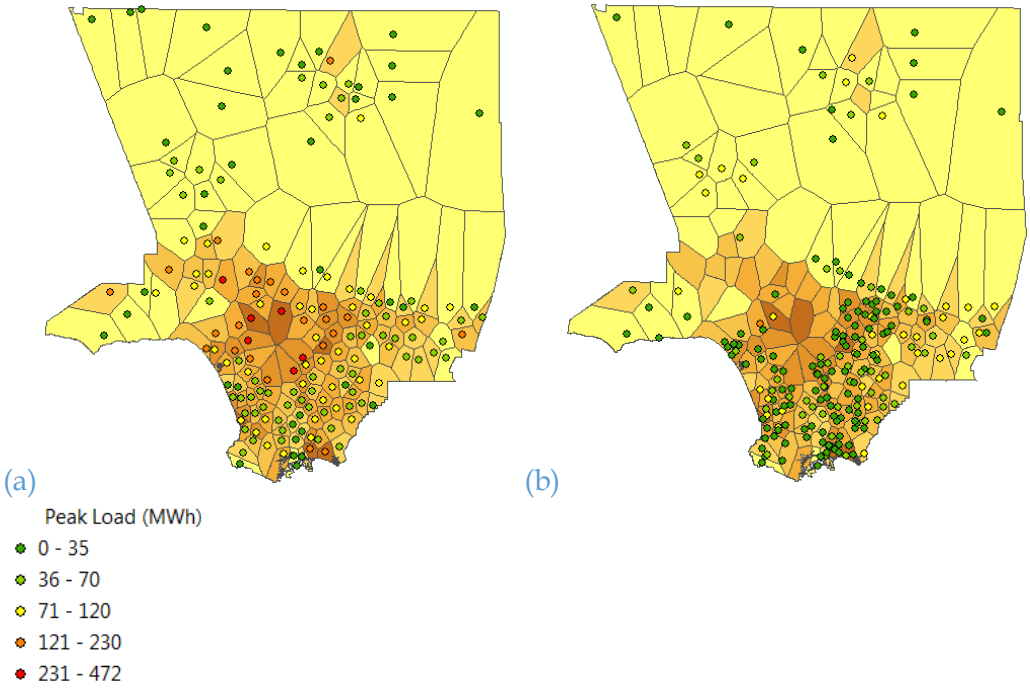

Figure 45. Base period loads for (a) model composite demand on substation clusters, and (b) SCE DERiM distribution substations and estimated peak load.

D.3 Preliminary Analysis of Substation Loading using SCE DERiM Data

This section details how substation load, capacity, and load factor estimations were developed for the base period. The EIA / homeland security substation data set, as previously described, was used as representative of LAC's installed components in terms of location and level in the delivery system. Components were separated into high voltage and low voltage layers in an attempt to represent parallel operations within each layer and series operations across the layers. Obviously this is not a perfectly accurate method, but given the data and tools available to work with this was considered a reasonable approach, within limits, as follows. The SCE DERiM data set [77] was used as a representative sample because data were available to estimate load, capacity, and load factor as detailed in the next paragraph. Shown in Figure 46, the DERiM's 21 "sub-transmission" substations were geo-located within 100m of the EIA's 59 high voltage ≥230kV substations, with matching names in the data. All but three were labeled as 220/66 kV, two were labeled 66/66 kV, and one as 12/66kV. Of the DERiM's 245 "distribution" substations, 202 were geo-located within 100m of the EIA lower ≤138kV and unknown voltage substations, 171 were listed as 66/16 kV or 66/12 kV, 73 as 16/4kV or 12/4kV, and 1 as 16/33 kV. Obviously, there is some amount of power flow in series amongst those substation layers, as there is between 500 kV and 230 kV substations. Again, this approach is an approximation. Of the EIA's 351 lower voltage substations, 37 had "unknown" names, otherwise unique, and 161 had names that matched to the DERiM's 245 substations. The DERiM data had 74 substations listed with the same name and different voltage ratings as the EIA data. Therefore, DERiM data were assumed representative of approximately 1/3rd of the high voltage substations, and 70% of the low voltage substations in LAC.

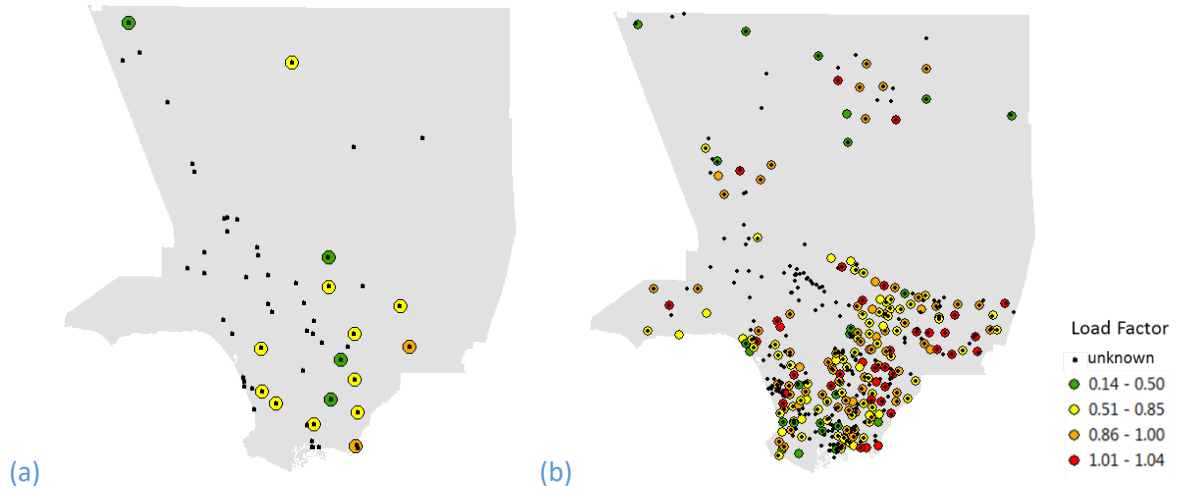

Figure 46. Overlay of EIA and SCE substations for (a) high voltage and (b) low voltage layers. EIA substations are shown as black dots, and SCE substations as colored circles.

Substation load, capacity, and load factor estimates were developed from the published DERiM data, and ranges allocated to the remaining substations in the LAC infrastructure. Equations for estimated values are listed in Table 18 below. Peak Load was a straightforward estimation per the definitions from SCE's data dictionary [77] quoted in the bullets points below. The formula

for Nameplate Capacity was assumed for a temperature adjusted loadability factor equal to 1 at 40°C. SCE's interconnection handbook guidelines [70] state 40°C in sections for Ambient conditions, and Transformer Emergency Ratings are stated as permissible with 10-20% overloading for 1-30 days. These values are consistent with the range of high voltage AC switchgear operations described in IEEE Std C37.30.1-2011 [8]. Load Factor is a straightforward calculation based on the previous two estimates. Descriptive statistics of results are summarized in Table 19, and shown in Figure 46, Figure 47, and Figure 48. Note: 7 substations were discarded from sample as Load Factor values were not considered reasonable equal to zero or greater than 2. UNIVERSAL 66/12 kV, TAHITI 66/16 kV, REDMAN 66/12 kV, NAVY MOLE 66/12 kV, GOULD 16/33 kV, GANESHA 66/12 kV, AUTOBODY P.T. 16/4 kV. Of the 238 remaining substations, the 72 substations labeled 16/4 kV and 12/4 kV had a total peak load of 509 MW (6% of the sample), capacity of 677 KVA (7% of the sample), and single largest capacity of 17 kVA.

Table 18. Equations used in estimating substation load factors.

Equation #	Expression	Units
1	Peak Load = Total Generation / Current Penetration Level * 100	MW
2	Nameplate Capacity = Existing Generation + Maximum Remaining Generation	MW
3	Load Factor = Peak Load / Nameplate Capacity	%

- Total Generation (MW) - "This value represents the sum of both Existing and Queued Generation. Total Generation includes all downstream [distributed energy] resources. For example, Total Generation at a substation includes all Existing and Queued Generation connected to all circuits fed from that substation."
- Current Penetration Level (%) - "This value represents the ratio of generating resources to peak load, expressed as a percentage. For example, if a circuit has a peak load of 10 MW, along with 4 MW of Total Generation (this includes existing and queued generation), the current penetration level is 40%."
- Maximum Remaining Generation (MW) – "This value represents the maximum amount of generation that the system may be capable of supporting within existing planning guidelines and criteria. The maximum remaining generation capacity often requires system upgrades to be fully realized."

Table 19. Summary of SCE DERiM substation estimated values.

Attribute	min	mean	max	total
High voltage (21/59)				
Peak Load (MW)	40	338	759	7,098
Nameplate Capacity (MW)	215	518	911	10,883
Load Factor (0-1)	0.188	0.632	0.893	0.652
Low voltage (245/351)				
Peak Load (MW)*	1	36	143	8,537
Nameplate Capacity (MW)	1	43	387	10,155
Load Factor (0-1)	0.145	0.807	1.042	0.841

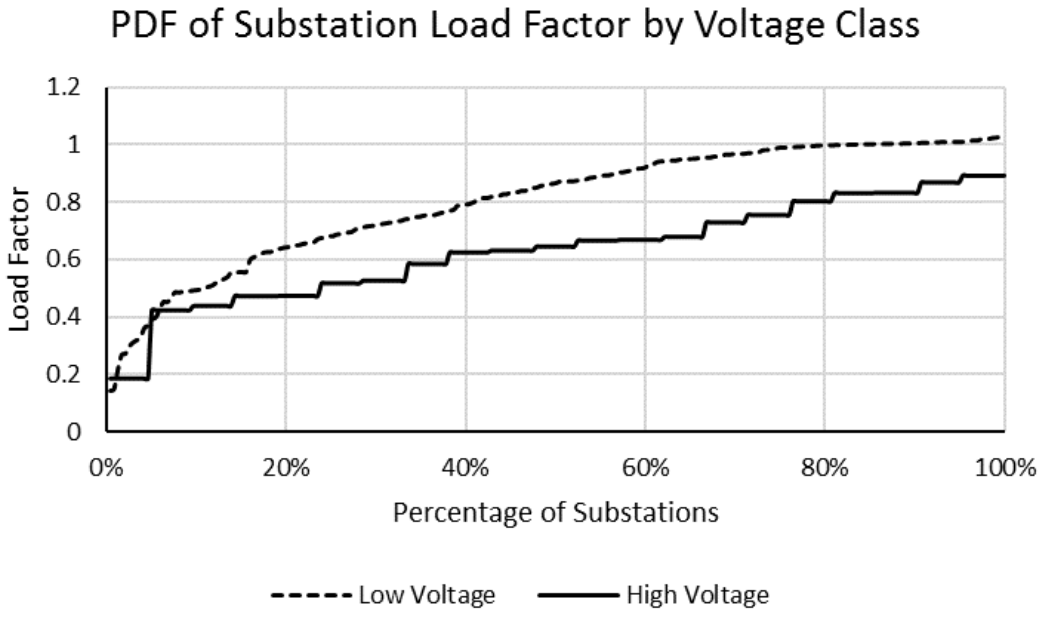

Figure 47. Probability density function of load factors on SCE substations

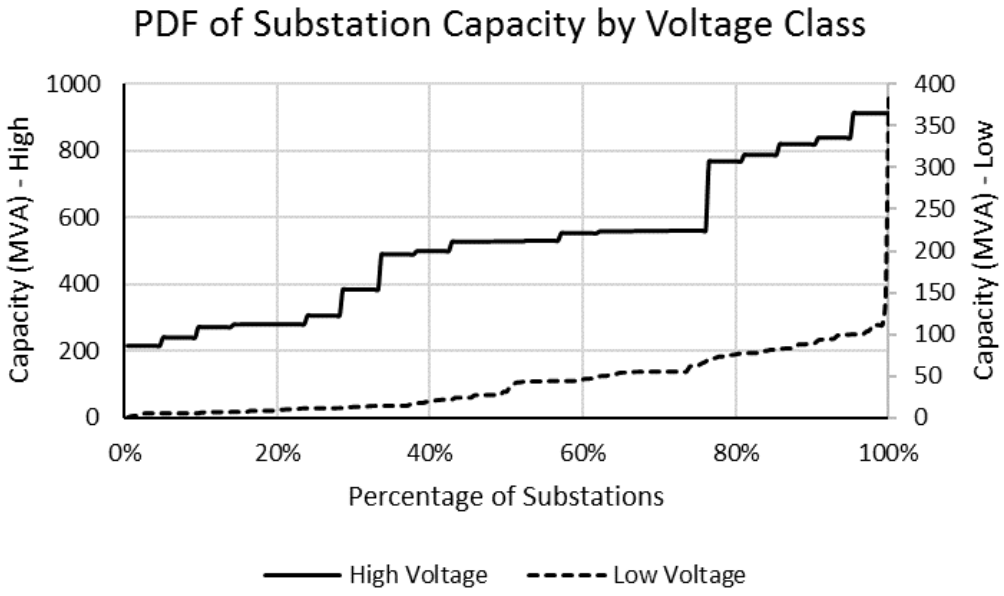

Figure 48. Probability density function of load factors on SCE substations

Total values for peak load for SCE at high- and low-voltage levels were considered as within a reasonable range to use for approximate verification purposes. Previous work in Task 3 estimated the range of base period peak demand for LAC as 15-20 GWh. If the total peak demand for SCE's high voltage substations is proportionally representative of the county, then total county peak demand on the high voltage layer would be equal to 7.1 GW * 59/21 = 19.9 GW. If the total peak demand for the low voltage substations is proportionally representative of the county, then total county peak demand on the low voltage layer would be equal to 8.5 GW * 351/245 = 12.2 GW. Possible explanations for the 25% shortfall at the low-voltage level are that SCE has about 1-2 GW of installed Solar PV capacity [93],[94] that is skewing the peak load lower in SCE substations relative to the rest of LAC, the other distribution substations may have disproportionately higher loads, and or the source data may erroneous beyond the 7 outliers identified.